MICROSTRUCTURE-CORROSION CORRELATION STUDIES ON THERMO-MECHANICALLY PROCESSED ZIRCONIUM BASED ALLOYS

By

SUNIL TONPE

(ENGG02200804021)

INDIRA GANDHI CENTRE FOR ATOMIC RESEARCH,
KALPAKKAM

A thesis submitted to the
Board of Studies in Engineering Sciences
In partial fulfillment of the requirements for the degree of

DOCTOR OF PHILOSOPHY

Of

HOMI BHABHA NATIONAL INSTITUTE

August, 2015

Homi Bhabha National Institute

Recommendations of the Viva Voce Board

As members of the Viva Voce Board, we certify that we have read the dissertation prepared by **Mr. Sunil Tonpe** entitled ***"Microstructure-corrosion correlation studies on thermo-mechanically processed zirconium based alloys"*** and recommend that it may be accepted as fulfilling the dissertation requirement for the Degree of Doctor of Philosophy.

(Dean-Academic) Date: 08.04.2016
Chair Person - Prof. T. Jayakumar Retired

UKamachi Mudali Date: 08/4/16
Supervisor-Convener –Sr. Prof. U. Kamachi Mudali

Date: 8-4-16
Member 1 Dr. M. Sai Baba

Date: 08/4/2016
Member2 - Dr. A. K. Bhaduri

Jyotsna Dutta Majumdar Date: 8.4.2016
Member3 - External Examiner

CERTIFICATE

I hereby certify that I have read this dissertation prepared under my direction and recommend that it may be accepted as fulfilling the dissertation requirement.

UKamachi Mudali

(U. Kamachi Mudali)

Research Supervisor

Date: 08/4/16

Place: Kalpakkam

STATEMENT BY AUTHOR

This dissertation has been submitted in partial fulfillment of requirements for an advanced degree at Homi Bhabha National Institute (HBNI) and is deposited in the library to be made available to borrowers under rules of the HBNI.

Brief quotations from this dissertation are allowable without special permission, provided that accurate acknowledgement of the source is made. Requests for permission for extended quotation from or reproduction of this manuscript in whole or in part may be granted by the Competent Authority of HBNI when in his or her judgment the proposed use of the material is in the interests of scholarship. In all other instances, permission must be obtained from the author.

(Sunil Tonpe)

DECLARATION

I, hereby declare that the thesis entitled "*Microstructure-corrosion correlation studies on thermo-mechanically processed zirconium based alloys*" submitted to Homi Bhabha National Institute (HBNI), Mumbai, India, for the award of Doctor of Philosophy in Engineering Science is the record of work carried out by me under the guidance of Sr. Prof. U. Kamachi Mudali, Associate Director, CSTG & MPEDG, Indira Gandhi Centre for Atomic Research (IGCAR). The work is original and has not been submitted earlier as a whole or in part for a degree, diploma, associateship, fellowship at this or any other Institution/University of higher learning.

(Sunil Tonpe)

List of Publications arising from the thesis

Journals

1. **Sunil Tonpe**, U. Kamachi Mudali, Effect of thermomechanical process on mechanical and corrosion properties of zircaloy-4 tubes of mock-up dissolver vessel, Journal Materials and Manufacturing Processes,2015, **DOI:** 10.1080/10426914.2015.1090589
2. **Sunil Tonpe**, N. Saibaba, R.N. Jayaraj, A. Ravi Kumar, U. Kamachi Mudali, Baldev Raj, Process development for fabrication of zircaloy-4 dissolver assembly for reprocessing of spent nuclear fuel, Energy Procedia 7 (2011) 459-467.
3. V. Deshmukh, Uppal Singha, **Sunil Tonpe**, N. Saibaba, Effect of process variables on texture and creep of preessurized heavy water reactor pressure tube, Transactions. IIM, 63 (2010) 397-402.

Conferences

1. **Sunil Tonpe**, Uppal Singha, V. Deshmukh, N. Saibaba, Fabrication of square channels through advanced pilgering route, INSAC-2008, Delhi.
2. **Sunil Tonpe**, A. M. Parsodkar, C.M. Prabhu, N. Saibaba Fabrication of reactivity control assemblies for 540 MWe PHWR, ibid.
3. **Sunil Tonpe**, Uppal Singha, V. Deshmukh, N. Saibaba, Fabrication of seamless pressure tubes and calandria tubes for PHWR through pilgering route, ibid.
4. V. Deshmukh, Kumar Vaibhav, SK Jha, **Sunil Tonpe**, N. Saibaba, Development of heat treated Zr-2.5Nb pressure tubes, ibid.
5. S. Srinivaslu Reddy, **Sunil Tonpe**, N. Saibaba, Optimization of process parameters for control of hydrogen in garter springs for PHWRs, HEM, BARC, Mumbai, 2008.
6. **Sunil Tonpe**, Uppal Singha, V. Deshmukh, N. Saibaba, Optimization of process parameters for control of hydrogen in Zr-2.5Nb pressure tubes for PHWRs, ibid.
7. **Sunil Tonpe**, Uppal Singha, V. Deshmukh, N. Saibaba, Hexagonal channel by seamless pilger route for Prototype fast breeder reactor, INSAC-2009, Chennai.
8. M. Kamesh, **Sunil Tonpe**, N. Saibaba, R.N. Jayaraj Manufacture of components for PHWR& BWR fuel bundles, ibid.
9. Uppal Singha, V. Deshmukh, **Sunil Tonpe**, N. Saibaba, Process development for manufacturing of square channels through seamless pilgering route, ibid.

10. V. Deshmukh, **Sunil Tonpe**, Uppal Singha, N. Saibaba , Development of heat treated Zr-2.5Nb pressure tubes, ibid.
11. V. Deshmukh, Uppal Singha, **Sunil Tonpe,** N. Saibaba and R. N. Jayaraj, Manufacture of Zirconium Alloy Square Channels for BWRs through Pilger Route, ibid, R-35, P. 220.
12. V. Deshmukh, K. Vaibhaw, S.K. Jha, **Sunil Tonpe** and N. Saibaba, Development of Zr-2.5% Nb Pressure Tubes through Heat Treated Route, In: Proceeding International Conference on Peaceful Uses of Atomic Energy-2009, September 29 - October 1, 2009, Vigyan Bhavan, New Delhi, Editors: A.V.R. Reddy, V. Venugopal, R. K. Sinha, S. Banerjee, Vol. 1. R-26, P. 202.
13. S. Srinivasulu Reddy, **Sunil Tonpe,** N. Saibaba and R. N. Jayaraj, Process Improvement for Enhanced Productivity of PHWR Garter Springs, ibid, R-37, P. 222.
14. **Sunil Tonpe**, Kiran Kumar, N. Saibaba, R.N. Jayaraj, Advances in the manufacture of clad tubes and components for PHWR fuel bundle, ANUP 2010, Kalpakkam.
15. V. Deshmukh, **Sunil Tonpe**, Uppal Singha, N. Saibaba, Effect of process variables on texture and creep of PHWR pressure tubes, Kalpakkam CF-8, 2010.
16. N. Saibaba, S.K. Jha, B. Chandrasekhar, **Sunil Tonpe,** R.N. Jayaraj, Advances in the Manufacture of Clad Tubes and Components for PHWR Fuel Bundle, 11th International Conference on CANDU Fuel, Ontario Canada, (2012).
17. **Sunil Tonpe**, N Saibaba, Development and manufacture of various advanced materials for aerospace application, 18th National Seminar on Aerospace Structures, NASAS, Dec 2014, Nagpur

Report

1. N. Saibaba , S.K. Jha, **Sunil Tonpe**, V. Kumar, V. Deshmukh, Ramana Rao, D. Srivastava S. Neogy, KV. Mani, G.K. Dey, E, Ramadasan, R. V. Kulkarni, B.B. Rath, S. A. Anatharaman, Microstructural studied of heat treaded 2.5% Nb alloy for pressure tube application. BARC Report: BARC/2010/E/010.

Awards and Recognitions

1) DAE Group Achievement Award in year 2009 for development of manufacturing process for production of Hexscan for PFBR reactor.
2) DAE Group Achievement Award in year 2011 for development of manufacturing process for production of coolant tube.
3) IIM Best Poster Awards at NMD ATM of IIM, Hyderabad, 2011.
4) DAE Group Achievement Award in year 2014 for record production of nuclear fuel complex.

(Sunil Tonpe)

Dedicated

to

My parents

ACKNOWLEDGEMENTS

The research work presented in this thesis has been primarily carried out at Nuclear Fuel complex, Hyderabad and Indira Gandhi Center for Atomic Research, Kalpakkam. I am very grateful to all the members of these Units who have been directly or indirectly related to this work for their help and support throughout these years.

I wish to express my sincere respect and gratitude to Sr. Prof. U. Kamachi Mudali, Associate Director, CSTG & MPEDG, Indira Gandhi Centre for Atomic Research (IGCAR) for his wholehearted support, encouragement and guidance during the entire research work. I am highly obliged to him, because of whom I could accomplish my project work, and I express my deep gratitude for his valuable suggestions. I am highly indebted to him for the meticulous guidance, inspiration, and motivation, because of which I could gain knowledge and expertise in my field.

I sincerely thank my Doctoral Committee Chairman, Dr. T. Jayakumar, former Dean, HBNI-IGCAR Campus and Director, Metallurgy & Materials Group (MMG), and members Dr. M. Saibaba and Dr. A. K. Bhaduri for time to time evaluation of the research work and useful suggestions which improved the dissertation.

I would like to thank Dr. N Saibaba, Chairman and Chief Executive, NFC for his encouragement in undertaking this doctoral study. I would like to thank all the members of the monitoring committee for their valuable suggestions and support throughout the course of the work.

The scope of this research involved working not only at laboratory scale but also at industrial scale. This would not have been possible without the solid support and help provided by my colleagues from NFC and IGCAR. I am thankful to every individual, who has been of help to me in carrying out my thesis work from both the Institutes. I would like to place on record the special contributions from my colleagues from NFC; Dr. Komal Kapoor and Shri S.V. Ramana Rao for microstructure and textural characterization and Smt K.S. Lakshmi for mechanical testing.

Working has always been great fun, thanks to the vibrant team of Corrosion Science and Technology Group (CSTG), IGCAR, which made complicated problems look simple. I would like to take this opportunity to specially thank, Dr. J. Jayaraj, CSTG, IGCAR, for helping in carrying out the corrosion experiments and for the endless help rendered by him during this research work. I thank Dr. C. Mallika, Head, ACSCS and Dr. S. Ningshen, PL, CPC of CSTG for their invaluable help. Also thanks are due to scientific and technical staff of CSTG for their help and support during my stay at IGCAR.

Finally, big thanks to my family for always being there for me. My wife Shubhangi, is my strength and it is her encouraging words at times of distress that drives me. My Son, Dr. Sudhanshu, always has belief in me and encouraged me to aim high.

Sunil Tonpe

CONTENTS

CHAPTER I

INTRODUCTION & LITERATURE REVIEW

CHAPTER II

EXPERIMENTAL DETAIL

CHAPTER III

EVOLUTION OF MICROSTRUCTURE AND MECHANICAL PROPERTIES AT DIFFERENT STAGES OF THERMO-MECHANICAL TREATMENTS FOR ZIRCONIUM ALLOYS

CHAPTER IV

CORROSION BEHAVIOR OF ZIRCONIUM BASED ALLOYS IN NITRIC ACID

CHAPTER V

CONCLUSIONS

SYNOPSIS

MICROSTRUCTURE-CORROSION CORRELATION STUDIES ON THERMO-MECHANICALLY PROCESSED ZIRCONIUM BASED ALLOYS

Zirconium based alloys are the natural choice for both fuel clad, and in-core structural components of the water cooled thermal reactors. The general requirements for zirconium structural components are low thermal neutron absorption cross-section, adequate strength and ductility at ambient and reactor operating temperatures. Apart from this, zirconium alloys possess good corrosion resistance, low hydrogen absorption and long term dimensional stability in nuclear environments. The performance of zirconium alloys in the nuclear reactor depends upon reactor environment (water chemistry, neutron flux and fluence, power history, temperature, etc.) and microchemistry and microstructure of the zirconium alloys [1, 2]. For the fast breeder reactor (FBR) spent nuclear fuel reprocessing plants, zirconium-based alloys are considered as a candidate material for its high corrosion resistance [3-7]. Reprocessing of spent nuclear fuel from fast breeder reactors (FBRs) with high plutonium content is carried by using Plutonium Uranium Recovery by Extraction (PUREX) based aqueous process [5, 6]. In the PUREX process, dissolution of spent nuclear fuel is carried out in boiling 11.5 M nitric acid. Nitric acid grade, and non-sensitized AISI 304 L stainless steels cannot be used for concentrated 11.5 M nitric acid under boiling conditions seen in dissolver vessels, as they undergo severe intergranular corrosion in such corrosive medium [7, 8] and titanium undergoes vapor and condensate corrosion [3, 5]. On the other hand, zirconium does not undergo sensitization or show complicated microstructures during welding and thus insensitive to intergranular corrosion in nitric acid [7, 9, 10]. Also it does not show any tendency for vapor and condensate corrosion similar to titanium.

The most common alloying elements to zirconium are tin and niobium apart from minor additions of nickel, iron, chromium, molybdenum, copper and oxygen to enhance the properties and performance. The Zr-2, Zr-4, Zr-1%Nb, Zr-2.5%Nb and Zr-2.5%Nb-O.5%Cu are the well-known alloys developed for structural and fuel cladding applications in the nuclear reactor[10-14]. Mock up dissolver vessel made of Zr-4 has been fabricated for reprocessing fuel form FBR [5, 6]. Thermo-mechanical processing plays an important role in the manufacturing of various zirconium alloys for meeting the stringent properties required for nuclear components. Zirconium and its alloys are amenable to various hot and cold working operations like extrusion, pilgering and rolling, etc., for the production of these components. The processing ability of these alloys is governed by the microstructure formed at different stages of its working. The chemical composition and microstructure of a zirconium alloy are critical factors that ensure its required mechanical properties and proper functioning in a corrosive environment. When choosing a material, its microstructure is of crucial importance, which in turn is a function of the material chemistry and the thermo-mechanical manufacturing processes. Thus, proper selection of alloying elements and the manufacturing process conditions are crucial to yield the appropriate microstructure resulting in the required mechanical and corrosion properties.

This thesis emphasis the importance of several thermo-mechanical treatments required for processing the zirconium alloys such as Zr-2, Zr-4, Zr-1%Nb and Zr-2.5%Nb. The evolution of microstructure at different stages of production of zirconium products was characterized using scanning electron microscopy (SEM). The optimized microstructure has been correlated with the obtained mechanical properties of the studied zirconium alloys. Microstructural properties depend strongly on the composition of the zirconium alloy and thermo-mechanical processing conditions. Corrosion behaviors of such processed zirconium, Zr-2, Zr-4, Zr-1%Nb and Zr-2.5%Nb alloys were evaluated in boiling 11.5 M nitric acid to evaluate their corrosion resistance and correlate with the microstructure obtained after various processing steps.

The thesis has been organized into different chapters as given below.

CHAPTER I:	Introduction & Literature Review
CHAPTER II:	Experimental Details
CHAPTER III:	Evolution of microstructure and mechanical properties at different stages of thermo-mechanical treatments for zirconium alloys
CHAPTER IV:	Corrosion behaviour of zirconium based alloys in nitric acid
CHAPTER V:	Conclusions

A brief overview of the individual chapters is presented below:

CHAPTER I:

INTRODUCTION & LITERATURE REVIEW

This chapter briefly describes different zirconium based alloys for nuclear reactor structural components, fuel cladding material and dissolver vessels for reprocessing of spent nuclear fuel. Thermo-mechanical processing plays an important role in processing various zirconium alloys for meeting the stringent properties required for nuclear components. This chapter also includes the phase diagram, phase transformation and microstructure of the zirconium based alloys. In addition, this chapter provides an introduction on aqueous corrosion of zirconium based alloys in nuclear reactor and reprocessing environments.

CHAPTER II:

EXPERIMENTAL DETAILS

This chapter describes the manufacturing processes and flow sheet for the production of various zirconium based alloys like Zr-2, Zr-4, Zr-1%Nb and Zr-2.5%Nb. This involves different thermo-mechanical treatments such as melting, extrusion, pillgering and heat treatment like β-quenching and annealing. Characterization techniques like an optical microscope (OM) and scanning electron microscope (SEM) have been used in the present study to optimize the desired microstructure. Tensile testing and Vickers hardness measurements were used for the evaluation of mechanical properties like yield strength (YS), ultimate tensile strength (UTS) and micro-hardness at room temperature. Three-electrode corrosion cell setup used to carry out the potentiodynamic polarization experiments to study the passivation behavior of zirconium based alloys in 11.5 M nitric acid at room temperature has been described. To evaluate the corrosion rates of the zirconium alloys, ASTM A262 practice-C and Zr-loop tests were carried out, and their experimental setup are described.

CHAPTER III:

EVOLUTION OF MICROSTRUCTURE AND MECHANICAL PROPERTIES AT DIFFERENT STAGES OF THERMO-MECHANICAL TREATMENTS FOR ZIRCONIUM ALLOYS

This chapter discusses in detail the effect of various thermo-mechanical treatments on the evolution of microstructure during fabrication of different zirconium based alloys such as Zircaloy-2, Zircaloy-4, Zr-1%Nb and Zr-2.5%Nb. This chapter presents a detailed description of the evolution of microstructure during thermo-mechanical processing of the above mentioned zirconium based alloys. This chapter describes a detailed description of microstructure of the weld region of TIG and EB welded Zr-4. Characterization techniques like OM and SEM have been used to understand the microstructural evolution to optimize the desired microstructure. Mechanical properties like YS, UTS and microhardness of various zirconium based alloys in as-cast and final product condition were discussed. The results are correlated with the initial and final microstructure of the individual alloys.

CHAPTER IV:

CORROSION BEHAVIOR OF ZIRCONIUM BASED ALLOYS IN NITRIC ACID

In this chapter, corrosion investigations were carried out for various zirconium and its alloys like Zircaloy-2, Zircaloy-4, Zr-1%Nb and Zr-2.5%Nb in nitric acid environments. The potentiodynamic polarization of these zirconium based alloys was carried out 11.5 M HNO_3 at room temperature to understand their passivation behavior. Similarly, corrosion experiments have been carried out in boiling 11.5 M HNO_3 to simulate dissolver condition in the nuclear reprocessing plant. This chapter describes the corrosion behavior of the zirconium based alloys that were subjected to boiling 11.5 M HNO_3 as per ASTM A262 Practice C for 240 h (5 periods of 48 h) and boiling 11.5 M HNO_3 in the Zirconium test loop facility. SEM investigation of the samples surface subjected to ASTM 262A practice C and zirconium test loop facility has been studied.

CHAPTER V:

CONCLUSIONS

In summary, this studies emphasis the importance of several thermo-mechanical treatments required for processing the zirconium alloys. The evolution of microstructure at different stages of production of zircaloy products was characterized using OM and SEM.

Microstructural evolution of the Zr-2 and Zr-4 samples follows the sequence as cast ingot with dendritic structure→β-quenched Widmanstätten structure→hot extruded bimodal grain size→pilgered heterogeneous deformed structure→partially recrystallized structure (final annealed). Similarly, Zr-2.5% Nb and Zr-1% Nb for samples follows the sequence as-cast ingot with dendritic structure→β-quenched martensitic parallel plate morphology→hot extruded martensitic microstructure→pilgered heterogeneous deformed structure→ α-Zr grains and fine β-Nb phase at α grain boundary (stress relived).

The mechanical properties of the for unalloyed zirconium and Zr-2, Zr-4, Zr-1%Nb and Zr-2.5%Nb and Zr-1%Nb alloy tubes & Zr-2.5%Nb alloys have been studied at various process steps like as cast, extruded and β quenched and final tube product. The as-cast unalloyed zirconium, Zr-2, Zr-4, Zr-1%Nb and Zr-2.5%Nb. Zr-2.5% Nb and Zr-1% Nb ingot exhibited YS of about 210, 250, 300, 335 and 230 MPa and % elongation of 24, 22, 19, 18.5 and 21.5% respectively. These low mechanical properties of as cast ingots were attributed to the course dendritic cast structure. For the hot extruded Zr-2, Zr-4, Zr-1%Nb and Zr-2.5%Nb, Zr-2.5% Nb and Zr-1%Nb the YS was about 340, 336, 418 and 351 MPa and % elongation was 14, 25, 18 and 19 %. The slight increase in mechanical properties could be attributed to the bimodal microstructure obtained after hot extrusion. For final pass pilgered and heat-treated condition, for Zr-2, Zr-4, Zr-1%Nb and Zr-2.5%Nb, Zr-2.5% Nb and Zr-1% Nb alloy mechanical properties increased significantly, and YS values are 325, 483, 504 and 310 MPa and % elongation was 25, 30 17 and 32 %. Mechanical and microstructural properties depend strongly on the composition of the zirconium alloy and thermo-mechanical processing conditions. The optimized microstructure has been correlated with the obtained mechanical properties of the studied zirconium alloys. In general, all the final products have better mechanical properties because of stress relieved cold worked microstructure.

Corrosion studies indicated that the corrosion rates of zirconium based alloys exposed to boiling 11.5 M HNO_3 as per ASTM A262 Practice C for 240 h (5 periods of 48 h) and boiling 11.5 M HNO_3 in the Zirconium test loop facility are below 0.1 mpy. The corrosion rate for most of the zirconium alloys in as-cast and final product is negligible. The corrosion rates clearly indicated that these zirconium alloys exhibited high corrosion resistance in boiling nitric acid medium. However, slightly higher corrosion rate was observed for Zr-2.5%Nb alloy samples, and it is due to the two-phase morphology of the alloy. SEM investigations showed insignificant corrosion attack due to the formation of a smooth and compact passive film present over the surface. LRS analysis confirmed that the high corrosion resistance behavior of the alloy is due to the formation of ZrO_2 passive film.

REFERENCES:

1. S. Banerjee, Role of basic research in the development of Zirconium Alloys for nuclear applications, Proceeding of ZIRC 2003 Symposium, Mumbai, p.40
2. C. Bernard, J.P. Mourox, J. Decours, R. Demay, J. Simonnet, “Zirconium Made Equipment for the New La Hague Reprocessing Plants,” Proc. Int. Conf. on Fuel Reprocessing and Waste Management -RECOD 91, (Sendai, Japan, 1991): p.570.
3. Baldev Raj, U. Kamachi Mudali, Materials development and corrosion problems in nuclear fuel reprocessing plants Prog. Nucl. Energy 48 (2006) 283
4. U. Kamachi Mudali, A. Ravi Shankar, R. Natarajan, N. Saibaba, Baldev Raj, Application of zirconium alloys for reprocessing plant components, Nucl. Technol. 182 (2013) 349
5. Sunil Tonpe, N. Saibaba, R. N. Jayaraj, A. Ravi Shankar, U. Kamachi Mudali, Baldev Raj, Process Development for Fabrication of Zircaloy–4 Dissolver Assembly for Reprocessing of Spent Nuclear Fuel, Energy Procedia 7 (2011) 459
6. U. Kamachi Mudali, R.K. Dayal, J.B. Gnanamoorthy, Corrosion studies on materials of construction for spent nuclear fuel reprocessing plant equipment, J. Nucl. Mater. 203 (1993)73.
7. Sunil Tonpe, U. Kamachi Mudali, Effect of thermomechanical process on mechanical and corrosion properties of zircaloy-4 tubes of mock-up dissolver vessel, Journal Materials and Manufacturing Processes, 2015, (in Press), DOI: 10.1080/10426914.2015.1090589
8. S. Ningshen, U. Kamachi Mudali, G. Amarendra, Baldev Raj, Corrosion assessment of nitric acid grade austenitic stainless steels, Corros. Sci. 51 (2009) 322

9. P. Fauvet, F. Balbaud, R. Robin, Q.T. Taran, A. Mugnier, D. Espinoux, Corrosion mechanisms of austenitic stainless steels in nitric media used in reprocessing plants, J. Nucl. Mater. 375 (2008) 52
10. K. Kiuchi, H. Hayakawa, Y. Takagi, M. Kikuchi, Proc. of the Fourth International Conf. on Nuclear Fuel Reprocessing and Waste Management (RECOD-94), London, UK, vol. 3 (1994)
11. C. Ganguly, Advances in Zirconium Technology for Nuclear Reactor Application, Proceeding of ZIRC 2003 Symposium, Mumbai, p.1
12. S.Neogy, D. Srivastava, G. K. Dey, J. K. Chakravartty and S.Banerjee, Annealing studies on Zr-1Nb and Zr-1Nb-1Sn-0.1Fe alloys, Trans. Indian Inst Met. 57 (2004) 509.
13. Sunil Tonpe, N. Saibaba, R.N. Jayaraj, A. Ravi Kumar, U. Kamachi Mudali, Baldev Raj, Process development for fabrication of zircaloy-4 dissolver assembly for reprocessing of spent nuclear fuel, Energy Procedia 7 (2011) 459-467.
14. V. Deshmukh, Uppal Singha, Sunil Tonpe, N. Saibaba, Effect of process variables on texture and creep of preessurized heavy water reactor pressure tube, Tran. IIM, 63 (2010) 397-402.

LIST OF FIGURES

LIST OF TABLES

LIST OF ABBREVIATIONS

BWR	Boiling water reactors
PHWR	Pressurized Heavy Water Reactor
FBR	Fast Breeder Reactor
FBTR	Fast Breeder Test Reactor
PFBR	Prototype Fast Breeder Reactor
EBR-II	Experimental Breeder Reactor-II
PUREX	Plutonium URanium EXtraction
MA	Minor Actinides
FP	Fission products
AISI	American Institute of Steel Industry
SS	Stainless Steel
ASTM	American Society for Testing Materials
XRD	X-ray Diffraction
SEM	Scanning Electron Microscopy
EBSD	Electron back scattered diffraction
EDX/EDS	Energy-Dispersive X-ray spectroscopy
LRS	Laser Raman Spectroscopy
IGCAR	Indira Gandhi Centre for Atomic Research
NFC	Nuclear Fuel Complex
BARC	Bhabha Atomic Reaserch Center
PUREX	Plutonium Uranium Reduction Extraction
HAZ	Heat Affected Zone
UHP	Ultra High Purity
HAZ	Heat affected zone
HTHP	High temperature and high pressure
IGSCC	Intergranular stress corrosion cracking
LTS	Low temperature sensitization
NWC	Normal water chemistry

SCC	Stress corrosion cracking
UTS	Ultimate tensile strength
YS	Yield strength
TCE	Total circumferential elongation
VAR	Vacuum Arc Remelting furnace
HEP	Horizontal Extrusion Press
EBW	Electron Beam Welding
TIG	Tungsten Inert Gas welding
SE	Secondary Electron
BSE	Back Scattered Electron
LRS	Laser Raman Spectroscopy
OCP	Open Circuit Potential
RX	Recrystalised
CR	Cold Rolled
CCD	Charged Coupled Device
LVDT	Linear Variable Differential Transformer

CHAPTER I

INTRODUCTION & LITERATURE REVIEW

This chapter briefly describes the different Zirconium based alloys for the structural components of nuclear reactors, fuel cladding material and dissolver vessels for the aqueous reprocessing of spent nuclear fuels. An introduction on the aqueous corrosion of Zirconium based alloys in nuclear reactors and reprocessing environments is also provided in this chapter. Further, the corrosion behavior of Zirconium based alloys in nitric acid environment prevailing in reprocessing plants was also reviewed. It also focuses on the aim and objective of the present thesis.

1.1 Introduction

Zirconium based alloys are the natural choice for both fuel clad, and in-core structural components of the water cooled thermal reactors. The general requirements for Zirconium based structural components are low thermal neutron absorption cross-section, adequate strength and ductility at ambient and reactor operating temperatures. Apart from this, Zirconium alloys possess excellent corrosion resistance, low hydrogen absorption and long term dimensional stability in nuclear environments. The performance of Zirconium alloys in nuclear reactors depends upon the reactor environment (water chemistry, neutron flux and fluence, power history, temperature,etc.), and microchemistry and microstructure of the Zirconium alloys [1-11].

For the spent fuel reprocessing plants of fast breeder reactors (FBRs), Zirconium-based alloys are considered as a candidate material for the dissolver due to its high corrosion resistance [2-5, 12, 13]. Reprocessing of spent nuclear fuel from fast breeder reactors (FBRs) with high plutonium content is carried out by Plutonium-URanium Extraction (PUREX) based aqueous process [2, 13, 14]. In the PUREX process, the spent fuel is dissolved in boiling 11.5 M nitric acid. Dissolvers made up of nitric acid grade and non-sensitized 304L stainless steels cannot be used for high concentrated 11.5 M nitric acid under boiling conditions, as they undergo severe intergranular corrosion in such corrosive medium [6-8] and titanium undergoes vapor and condensate phase corrosion in nitric acid [9]. On the other hand, Zirconium neither undergoes sensitization nor shows complicated microstructures during welding and thus, insensitive to intergranular corrosion in nitric acid [10, 11].

Thermo-mechanical processing plays a significant role in manufacturing various Zirconium alloys for meeting the stringent properties required for the fabrication of components for applications in nuclear reactors and reprocessing plants. Zirconium and its alloys are subjected to various hot and cold working operations like extrusion, pilgering, rolling etc., for the production of these components. The processing ability of these alloys is governed by the microstructure formed at different stages of its working. The chemical composition and microstructure of a Zirconium alloy are critical factors that ensure its required mechanical properties and its performance in corrosive environment. While choosing a material its microstructure is of paramount importance, which in turn is a function of the material chemistry and the thermo-mechanical manufacturing processes. Thus, proper selection of alloying elements and the manufacturing process conditions are crucial to yield the appropriate microstructure resulting in the required mechanical and corrosion properties.

1.2 Overview on aqueous reprocessing

Most of the countries in the world follow the once-through fuel cycle (open fuel cycle), which does not include reprocessing of the spent nuclear fuel. Closing of the fuel cycle is an important part of the strategy to ensure the growth of nuclear energy production [9]. Reprocessing of spent nuclear fuel [12-14] refers to the separation process with the fractionation of useful radionuclides for the fabrication of fresh fuel, and safe waste management. Two types of processes available for the reprocessing of spent nuclear fuels are aqueous reprocessing and pyrochemical reprocessing. The PUREX process is well developed and has been used to treat spent nuclear fuels and irradiated uranium for over 40 years [15, 16]. PUREX process is well suited for the reprocessing of oxide/carbide fuels discharged from thermal and fast breeder reactors (Figure 1.1). The fission products, other actinides and corrosion products are separated and immobilized with various stabilization matrices like borosilicate glass or pyrochlore based ceramic system and finally disposed.

The spent fuel is chopped and dissolved in boiling concentrated nitric acid. In the first stage the concentration of nitric acid and the oxidation state of plutonium in the dissolver solution are conditioned to facilitate the separation of uranium and plutonium from the aqueous nitric acid stream containing the fission products and minor actinides, by a countercurrent solvent extraction process using tributyl phosphate dissolved in kerosene or dodecane. In the extractor (pulsed column, mixer-settler or centrifugal extractor), uranium and plutonium are extracted into the organic phase while the fission products and corrosion products remain in the aqueous nitric acid phase (known as raffinate) [17]. In a second stage, plutonium is separated from uranium by adding excess U^{4+} to the loaded organic phase in order to reduce plutonium to Pu^{3+}. Plutonium in its third valence state is then extracted to the aqueous phase while the mixture of U^{4+} and U^{6+} remain in the organic phase. It is then stripped from the organic solvent using dilute nitric acid.

Plutonium nitrate solution is concentrated by evaporationand subjected to an oxalate precipitation process followed by calcination to produce Plutonium Oxide (PuO_2) in powder form. The uranium nitrate solution is concentrated by evaporation, precipitated as ammonium diuranate and calcined to produce UO_3 in powder form. It is then converted to UO_2 product by a reduction in hydrogen.

The aqueous stream, left over after the recovery of Pu and U, is high-level liquid waste (HLLW) or the raffinate, and it comprises about 3% of the used fuel in the form of fission products and minor actinides (Np, Am, Cm) in about 3-4 M nitric acid. It is highly radioactive and continues to generate heat. It is conditioned by calcining, and the dry material is incorporated into borosilicate glass and stored for final disposal. In principle, any compact, stable and insoluble solid matrix is adequate for disposal.

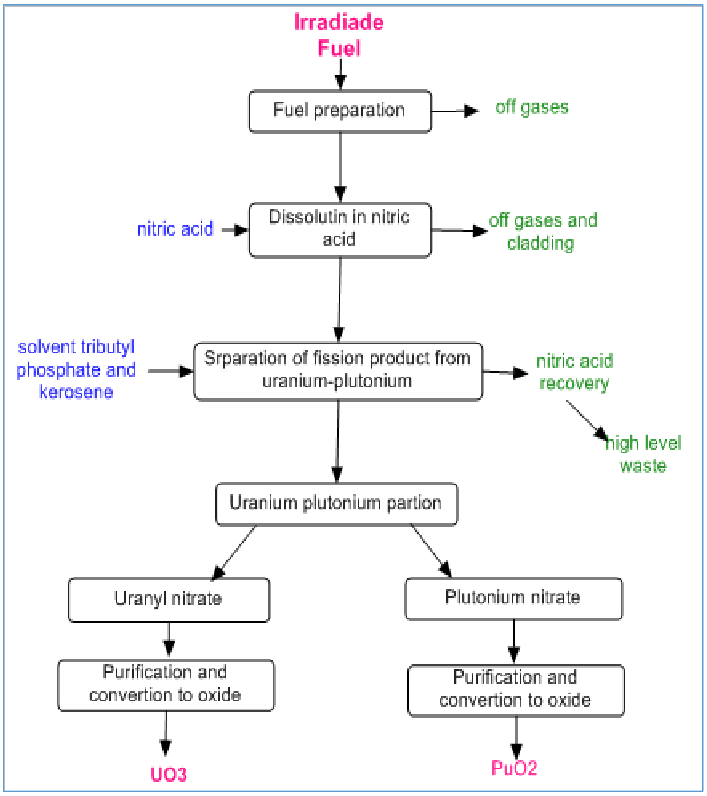

Figure 1.1: Overview of PUREX process flow-sheet for reprocessing of spent nuclear fuel.

In the PUREX process nitric acid concentrations from 0.01 M up to the azeotropic one (14.4 mol/L) and temperatures from ambient up to their boiling temperature (120°C) are employed all along the processes. Dissolved species in nitric acid consist of oxidizing ions such as Pu(VI), Np(VI), U(VI), alkali, alkaline earth, lanthanide and actinide fission products, non-metallic iodine, selenium and tellurium as well as cations like Fe(III), Cr(III) etc. from the corrosion of equipment and insoluble solid species such as platinoïds (Pd, Rh and Ru). In order to properly handle these highly acidic and oxidizing media and to ensure the safety and economical operation of nuclear reprocessing plants, high corrosion resistant metallic materials have been chosen [14, 17].

1.2.1 Materials challenges for reprocessing plant

The integrity and availability of fuel reprocessing plants for uninterrupted operation depend on the quality and performance of critical engineering components, vessels, and piping. Any failure of the components of unit processes would lead to the release of radioactivity and slowing down the recovery of useful fissile material required for sustained operation of power plants. Out of several critical issues, material challenges are of utmost important for safe operation of the fuel reprocessing plant as well as for determining the overall service life of the plant [18,19]. This demand dictates many challenges with respect to the reprocessing of plutonium-rich spent fuels of FBRs inparticular, as various fission products and transuranium elements are produced in large yields due to the significantly high burn ups in FBRs. The selection criterion of materials of construction for nuclear fuel reprocessing plants is a complicated procedure involving various parameters such as availability, cost effectiveness, mechanical properties, corrosion resistance, etc.. The radiation dose, corrosive chemicals and high temperature make it difficult to have access in the operating areas of the plant for maintenance. These aggressive conditions prevailing in the reprocessing plant demand structural materials and accessories of the unit operations with good mechanical integrity and thermal stability combined with corrosion resistance to provide high performance and long service life [19-24].

In general, metals and alloys can be employed for high-temperature operation; however, during service in addition to high-temperature corrosion and scaling, creep properties begin to dominate. Recrystallisation, grain growth, oxidation and scaling, and high-temperature corrosion affect the properties and stability of materials as the temperature of application increases further. Thus, limited materials only have been identified for applications at high temperatures in a corrosive environment and under intense radiation field, to avoid the need for repair and replacement. The dependence of equipment performance on variables like material properties, environment, assembly design, chemical composition and manufacturing process is shown in Figure 1.2.

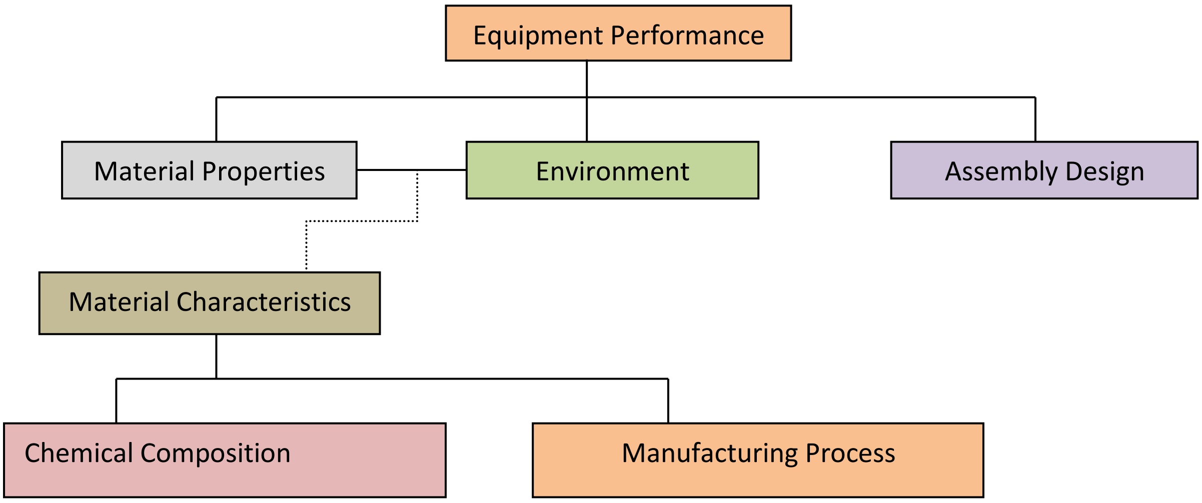

Figure 1.2: Factors affecting the performance of equipment with various variables like material properties, environment, assembly design and material characteristics material composition and manufacturing process.

Based on the corrosion data, the acceptance criteria for the selection of structural materials used for reprocessing plants are as follows:

- The materials should not have undergone any kind of localized corrosion (intergranular, pitting, tunnel corrosion,etc.) that would affect the definite equipment service life and would complicate any monitoring during operation.
- The generalized corrosion rate of the materials remains acceptable in the nominal operating configuration; the corrosion values must remain reasonable to ensure the construction and the functioning of the equipment.

1.2.2 Corrosion in nuclear spent fuel reprocessing plants

Reprocessing of spent fuel discharged from fast breeder reactors involves the use of nitric acid at high concentrations and temperatures for the dissolution of the fuel in the dissolver vessel and for concentrating the high-level liquid waste by evaporation to reduce the waste volume. Both processes create the highly corrosive environment. Hence, the materials to be chosen for the fabrication of equipment such as dissolver and evaporator should possess excellent corrosion resistance, ease of fabrication and reliability. Conventional austenitic stainless steels are not preferable in such highly oxidizing conditions as these materials undergo severe intergranular corrosion. Extensive studies have been carried out worldwide for selecting suitable materials for the fabrication of equipment for highly oxidizing nitric acid applications in spent fuel reprocessing plants. Studies conducted earlier on AISI type 304L stainless steel (SS), nitric acid grade SS, commercially pure Ti (CP-Ti) and Ti-Ta based alloys indicated good corrosion resistance of CP-Ti and Ti-5%Ta and Ti-Ta-Nb compared to AISI type 304LSS in concentrated nitric acid [14, 15]. The corrosion resistance of unalloyed titanium improves dramatically as the impurity levels in hot nitric acid solutions increase. Titanium exhibits excellent resistance to recirculating nitric acid process streams. However, in hot and pure nitric acid solutions and vapour condensates of nitric acid, significant corrosion was observed for titanium [15, 17]. Zirconium is highly resistant to the nitric acid environment and is considered as a candidate material for various applications in spent fuel reprocessing plants involving concentrated nitric acid medium. In France, 80 ton of Zirconium and 5500 m of piping were employed in La Hague reprocessing plant for the manufacturing of various components like dissolvers, oxalic mother liquor evaporator and heat exchangers, vitrification dust scrubber, and liquid waste treatment reactors [18, 24, 25]. Zirconium is much more corrosion resistant to nitric acid than titanium, but the only concern in using Zirconium is its susceptibility to corrosion fatigue and stress corrosion cracking (SCC) in high concentrations of nitric acid. Particularly, the heat affected zone of Zirconium weldments is considered to be more sensitive to SCC. However, based on the tests carried out in nitric acid up to 65 wt%, it was concluded that the risk of stress corrosion cracking was extremely low in industrial application [26].

1.2.3 Development of materials for reprocessing plant

All along the process line nitric acid containing dissolved species such as oxidizing ions as well as undissolved solid particles are being found at various concentrations and at temperatures up to and marginally higher than their boiling point as nitric acid is being used to dissolve the spent fuel in the PUREX process. Thus, it is essential to choose the metallic materials according to their corrosion limits in the nitric acid environment and qualify them before building the plants.

The materials considered are mainly;

- Zirconium, titanium and their alloys for the construction of the most critical equipment in term of high corrosion resistance such as fuel dissolvers and nitric acid recovery concentrators.
- Austenitic stainless steels with very low carbon (type AISI 304L and nitric acid grade 316L) for the major part of the extraction equipment and piping
- A special stainless steel with 4% silicon for evaporators for concentrating HLLW.

All these materials are protected by a stable passive oxide layer in nitric acid. However, conditions that promote the deterioration of the passive oxide layer will result in severe corrosion phenomena.

In the future reprocessing plants for FBR spent fuels, Zirconium-based alloys are proposed as a candidate material for dissolver in the highly corrosive environment [21].

1.3 Zirconium and Zirconium alloys

Zirconium and its alloys are extensively used as structural materials in nuclear reactors, because of their unique combination of good corrosion resistance in steam at 300°C, good mechanical properties and low capture cross section for thermal neutrons. The alloys of Zirconium are mainly used in the form of tubes of different sizes for applications such as fuel sheathing, guide tubes/calandria tubes and pressure tubes [26, 27]. In designing Zirconium alloys for nuclear applications care should be taken that thermal neutron absorption cross-section of pure Zirconium does not increase significantly. Therefore, only relatively small amounts of alloying elements are added. Alloying elements are added to Zirconium, primarily to improve its corrosion resistance in water [1, 2, 6]. Tin is added to counteract the detrimental action of nitrogen on corrosion resistance. Small amounts of iron, chromium and nickel are found to improve the corrosion resistance of Zirconium-tin alloys due to the formation of intermetallic second phase particles (SPPs) [1,26]. The size and distribution of the SPPs strongly influence the corrosion resistance. Table 1.1 gives the composition of some of the Zirconium alloys developed for cladding and structural components in nuclear reactors [26, 27]. The addition of alloying elements produces alpha–beta structures over a broad range of temperature and greatly improves mechanical properties and the corrosion resistance of pure Zirconium at high temperatures.

Table 1.1: Composition of major Zirconium alloys produced at Nuclear Fuel Complex and equivalent ASTM reference.

ASTM Ref.	R60802	R60804	R60901	R60901
Common name	Zr-2	Zr-4	Zr-2.5%Nb	Zr-1%Nb
Alloying Elements (mass %)				
Sn	1.2 – 1.7	1.2 – 1.7	-	-
Fe	0.07 – 0.2	0.18 – 0.24	-	-
Cr	0.05 – 0.15	0.07 – 0.13	-	-
Ni	0.03 – 0.08	-	-	-
Nb	-	-	2.4 – 2.8	0.9- 1.1
O	1000 – 1400ppm		0.09 – 0.13	0.09 – 0.13
Impurities(max ppm)				
Sn	-	-	50	100
Fe	-	-	1500	650
Cr	-	-	200	100
Ni	-	-	70	35

1.3.1 Physical metallurgy of Zirconium alloys

Zirconium based alloys are stable in the alpha phase (α) with a hexagonal close-packed (hcp) structure at temperatures below 800°C (Figure 1.3 (a)) [27-29]. The typical lattice parameters are a=0.323 nm and c=0.515 nm, resulting in a c/a ratio of 1.593 (i.e. marginally lower than the ideal ratio of 1.633). The three parallel planes contain Zr atoms at each of the corners and the center of the hexagon. These planes are called basal planes, and the direction normal to them is the c direction (or<c>), also called as the basal pole. The basal planes are close-packed planes. The other important family of planes in this structure is located on the six sides of the hexagonal prism and is called as prism planes (Figure 1.3 (b)). For an ideal c/a ratio, the atom density on these planes is less than that of close-packed planes. The directions perpendicular to these planes are collectively calledas a direction (or <a>).

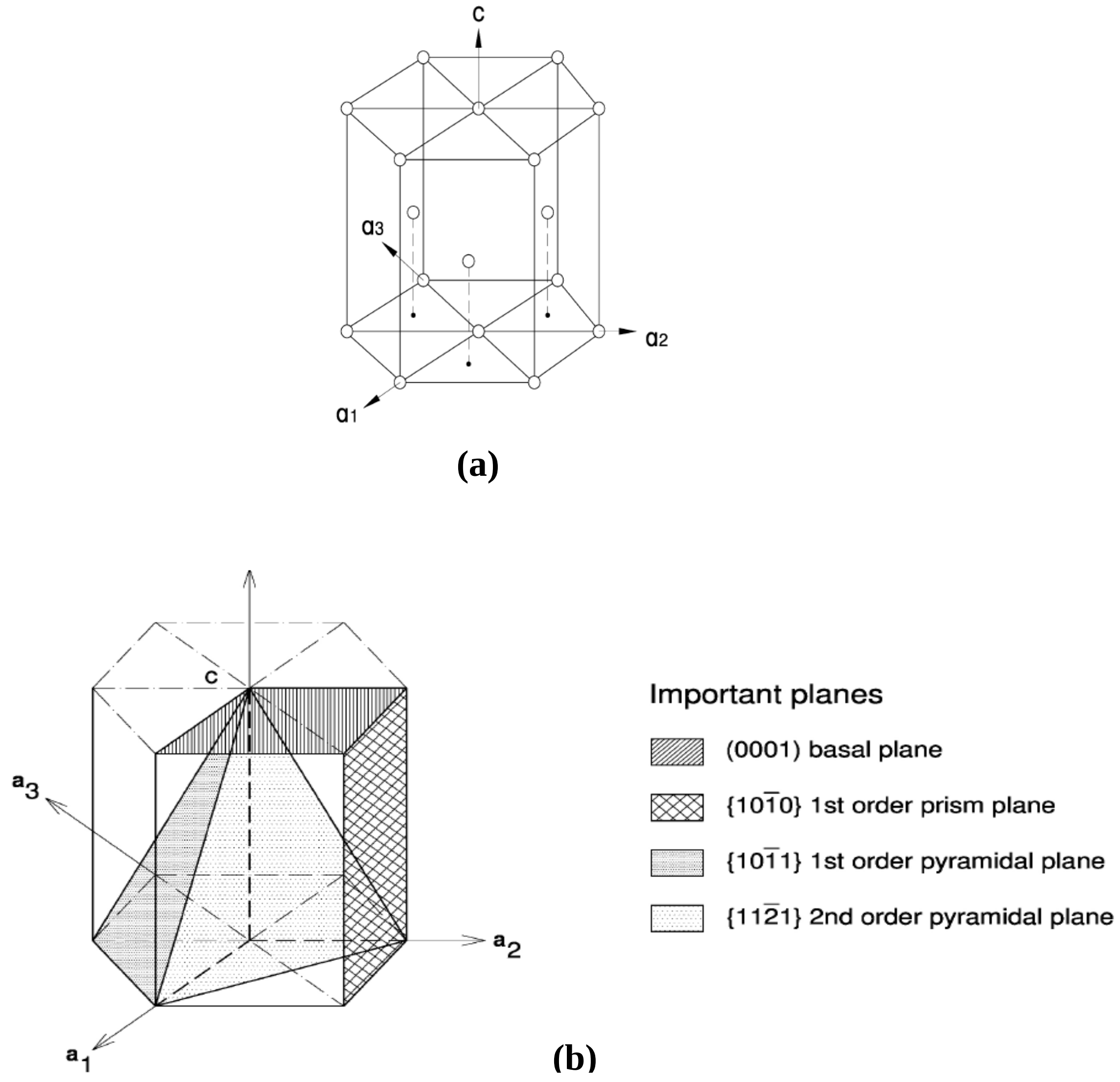

Figure 1.3: (a) Unit cell of hexagonal closed packed (hcp) crystal and (b) Some of the important planes and directions of the hcp crystals [27 - 29]

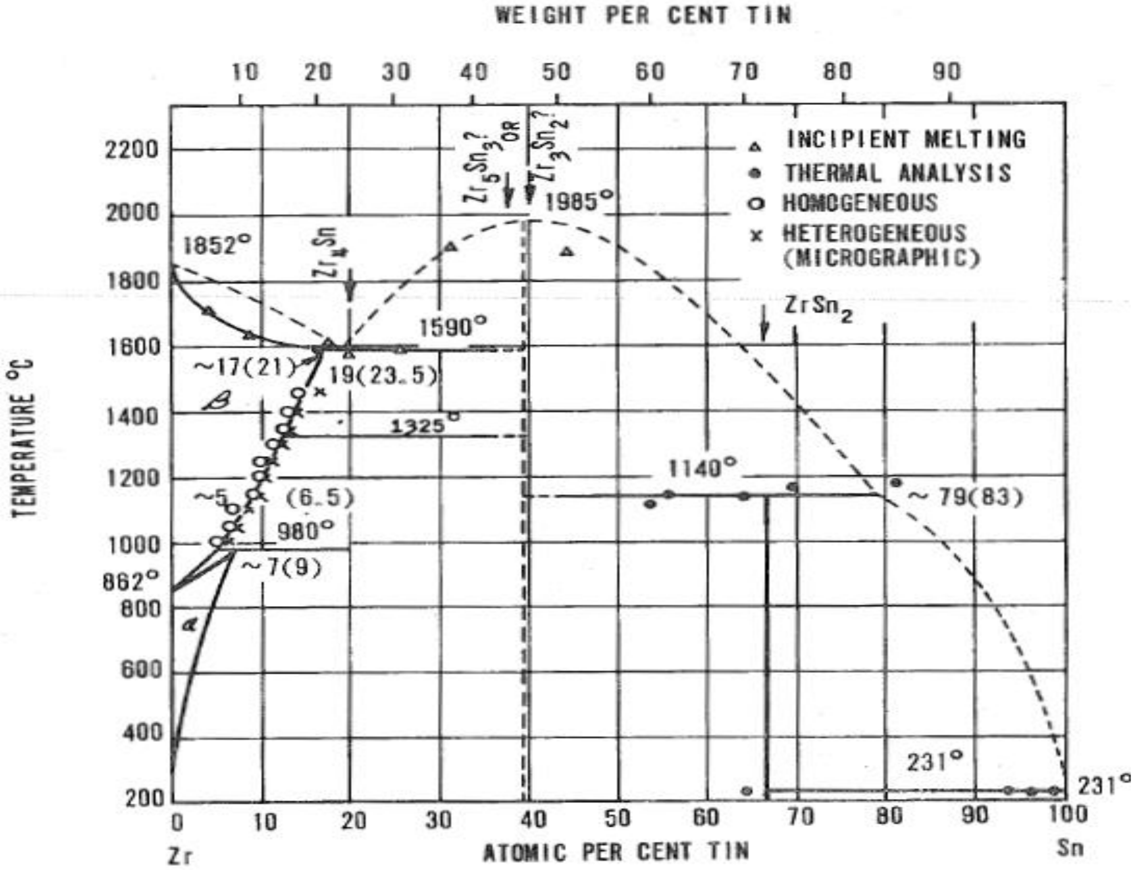

Figure 1.4: The phase diagram of binary Zr-Sn system [29].

Alloying elements in Zirconium alloys can be classified into α-stabilizers and β-stabilizers. Aluminum, tin, hafnium, nitrogen, and oxygen are the important stabilising elements. Phase diagrams for many of the Zirconium -α-stabiliser binary alloy systems show a peritectic or a peritectoid reaction at the Zirconium-rich end [6, 26, 27],whereas β-stabilisers(including iron and chromium) with Zirconium exhibit a peritectoid reaction at the Zirconium-rich end [6, 26,27]. In the binary alloys between Zirconium and its stabilizing elements, there usually exists a eutectoid reaction, and often a eutectic reaction at the Zirconium-rich end of the phase diagram. Some β-stabilizing elements such as iron, nickel, chromium, and molybdenum have a very little solubility in the α phase, and they form ordered intermetallic phases that are readily precipitated even in very dilute Zirconium alloys, resulting in precipitation hardening [27, 28]. The major metallurgical characteristics of Zirconium originate from its high reactivity with oxygen, from different types of chemical interactions with the alloying elements (complete solubility and intermetallic compound formation) and its strongly anisotropic hexagonal crystal structure, the latter leading to the development of textured material after thermomechanical processing. At 865°C, Zirconium undergoes an allotropic transformation from the low-temperature HCP α phase to BCC β phase. On cooling, the transformation is either martensitic or bainitic, depending on the cooling rate.

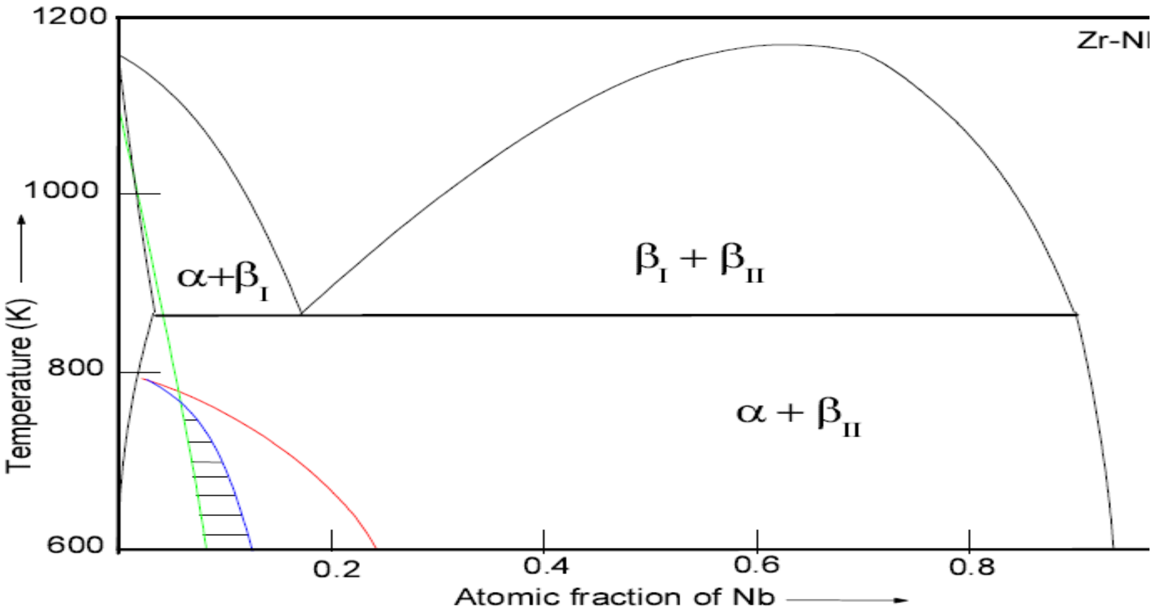

Figure 1.5: The phase diagram of binary Zr-2.5%Nb system showing meta-stable phase transformation

Figure 1.4 shows the Zr-Sn equilibrium diagram that provides the basis for studying the equilibrium transformations [29]. Zirconium alloys consist of an alpha-Zr matrix with alloying elements in solution and second phase particles made up of the alloying elements whose concentrations exceed the solubility limits in the alpha-Zr matrix [29]. The main alloying elements Sn, Nb, and oxygen have a significant solid solubility in α Zr. Tin is an α stabilizer, and when added in the concentrations of 1.2-1.8 %, it forms the α phase in solid solution. Tin was originally used to improve the corrosion resistance especially by mitigating the deleterious effect of nitrogen. Tin also has a significant impact on mechanical properties and increases the tensile yield strength.

Iron, chromium, and nickel are considered as “β-eutectoids” because, in their phase diagrams, these elements undergo eutectoid decomposition of the β-phase at their usual concentrations, and these elements are completely soluble in β-phase. This temperature of dissolution in the range 835-845°C is in the upper α+β range. In the α phase, their solubility is very low (about 120 ppm for Fe and 200 ppm for Cr at the maximum solubility). In the binary Zr-Cr and Zr-Ni systems, the stable binary phases are $ZrCr_2$ and Zr_2Ni respectively. Iron substitutes the corresponding transitional metal and the intermetallic compounds found in the Zirconium alloys are $Zr_2(Ni,Fe)$ and $Zr(Cr,Fe)_2$. The $Zr(Cr,Fe)_2$ precipitate is either hcp or fcc – laves phase depending on the composition and heat treatment and it usually shows the characteristic stacking fault [28]. In Zr-2 alloys, the partitioning of Fe between the two types of intermetallic phases leads to a more complex relationship between nominal composition and precipitate composition, giving a broad range of Fe/Cr ratio in $Zr(Cr,Fe)_2$, and Fe/Ni ratio in $Zr_2(Fe,Ni)$. The orthorhombic Zr_3Fe phase which appears in the binary Zr-Fe diagram is found only in Zr-4 with very high Fe/Cr ratios, probably because its formation is too sluggish compared to the formation of the $Zr(Cr,Fe)_2$ precipitates. As a result, upon cooling from the β-phase the $Zr(Cr,Fe)_2$ precipitates form first and consume the available Fe [6, 26, 27].

Oxygen is to be considered as an alloying element, rather than an impurity. It is added to the compacts before melting as small additions of ZrO_2 powder. The α-stabilizer and oxygen expand the α region of the phase diagram by formation of an interstitial solid solution strengthening. The usual oxygen content is in the range of 800-1600 ppm, and its purpose is to increase the yield strength by solution strengthening [28, 31].

The equilibrium diagrams of Zr-Nb binary system are presented in Figures 1.5 and 1.6. Analysis of the phase diagrams facilitates in understanding the meta-stable steps in the sequence of transformation events [26, 27]. The Zr-Nb system is characterized by complete solid solution in the β (bcc) phase at sufficiently high temperatures and there is a tendency for phase separation in the β phase, as reflected in the miscibility gap at temperatures below 970°C ($\beta_{Zr} + \beta_{Nb}$ miscibility gap); the following monotectoid reaction occurs at 610°C.

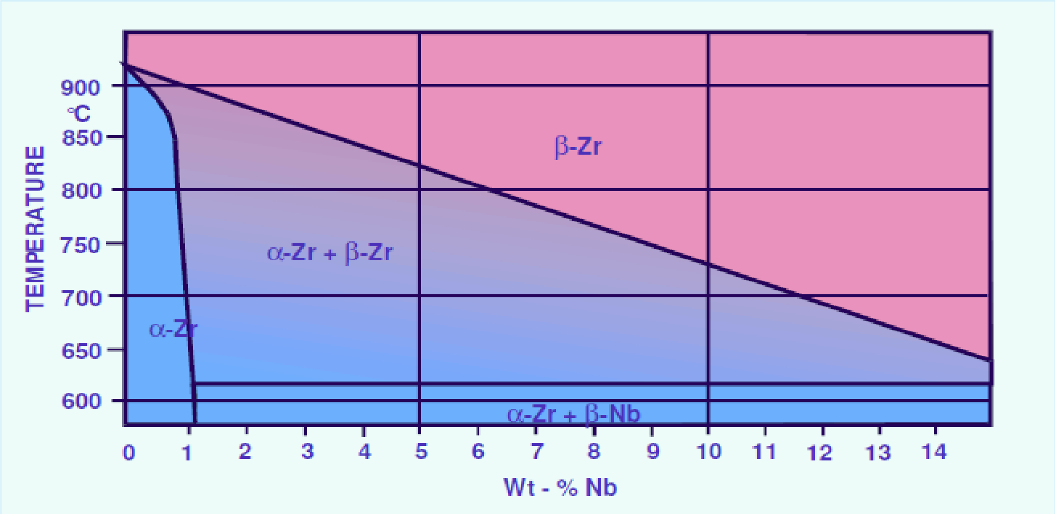

Figure 1.6: Phase diagram of binary Zr-2.5%Nb system, showing meta-stable region.

$$\beta_{Zr} \longrightarrow \alpha_{Zr} + \beta_{Nb} \qquad (1)$$

A variety of equilibrium and meta-stable phases can be obtained from the high-temperature β phase in Zirconium-rich Zr-Nb alloys. The β phase in the Zr-Nb system exhibits the tendency for β→α martensitic transformation and $\beta \rightarrow \beta_{Zr} + \beta_{Nb}$ phase separation reaction in different composition and temperature domains. This β phase instability is known to influence the sequence of phase transformations in Zirconium alloys. In dilute Zr-Nb alloys, it is well known that the β phase, having the same composition as that of the alloy cannot be retained at ambient temperatures even by very rapid quenching. In the alloys containing upto 8% Nb, quenching from the β phase field rapidly through the equilibrium α + β region results in a martensitic structure [29, 30]. Less rapid cooling of dilute Zr-Nb alloys from the β phase field results in the formation of characteristic widmanstatten α plates by nucleation and growth process. The approximate phase boundaries for the meta-stable phase transformations from the high-temperature beta phase are shown in Figures 1.5 and 1.6. In the niobium lean alloys wherein the β phase transforms martensitically to α' phase, the β phase can reappear on tempering the martensite either on the martensite plate boundaries or within the martensite plates [6, 26-28].

1.3.2 Deformation of Zirconium and its alloys

Owing to non-symmetric hexagonal closed packed structure, Zirconium exhibits a limited number of slip systems. The main slip planes in a HCP structure are basal {000l}, prism $\{l0\bar{1}0\}$ and pyramidal $\{l0\bar{1}1\}$. In Zirconium alloys both slip and twinning, mechanisms play equally important roles in the deformation [30-33].

1.3.2.1 Slip modes

Slip is the usual plastic deformation for most of the metallic materials. Slip occurs when shear stress exceeds a critical value for one definite slip plane. Slip occurs readily in specific directions on certain crystallographic planes. Slip operates on a plane and direction for which critical resolved shear stress (CRSS) is the lowest. This is because of the fact that the slip plane is the plane with highest atomic density, and the slip direction is the direction that contains the shortest Burgers vector. The slip plane together with the slip direction establishes the slip system. Lattice constant ratio c/a varies from one HCP material to another. The c/a ratio is an important parameter to explain the deformation behavior of HCP materials and to predict the dominance of any particular slip system at a given temperature and stress conditions [34, 35]. The c/a value of ideal sphere packing is 1.633. For a given HCP material it can be larger than, equal to or smaller than the ideal c/a value. The HCP crystal possesses three slip systems compared to 12 possible slip systems for FCC and 48 possible slip systems for BCC crystal structures. The limited number of slip systems is the reason for the ductility, which is a strong function of orientation in HCP materials. Prism slip is more commonly observed in recrystallized Zirconium alloys, and basal slip is found in cold-worked Zirconium alloys.

1.3.2.2 Twinning

The second important deformation mechanism in Zirconium alloys is twinning. Twinning occurs when a portion of the crystal moves with respect to the adjacent zone. The interface between the twinning area and untwinned area is called as twinning plane [36-39]. In a simple lattice, each atom in the twinned region moves by a homogeneous shear and the distance is proportional to its distance from the twin plane. Lattice strains produced by twinning configuration in a crystal are small so that the amount of gross deformation due to twinning is small. The important consequence of twinning is not only the deformation arising from the twinning process, but also the changes in orientation resulting from twinning, which may produce new slip system in a favorable orientation, and additional slips can take place [40]. Thus, twinning is important in the overall deformation of metals having a low number of slip systems, such as HCP materials.

1.3.3 Thermomechanical processing

Mechanical processing is an essential step in the shaping of materials into engineering components which require dimensional accuracy along with specified mechanical properties and microstructures. The techniques for mechanical processing involve bulk metal working e.g. rolling, forging or extrusion. Cold working is carried out to ensure surface finish, high dimensional tolerance and better strength. Cold working involves a number of steps with intermediate annealing to restore ductility. The important properties such as mechanical properties and corrosion resistance are significantly controlled by the microstructure and texture of the final tube product. The initial condition of the input material, intermediate and final heat treatment processes prior cold work, etc. affect these properties.

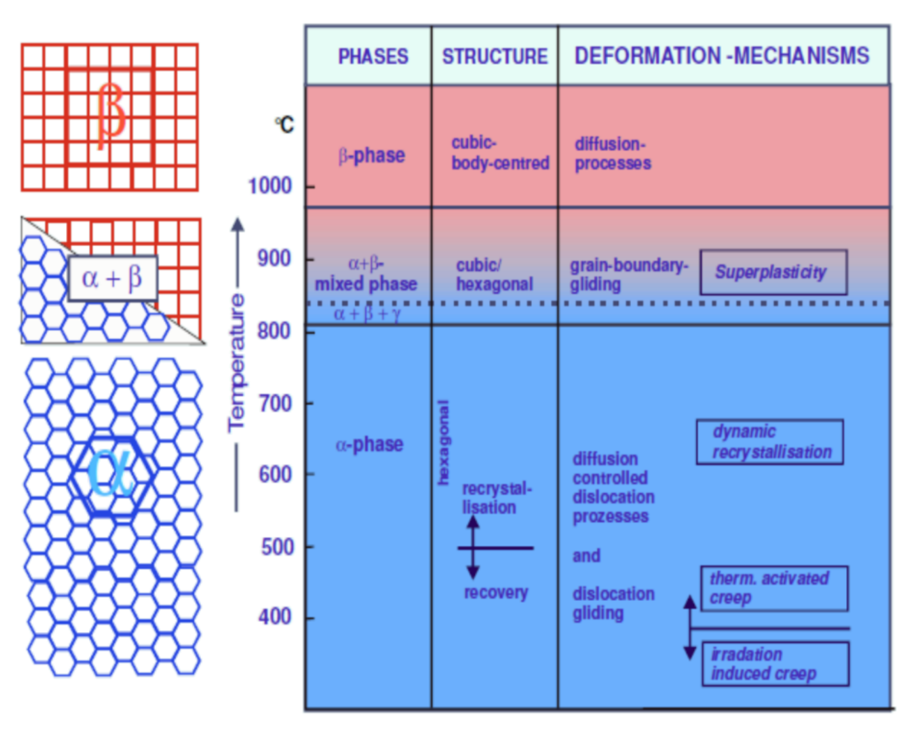

Figure 1.7: Phases, crystallographic structure and deformation mechanisms of Zirconium alloy

The indirect compression force is applied to the surface and the metal flows at right angles to the direction of the compression during mechanical processing like forging, pilgering and rolling. During deformation process, distribution of stress, strain, material flow and overall force are required to perform the operation. The applied forces must cause only yielding and should not create a fracture. Metallurgical phenomena such as strain hardening, recrystallization and fracture are important, under specific conditions of strain rates or high temperature. The flow stress of the material is a strong function of the stress, strain rate and temperature [41, 42]. The phases, crystallographic structure and deformation mechanisms operating in Zirconium alloys are shown in Figure 1.7.

1.3.3.1 Hot working

Hot extrusion is a significant bulk deformation process in the manufacturing of seamless tubes of Zirconium alloys. In order to break the cast structure, vacuum arc melted ingots are further extruded to billets of 150/230 mm diameter size. High-temperature deformation (800 to 840°C) is carried out above the recrystallization temperature to enable imposition of large strains in a single step. This deformation causes a significant change in the microstructure of the material, and it depends on the extrusion process parameters such as temperature and strain rate (1-5 s^{-1}). Basic microstructure developed at this deformation stage has a significant bearing on the final properties of the material fabricated with subsequent cold working steps [26].

1.3.3.2 β-Quenching

Process steps in β-quenching are shown in Figure 1.8.After the completion of hot working and first extrusion, the billets are heated to 1040 ± 10°C, soaked for half an hour (not less than 20 min. and not more than 45 min.) and quenched in water. β-quenching is used to homogenize alloying elements during the processing of Zirconium, to control the second phase particle’s size and to randomize the texture. The transformation temperature of Zirconium from the β-BCC to α-HCP phase during cooling depends on the cooling rate (delayed transformation). Together with process temperatures and durations, β-quenching governs the final second phase particle, types and their size distributions in the Zr α-matrix. The β-heat treatment performed in the β-range (>900-960°C, depending on oxygen content; typically at 1050°C) results in microstructure homogenisation after very short durations. The size of the β-grains formed during this treatment depends on the temperature and soak time. During fast cooling the β-phase decomposes to different phases depending on the composition of the material and cooling rate. β-quenching leads to grain refinement of the as-cast structure, since large grains are broken down into smaller grains and enabled the formation of widmanstatten basket weave morphology and a randomized texture [11, 26].

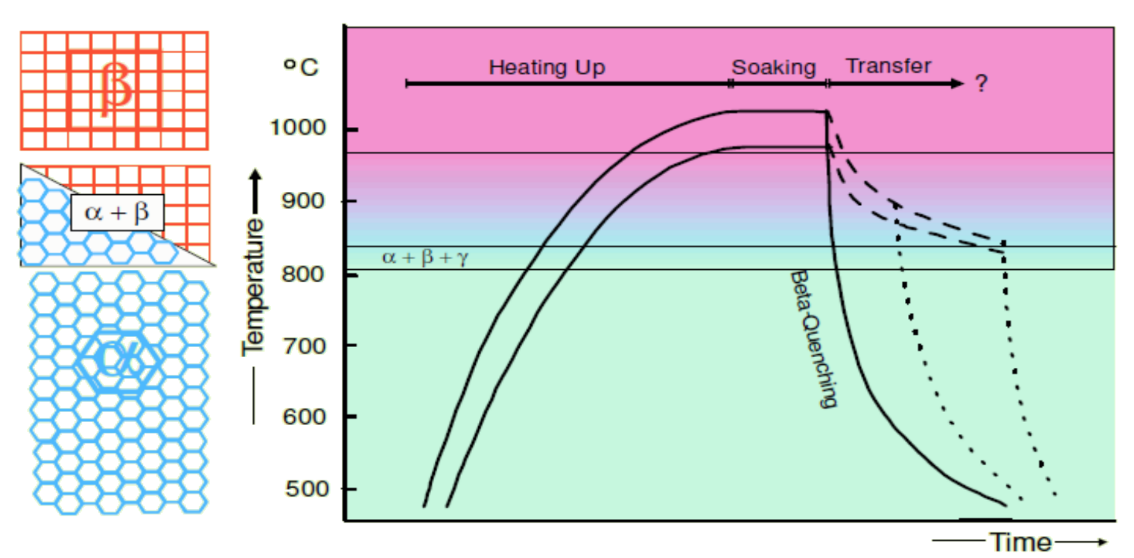

Figure 1.8: Key process steps in β–quenching

1.3.3.3 Cold working

Cold work is defined as the plastic deformation of a material at lower temperatures (below recrystallization temperature). Cold working increases the concentration of dislocations and results in increase in strength & hardness and decrease in ductility. When cold work is beyond the threshold value, the material will fracture before reaching the desired size and shape. Hence, cold working operations are generally carried out in several steps, with intermediate heat treatment operations, where recovery and recrystallization reduce the dislocation density and restore the ductility. The sequence of repeated cold working and annealing is frequently called as the cold work-anneal cycle. The schematic given in Figure 1.9 illustrates the property changes involved in this cycle. If the cold worked material is heat treated, its hardness and strength decrease whereas its ductility increases. Cold worked material’s grains are elongated type whereas annealed material has grains of equiaxed type. If the finished product is required to be stronger than the fully annealed material, the final operation must be a cold working step with proper degree of deformation to produce the desired strength, and subsequently stress relieving needs to be carried out to remove residual stresses [4, 6, 11].

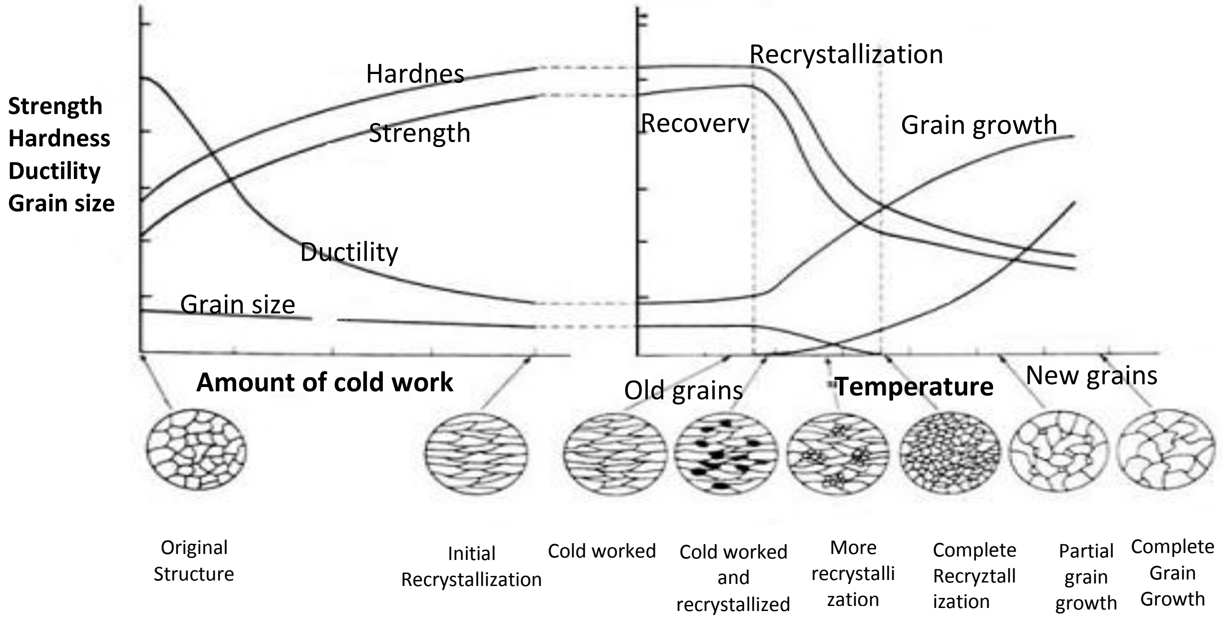

Figure 1.9: Schematic of the cold work-anneal cycle showing its effect on the properties and microstructure

1.3.3.4 Annealing

Zirconium alloys require intermediate annealing before they are subjected to further cold work operations. Annealing operation is carried out at a high vacuum of 10^{-5} mbar and high temperature in vacuum annealing furnaces, with precise temperature control. Annealing restores the original ductility in the material and makes it suitable for further operations.

Thermo-mechanical processing, therefore plays an important role in the processing of Zirconium alloys for meeting the stringent properties required for the fabrication of dissolvers. Control of microstructure by suitable thermo-mechanical processing is the key to the successful fabrication of structural components [42].

1.4 Corrosion of Zirconium alloys

The primary mode of corrosion of Zirconium alloys in an aqueous environment is due to the oxidation of Zirconium by the oxygen in the coolant, dissolved or produced by radiolysis of water. Radiolysis of steam/water mixture or water solution can take place when exposed to high-energy particles (neutrons, alpha particles, gamma quanta and fission fragments). Radiolysis effect is following the theory of high-energy particles flying in the medium break the existing bonds between atoms in molecules. Further, after quick recombination of intermediate particles, the stage of interaction of radicals is set in according to kinetic equations of radiation chemistry and the main reactions are governed by behavior of radicals H, OH, O and molecules H_2O, H_2, O_2, H_2O_2; formation and interaction with radical HO_2. A small amount of oxygen may dissolve in the metal, but once the thermodynamic solubility limit is exceeded, ZrO_2 is formed on the metal. It is reported that Zr oxidation occurs by inward migration of oxygen ions through the oxide layer [43, 44], as shown in Figure 1.10.

$$Zr + O_2 = ZrO_2 \qquad (2)$$

The growth of the oxide layer on the metal surface depends on the kinetics of oxygen diffusion through this layer. The corrosion kinetics slows down as the thickness of the oxide scale increases; the rate controlling step in the oxidation process is the transport of atomic species in the protective oxide, by either diffusion of oxygen or electrons through the oxide film. These processes are necessarily coupled to maintain electro neutrality. Electron transport is, however, difficult in Zirconium dioxide, as it is an electrical insulator when undoped. Although this is not confirmed, it is likely that the role of doping elements in the determination of corrosion kinetics is done through their influence on the electron or oxygen transport in the oxide layer [43-45]. The most important types of corrosion morphologies, which have been observed in nuclear reactors and autoclave experiments are:

1. Uniform: Formation of a thin uniform layer of Zirconium dioxide on the surface of a Zirconium alloy component.

2. Nodular: Formation of local, small, circular Zirconium oxide blisters

3. Shadow: Formation of local corrosion regions that mirror the shape (suggestive of a shadow) of other nearby noble reactor core components.

The occurrence of these morphologies is strongly dependent on the reactor operating conditions and chemical environment.

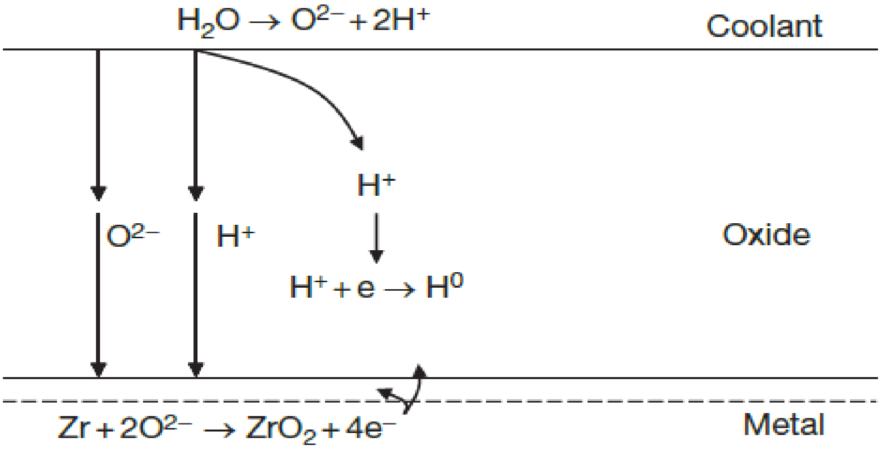

Figure 1.10: Schematic of the corrosion mechanism of Zirconium alloys

1.4.1 Controlling factors for corrosion of Zirconium in nuclear application

The oxidation and hydrogen uptake of Zirconium alloys is dictated by several factors, including the chemical and physical states of the material such as composition, metallurgical condition, and surface condition. These are often specific to the material and sometimes batch-specific and also related to the fabrication process [45-47].

1. Coolant chemistry: It is well known that the dissolved oxygen and hydrogen play a major role in the corrosion process, but other dissolved species must also be taken into account. To control the pH of the coolant at marginally alkaline conditions, LiOH is added, and H_3BO_3(boric acid) is added for reactivity control in PWRs. Further, impurities (chloride, fluoride) and coolant-borne species (Cu, Ni, etc.) must also be considered.

2. Radiation: In the reactor, the Zirconium alloys and the coolant are subjected to the effect of energetic particles. The principal effect is the production of oxidizing species such as O^{2-} in the coolant.

3. Temperature: In the range of operation of light water reactors (240-33°C), the combined effect of temperature and radiation on Zirconium alloy oxidation and hydriding has been investigated extensively, which varies from almost no effect to accelerated oxidation by a factor of up to two orders of magnitude, depending on the environment and radiation level.

1.4.2 Corrosion of Zirconium alloys in nitric acid medium

Zirconium is resistant to many powerful oxidizing acids at various concentrations. While reacting with acids, Zirconium has a tendency to decompose water with the evolution of hydrogen, and it goes into solution as zirconic ions, $Zr^{4+}$and as zirconyl ions, ZrO^{2+} in very acidic solutions.

$$Zr \rightarrow Zr^{4+} + 4e \qquad (3)$$

$$Zr^{4+} + 2H_2O \rightarrow ZrO_2 + 4H^+ \qquad (4)$$

Zirconic ions form a stable ZrO_2 film on the surface according to reaction (4). Even a marginal positive shift in the equilibrium potential could lead to the formation of a 40–200Å thick oxide film on the surface of Zirconium. It has been reported that in electrolytes containing oxidizing agents, Zirconium forms nearly 1000Å thick oxide film which behaves like an inert surface with high ohmic resistance [47, 48].The excellent corrosion resistance of Zirconium to acids is attributed to the crystal structure and stability of the ZrO_2 film formed. Addition of alloying elements to Zirconium and their introduction in to the Zirconium oxide can basically change the properties of the metal and oxide as well as the interaction between metal and oxide. Replacement of oxygen by nitrogen in the oxide lattice leads to dilation of the oxide lattice and thus, has a negative effect in matching with the lattice of the metal. However, replacement of Zirconium ion in the oxide lattice by at in ion leads to the contraction of the lattice and nullifies the negative effect to nitrogen in Zirconium alloys. The elements Fe, Ni and Cr form insoluble intermetallic compounds that can act as microcathodic zones leading to the development of stronger thin layers of ZrO_2. It has also been reported that the corrosion rates of Zirconium and its alloys were extremely low, less than 0.1 mpy for most of the metallurgical conditions with different microstructural features.

The redox potential of boiling nitric acid is a measure of its aggressiveness towards the metal in contact with nitric acid [49, 50], and is calculated from the free energies of formation of appropriate oxides and chlorides. The higher the oxidizing power of the nitric acid, the more will be the metal corrosion giving rise to metal ions, before reaching the equilibrium. The reactivity of the acid towards metals depends on the nature of the cation. From thermodynamic stability calculations, it is found that boiling nitric acid does not react with Zr and alloys and corrosion of Zirconium and its alloys in nitric acid is due to the trace impurities. Water and oxygen are the main contaminants in nitric acid and complete removal of impurities is necessary to prevent corrosion [49, 50].

1.4.3 Behavior of Zirconium alloys in nitric acid

Zirconium alloys exhibit excellent corrosion resistance to all concentrations of all the industrial acids (up to approximately 75% concentration). Oxidizing species present in these acids can accelerate the corrosion of Zirconium in a localized manner. Besides oxidizing contaminants, there also appears to be a correlation between the surface condition of Zirconium and its susceptibility to localized corrosion. Austenitic stainless steels do not exhibit satisfactory corrosion resistance in highly oxidising boiling nitric acid media and occasionally intergranular corrosion failures are observed which are ascribed to corrosion in the transpassive range. This is aggravated by the presence of oxidising ions such as Cr (VI) and Pu (VI). Titanium alloys also possess a low corrosion rate in these media, but a specific form of corrosion is observed in the vapour phase. The vapour phase corrosion appears in the form of white, non-adhesive oxide (Ti_2O_3) above liquid level in the condensation zone. Zirconium does not suffer from this drawback and aids in solving corrosion problems in these particularly aggressive conditions for stainless steels. It is reported that Zirconium alloys have a uniform brown or black appearance without any sign of intergranular or local corrosion. This corrosion resistance does not depend on metallurgical factors such as grain size, cold work, annealing, β-quenching temperatures etc. Thus, Zirconium proves to be a versatile metal that is mainly used in the chemical and nuclear sectors. As mentioned earlier, Zirconium is also a good choice in the preparation and processing of nitric acid [48-51].

1.4.4 Advantages of using Zirconium alloys for reprocessing applications

The excellent corrosion resistance of Zirconium in nitric acid has been known for 5 decades. Even though Zirconium is seven times more expensive (per unit weight) and fabrication cost is five times more expensive than that for conventional 304L SS, the value of Zirconium is realized through the improved performance and extended service life of the component. Zirconium has several advantages for use in nitric acid applications. Unlike titanium, Zirconium is unaffected by vapour condensates in boiling nitric acid. The density of Zirconium is lower than that of iron and nickel, i.e. Zirconium is 20% lighter than stainless steel. Thermal conductivity is high for Zirconium, i.e. 18% more than that of Type 316 stainless steel; thus, fewer tubes are needed for Zirconium compared to stainless steel for heat transfer purpose. The coefficient of thermal expansion is about one-third of Type 316 stainless steel and two-thirds of titanium. No difference in corrosion behaviourwas observed between different grades of Zirconium in boiling nitric acid, and the corrosion rate was unaffected by an increase in acidity or by the presence of hexavalent chromium [52-55].

Investigation of the effect of metallurgical state on the corrosion resistance of the Zirconium also indicated that the corrosion rate is unaffected by the metallurgical state. Since the corrosion of Zirconium is negligible, maintenance and in-service inspection are not necessary for a radioactive environment, and extended component plant life can be realized. In view of all these advantages, studies on Zirconium and its alloys were initiated in order to consider it as a candidate material for dissolver and evaporator applications in future FBR reprocessing plants.

1.5 Objective of the study

The chemical composition and microstructure of a Zirconium alloy are critical factors that ensure its proper functioning in corrosive environment. While choosing a material its microstructure is of crucial importance, which in turn is a function of the material chemistry and the thermo-mechanical manufacturing processes. Thus, proper selection of alloying elements and the manufacturing process conditions are important to yield the appropriate microstructure resulting in the required properties. Zirconium with the optimized proportion of alloying elements in combination with a suitable thermomechanical manufacturing process will provide appropriate microstructure and corrosion resistance in nitric acidic environment at various concentrations.

The aim of the present study is to

1. Establish process flow sheet for Zr-2, Zr-4, Zr-1%Nb and Zr-2.5%Nb alloy tube production.
2. Study the evolution of microstructure during thermo-mechanical processing of Zr-2, Zr-4, Zr-1%Nb and Zr-2.5%Nbusing characterisation techniques like optical, scanning electron microscopy and Electron Backscattered Diffraction (EBSD).
3. Study of microstructure of the weld region of TIG and EB welded Zr-4 used for

fabrication of dissolver assembly for reprocessing.

4. Evaluate the mechanical properties like YS, UTS and hardness for unalloyed Zirconium, Zr-2, Zr-4, Zr-1%Nb and Zr-2.5%Nb alloy.
5. Study the electrochemical behaviour of Zirconium based alloys in 11.5 M nitric acid at room temperature using three-electrode corrosion cell setup used to carry out the open circuit potential and the potentiodynamic polarization experiments.
6. Evaluate the corrosion behaviour of Zirconium and its alloys like Zr-2, Zr-4, Zr-1%Nb and Zr-2.5%Nb in boiling 11.5 M nitric acid environment on short-term (per ASTM practice C) and long-term basis (in specially fabricated Zirconium alloy loop setup for 1000 h)
7. Characterisethe mixed monoclinic and tetragonal phases of ZrO_2 formed on Zirconium pilgered tube and autoclaved tubes by Laser Raman Spectroscopic (LRS) analysis after corrosion testing and the oxidation state of the components of the passive film of final pilgered and subsequently annealed Zr-4 sample exposed to boiling 11.5 M HNO_3 for 1000 h by analyzing the surface film by XPS.
8. Correlate the process parameters with mechanical properties; micro-structural evolution and corrosion behaviour of Zirconium based alloys for spent fuel reprocessing plants.

CHAPTER II

EXPERIMENTAL DETAILS

2.1 Introduction

This chapter describes the manufacturing processes and flow sheet for the production of various Zirconium based alloys like Zr-2, Zr4, Zr-1%Nb and Zr-2.5%Nb. The different thermo-mechanical treatments employed for Zirconium alloys have been explained. The process flow sheet developed and the acceptance criteria evolved for fabrication of dissolver for nuclear fuel reprocessing by adapting better and robust fabrication methods like Electron Beam welding (EBW), conventional TIG welding and optimization of welding parameters have been discussed briefly. Characterization tools like an optical microscope (OM), scanning electron microscope (SEM), Energy-dispersive X-ray spectroscopy (EDS), X-ray diffraction (XRD) and electron backscattered diffraction (EBSD) used in the present study to obtain the desired microstructure were described. Experimental methods used for the evaluation of mechanical properties like yield strength (YS), ultimate tensile strength (UTS) and microhardness at room temperature have been discussed. Three-electrode corrosion cell setup employed to measure the open circuit potential and the potentiodynamic polarization experiments conducted to evaluate the passivation behavior of Zirconium based alloys in 11.5 M nitric acid at room temperature were covered. To evaluate the corrosion rates of the Zirconium alloys, ASTM A262 practice-C and Zr-loop tests were carried out, and their experimental setup are described. After corrosion testing, Laser Raman Spectroscopic (LRS) analysis was carried out to study the phases formed on the passive film. The oxidation state of the elements in the passive films of final pilgered and subsequently annealed Zr-4 samples exposed to boiling 11.5 M HNO_3 for 1000 h was analyzed by X-ray Photoelectron Spectroscopy (XPS).

2.2 Manufacturing methods of Zirconium alloys

The manufacturing process for the various Zirconium based alloys changes as per the alloys type and the end product size. The single phase tin based alloys like Zr-2 and Zr-4 are manufactured specifically with different set of thermo mechanical processing (TMP) steps compared to the two-phase niobium based alloys like Zr-2.5%Nb and Zr-1 Nb. Steps used for the fabrication of Zirconium components are aimed at obtaining the required dimensional tolerances and optimized microstructure. The structural evolution at each of these TMP steps is important. The texture and microstructure obtained at the end of one stage decide the ease or difficulty of the next stage of processing. The final microstructure, and associated properties is often a cumulative outcome of a series of changes occurring at each stage of processing. Hence, characterization of microstructures associated with TMP stages of Zirconium tubes is important in optimizing the processing parameters [1, 56-60].

General flow sheet adopted for manufacturing of Zirconium alloys is as follows (Figure 2.1):

- Double/triple melting
- First extrusion/
- β-Quenching
- Second extrusion/hot rolling
- Cold working process
    - Pilgering
    - Cold rolling
    - Drawing

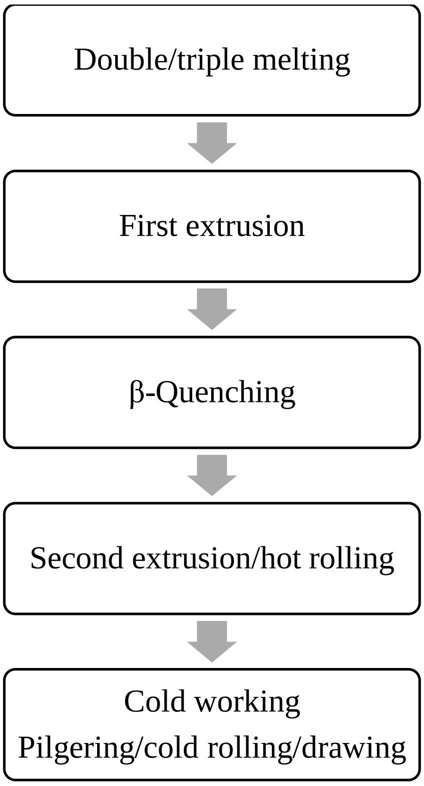

Figure 2.1: General flow-sheet for fabrication of Zirconium alloys

Zirconium and its alloys are amenable to various hot and cold working operations like extrusion, pilgering, rolling, drawing, swaging, stamping etc. Zirconium suffers from three main problems during fabrication, viz., (i) the material has a strong tendency to work harden during cold working, (ii) it has a tendency to stick or gall to the dies and tools, especially during drawing and (iii) the material gets contaminated with atmospheric gases during hot working or annealing. The effect of work hardening can be removed by annealing / stress relieving the material between two cold working operations [26, 27].

2.2.1 Melting

Zirconium sponge is mixed with alloying elements in required proportion and is compacted into briquettes. Several such briquettes are electron beam welded to form long consumable electrodes, which are melted in vacuum arc (VAR) furnace. Double melting is carried out to obtain homogenous Zirconium alloy ingots. Figure 2.2 shows the double melted Zr-4 ingot of Ø 350 mm by VAR melting. Melting parameters for Zirconium alloys is listed in Table 2.1.

Process parameters that influence the characteristics and quality of the ingot are:

(1) The quality of the raw material.

(2) Molten pool diameter and depth that are functions of amperage and speed of melting.

(3) Number of remelts of the ingot; an increased number of remelts tends to increase the homogeneity in the material and

(4) Welding electrode, copper mould (VAR furnace) and atmosphere composition.

The alloying elements and impurities of advanced Zirconium alloys such as Sn, Nb, Fe, Cr, Ni, O, Si and C are either fully dissolved in the alloy matrix (Sn, O) or dissolved to a large extent (Nb) or almost fully precipitated as small intermetallic (Fe, Cr, Ni, Si, C) Second Phase Particles (SPPs).

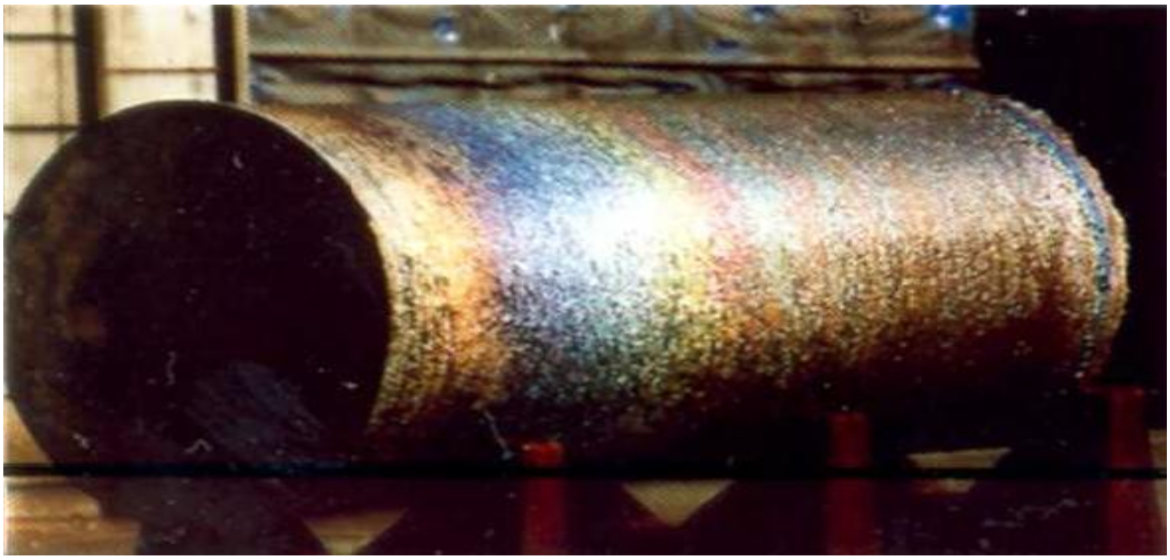

Figure 2.2: Double melted Zr-4 ingot of Ø350 mm by VAR melting

Table 2.1: Melting parameters for Zirconium alloys

Melting parameters			
	Zr-2/ Zr-4	Zr-2.5%Nb*	Zr-1%Nb
Ingot diameter	Ø 350 mm	Ø 350/550 mm	Ø 350 mm
Melting current and voltage	10 to 12 kA at 34 volt	10 to 20 kA at 38volt	11 to 13 kA at 35 volt
Melt-rate	10 to 15 kg/h	10 to 20 kg/h	10 to 15 kg/h
Vacuum Level	1x 10^{-3} mbar	0.5x 10^{-4} mbar	0.5x 10^{-4} mbar

(* Quadruple Melted)

2.2.2 Extrusion Process

Hot extrusion is a bulk deformation process used in the primary breakdown of cast structure for VAR double /quadruples melted ingots. High-temperature deformation (800 to 840°C) which is carried out above the recrystallization temperature, enables imposition of large strains in a single step. This deformation causes a significant change in the microstructure of the material, and it depends on extrusion process parameters such as temperature and strain rate (1-5 s^{-1}). The basic microstructure developed at this deformation stage has a significant bearing on the final properties of the material fabricated with subsequent cold working steps. The extrusion flow lines are represented in Figure 2.3, and the schematic arrangement of extrusion tooling like die, mandrel, main ram and billet for extrusion and extruded tube are shown in Figure 2.4. Processing maps (Figure 2.5) based on the dynamic material model have been adopted for the selection of hot extrusion parameters [61]. Extrusion parameters like temperature and strain rate are selected as per the stable region indicated in the processing maps. Extrusion press of 3780 T (Figure 2.6) capacity, horizontal with semi-floating mandrel as well as normal mandrel has been used [59, 60]. Extrusion parameters for various Zirconium alloys aregiven in Table 2.2.

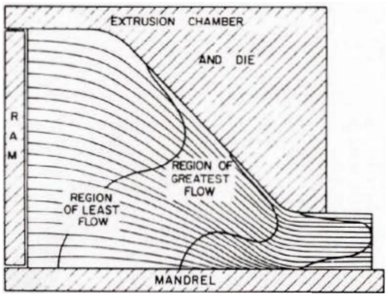

Figure 2.3: Schematic representation of extrusion flow lines

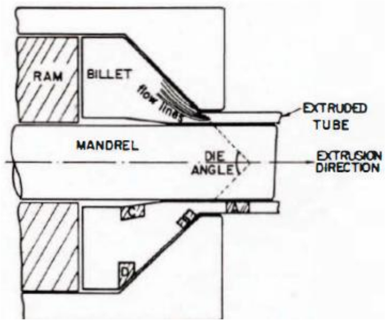

Figure 2.4: Schematic arrangement of extrusion tooling

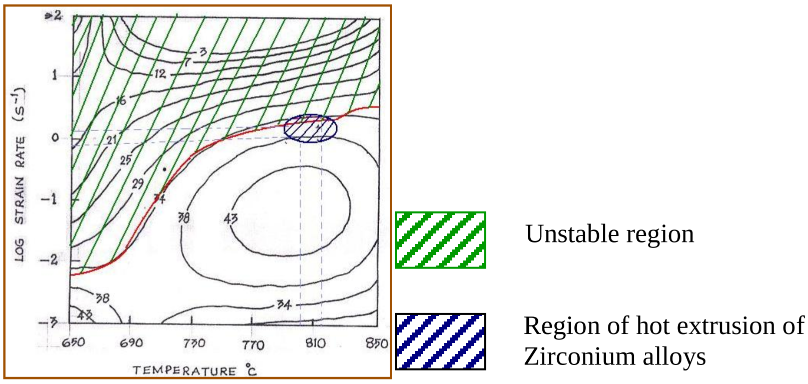

Figure 2.5: Processing map showing hot extrusion domain for Zirconium alloys

Figure 2.6: Hot extrusion press used for extrusion of Ø 350 mm ingot

Table 2.2: Extrusion parameters for Zirconium alloys (3780 T capacity Extrusion press)

Extrusion parameters			
	Zr-2/ Zr-4	Zr-2.5%Nb	Zr-1%Nb
Input ingot diameter	Ø 350 mm	Ø 350 mm	Ø 350 mm
Output billet/rod diameter	Ø 150 mm	Ø 230 mm	Ø 150 mm
Extrusion temp.	825-850°C	700-750°C	850°C
Extrusion press speed	25–30 mm/s	20–25 mm/s	25–30 mm/s
Strain rate	1-5 s^{-1}	1-5 s^{-1}	≈2s^{-1}
Lubricant		Copper	

2.2.3 β-Quenching

After completion of first extrusion hot working, billets are heated to 1040 ± 10°C, soaked for half an hour (min. 20 minutes to max. 45 minutes) and quenched in water. β-quenching is used to homogenize alloying elements during the Zirconium processing for the purpose of controlling the size of second phase particles and to randomize the texture. Zirconium undergoes an allotropic transformation from the β-bcc to α-hcp phase upon cooling. The transformation temperature depends on the cooling rate (delayed transformation). Together with process temperatures and cooling times, β-quenching governs the final SPPs, types and their size distributions in the Zr α-matrix. The β-heat treatment is performed in the β-range (>900-960°C, depending on the oxygen content) typically at 1050°C and it results in microstructure homogenisation after very short times. The size of the β-grains that form during this treatment depends on temperature and soak time. During fast cooling the β-phase decomposes into different phases depending on material composition and cooling rate. Key process steps in β-quenching of Zirconium billets were shown in Figure 1.8. β-quenching leads to grain refinement of the as-cast structure as large grains are broken down into smaller grains and forms widmanstatten basket weave morphology and a randomized texture [1, 11, 26]. β-quenching parameters for various Zirconium alloys are shown in Table 2.3.

Table 2.3: β-Quenching parameters for Zirconium alloys

β-quenching parameters			
	Zr-2/ Zr-4	Zr-2.5%Nb	Zr-1%Nb
Temp.	1050°C	1050°C	1000°C
Soaking Time	20-45 min.		
Quenching medium	Water (forced circulated)		

2.2.3.1 Production of mother blank for seamless tubes

The hot extruded and β-quenched billets are machined to hollow billet. These billets are heated and extruded in the extrusion press to get mother blank. It is important to ensure that the heat treatment temperature is below the monotectoid temperature and that the extrusion speed is limited so that the deformation heat produced during extrusion will not result in material temperatures higher than the monotectoid temperature.

2.2.4 Pilgering process for tube production

Pilgering is a method of step-wise reduction of tubes effecting their diameter as well as thickness, over a fixed mandrel, with to and fro rocking action of grooved rolls that exert a compressive force on the tube as it is forced into the roll pass. In this process, OD and wall tickness (WT) are simultaneously reduced. During manufacturing, cold pilgering may result in tube defects. Generally, a larger degree of cold reduction in the clad radial versus tangential direction will result in a more radial texture. More cold reduction in each pilgering step may reduce the number of necessary pilgering steps to bring down the tube to its final dimensions. However, too much of cold reduction may result in tube defects. Grain size and shape, as well as dislocation density are affected by the degree of cold deformation applied in the pilger steps, intermediate annealing and final annealing [62-64]. The final annealing affects the degree of recrystallization and the grain size (typically between 2 to 4 μm). In the pilgering process (Figures 2.7 and 2.8) there are two circular or semicircular dies with matching, tapering, semicircular grooves machined into their curved faces. During the operation, one die is placed over top of the other die so that the matching semicircular grooves make a circular pass. The dies are geared to each other in such a fashion that they rotate in opposite directions when they are moved laterally (in the plane of the groove) and a converging (or diverging, depending on the direction of lateral movement) circular pass is traced by the die grooves. The mandrel, which has a tapered shape in the rolling direction, is located inside the tube. Diameter and wall thickness are reduced in a number of forming steps, and the tube is elongated in the axial direction. In each stroke, the mother tube is advanced and rotated during the idle zone at a fixed feed rate and a fixed turn angle, respectively, to repeat the rolling in cold pilgering continuously. A large cross-sectional reduction is possible in cold pilgering. Cold pilgering is a longitudinal cold-rolling process that reduces the diameter and wall thickness of metal tube in one process step. A large number of small forming steps helps to ensure a constant reduction in wall thickness and nearly homogeneous material characteristics in the rolled tube. Pilgering process improves the dimensional tolerances to a great extent, reduces internal material defects due to the application of high compressive stresses during pilgering and imparts excellent surface finish on the ID and OD resulting into uniform microstructure.

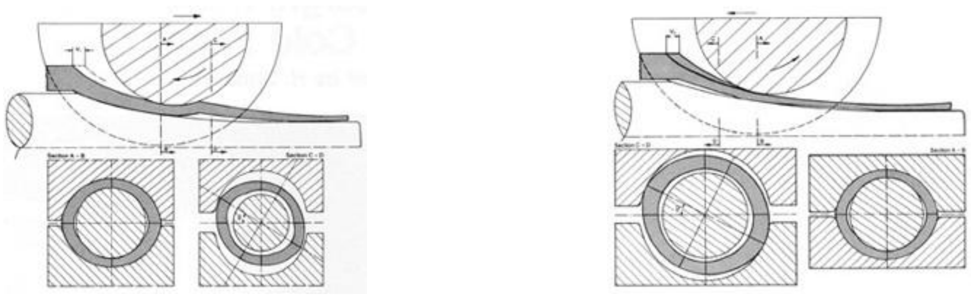

Figures 2.7: The cold pilger mill's forward motion (left) and backward motion (right) rely on the tapered cross section between the dies and the mandrel to reduce the tube's diameter and wall thickness simultaneously

2.2.4.1 *Operational parameters influencing the pilgering operation*

Optimizing the parameters for pilgering process is achieved by matching the feed rate and the rotation angle in the two dead-centre positions with the tube material [62-64]. For the production of Zirconium alloys tubing, feed rate has been optimised at 2.3 to 4.5 mm/min and 150 to 180 strokes/min. Copious flooding lubricant is used for better surface finish and longer tooling life and to control tube temperature, which increases due to cold-work.

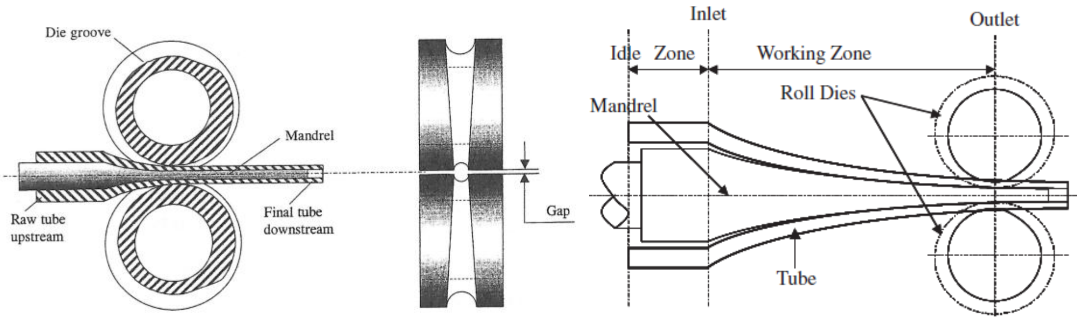

Figure 2.8: Schematic of cold pilgering process

Table 2.4: Pilgering parameters for Zr alloys

	Pilgering parameters		
	Zr-2/ Zr-4	Zr-2.5%Nb	Zr-1%Nb
Pilger strokes/min	150 to 180	100 to 120	150 to 180
Reduction Ratio	70-90 %	40 %	40-50 %
Die	AISI H13		

Figure 2.9: Pilgering used for production of seamless tubes

2.2.4.2 Annealing

Zirconium alloys require intermediate annealing before they are subjected to cold work operations. The de-jacketed hollows and the pilgered tubes at intermediate stages are thoroughly degreased and vacuum annealed at 730°C for 3 h. Annealing operation is carried out in a high vacuum-high temperature horizontal annealing furnace (Figure 2.10), with close temperature control and very high vacuum of the order of 10^{-5} mbar or better. The material after annealing attains original ductility and becomes suitable for further operations. Thermo-mechanical processing, therefore, assumes an important role infabricating Zr-based alloys for meeting the stringent properties required for dissolver applications. The control of microstructure by suitable thermo-mechanical processing is the key to the successful fabrication of structural components. Heating rate for the annealing treatment was 1°C/s [30, 65].

The pilgering schedule is based on the consideration of the maximum amount of cold work imparted in each pilger stage. After each cold working step an intermediate annealing (at 760°C/4 h) is performed to restore the material ductility for further cold working. It is also important that these heat-treatments are done below the monotectoid temperature.The annealing parameters for Zirconium alloys are given in Table 2.5.

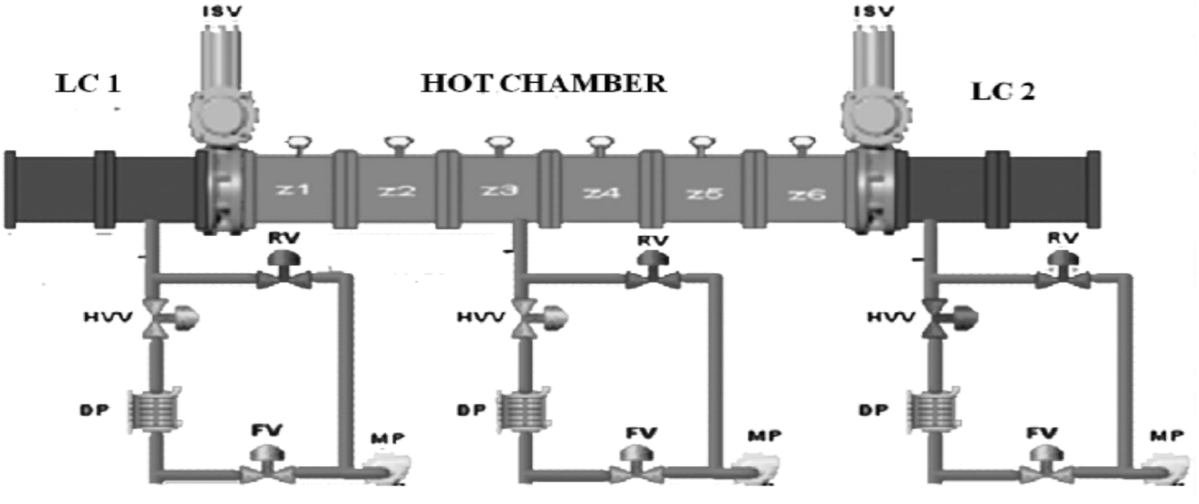

Figure 2.10: Representation of Horizontal Vacuum Annealing Furnace

The thermo-mechanical treatment followed in the processing of clad tubes is adequate to meet the requirements of UTS, % elongation and hoop stress consistently. However, YS and total circumferential elongation (TCE) are more sensitive properties and sometimes require re-heat-treatment in order to meet the specifications. The mechanical properties depend on several factors such as stress-relieving temperature, eccentricity, ID defects, and cold work after stress relieving like straightening, etc. [42].

Table 2.5: Annealing parameters for Zirconium alloys

Annealing parameters			
	Zr-2/ Zr-4	Zr-2.5%Nb	Zr-1%Nb
Annealing temp.	575-760°C*	580°C	555-575°C
Time	3-4 h	3 h	4 h
Vacuum Level	1x 10^{-5} mbar		

(* depending on cold-work)

Zr-2 and Zr-2.5%Nb tubes manufactured were autoclaved to get corrosion resistant black monoclinic oxide layer. Autoclaving is carried out at 290-400°C at 10 bar pressure in steam medium for 72 to 120 h depending upon the thickness required for product oxide layer. Autoclaving parameters for Zr-2/ Zr-4 and Zr-2.5%Nb are presented in Table 2.6.

Table 2.6: Autoclaving parameters for Zr-2/ Zr-4 and Zr-2.5%Nb

	Zr-2/ Zr-4	Zr-2.5%Nb
Autoclaving temp.	400°C	290°C
Pressure	10 bar	
Medium	Steam	
Time	72 h	120

2.3 Manufacturing of Zirconium alloys

2.3.1 Manufacturing of Zr-2 and Zr-4

The flow chart employed at NFC for the production of Zr-4 and Zr-2 tubes are shown in Figures 2.11 and 2.12 respectively. As a first step, Zr-2 and Zr-4 ingots of dia350 mm were produced in vacuum arc furnace by melting Zirconium sponge and the other alloying elements. The as-cast Zr-2 and Zr-4 ingots were extruded (Figure 2.6) at a temperature close to 850°C in a 3780 T horizontal extrusion press (HEP) to form billets of Ø 150 mm. These billets are subjected to β-quenching where they are homogenized at 1050°C for 30 min and are quenched in water. β-quenched billets are jacketed with seamless copper tubes and extruded in a 3780T HEP, maintaining the extrusion ratio of 14:1 and extrusion speed of 25-30 mm/s at 800°C. After extrusion, the copper jacket on the surface of the Zr-2 and Zr-4 blanks is removed by dissolution in a bath containing HNO_3 and HF solution. After these operations, the extruded blanks are stress relieved at 700°C for 2 h and subjected to pilgering operations. All seamless tubes of Zr-2 and Zr-4 are manufactured by either 3 or 4 pilgering steps with intermediate annealing to restore the ductility of Zr-2 and Zr-4 tubes. Pilgering

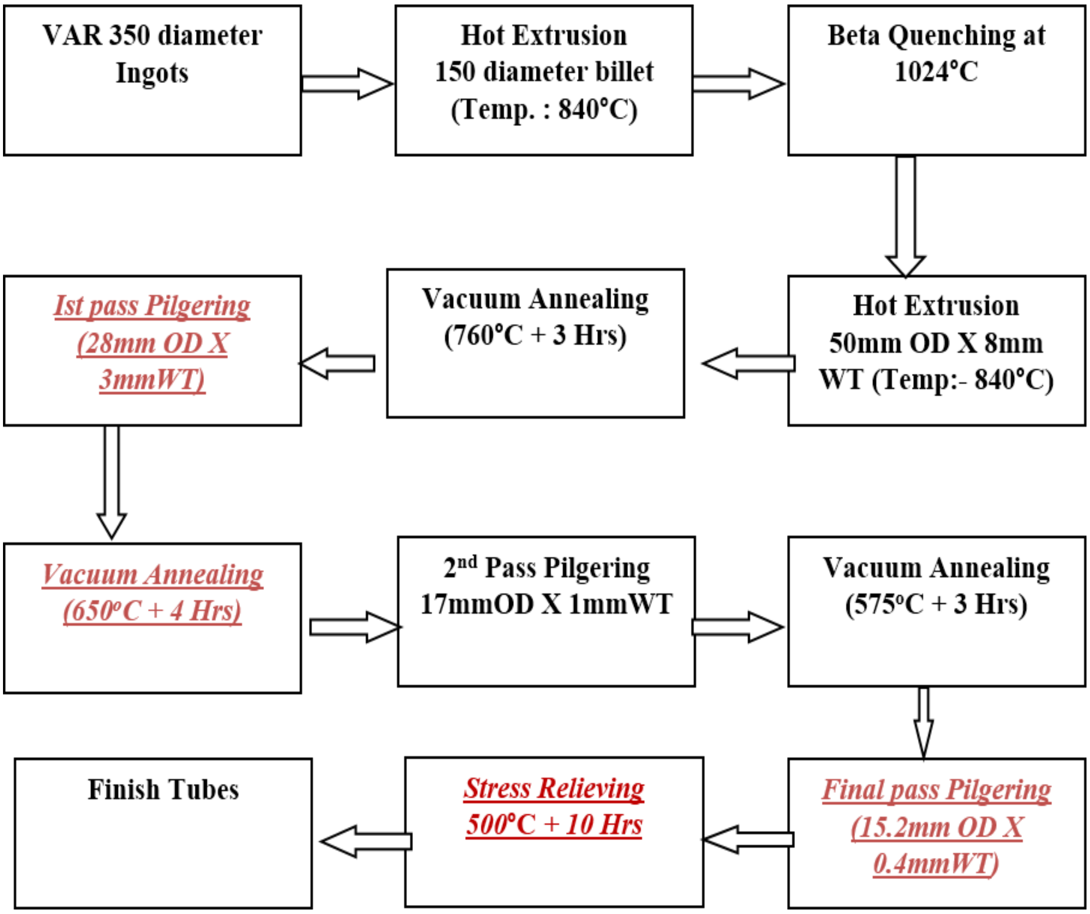

Figure 2.11: Flow-sheet followed at NFC for fabrication of Zr-4

was carried out in 50 VMR MIR make German mill (Figure 2.9) and 10/20 and 16/32 in Russian make HPTR mill available at NFC, Hyderabad. All the annealing operations were carried out in horizontal vacuum furnaces, with vacuum of the order of 10^{-5}mbar [26].

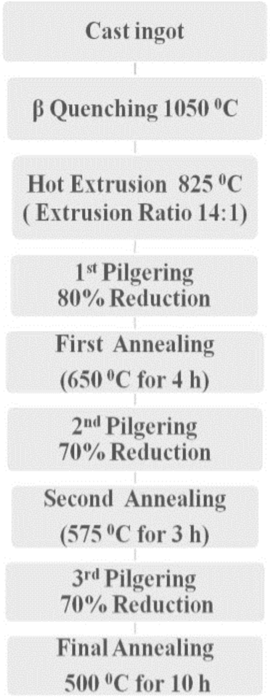

Figure 2.12: Flow-sheet followed at NFC for fabrication of Zr-2

2.3.2 Manufacturing of Zr-2.5%Nb and Zr-1%Nb alloy

Zr-2.5%Nb alloy tubes were produced as per the flow sheet in Figure 2.13(a). The ingots of Ø350 mm were produced in a consumable vacuum arc melting furnace (VAR). For Zr-2.5%Nb alloy, quadruple melting has been carried out to reduce the impurity elements. In order to break the cast structure, these ingots were further extruded to billets of Ø230 mm size. Hollow machined billets were subsequently water quenched to achieve compositional and microstructural homogeneity; the quenched billetswere soaked at 800°C for 1h followed by extrusion with an extrusion ratio of 7.3:1. The hot extruded blank of Zr-2.5% Nb alloy was further subjected to cold deformation of 41 % by pilgering [66]. Followed by 2nd Pass Pilgering (23% cold-working), intermediate annealing operations were carried out in a vertical vacuum furnace, with vacuum of 10^{-5}mbar, followed by ageing at 515°C / 540°C for

24 h and autoclaving (290°C for 120 h) . Zr-1%Nb alloy tubes were produced as per flow sheet in Figure 2.13 (b). The ingots of Ø 350 mm were produced in VAR furnace by double melting. Zr-1%Nb ingots are extruded at a temperature close to 850°C and atthe strain rate ($\approx 2s^{-1}$) in a 3780 T horizontal extrusion press to form billets of Ø 150 mm. These billets are subjected to β-quenching where they are homogenized at 1000° C for 30 min. and are quenched in water. The hot extruded blank of Zr-1%Nb alloy is further subjected to repeated cold deformation by pilgering operation (six times) followed by intermediate annealing at 610°C [20, 42].

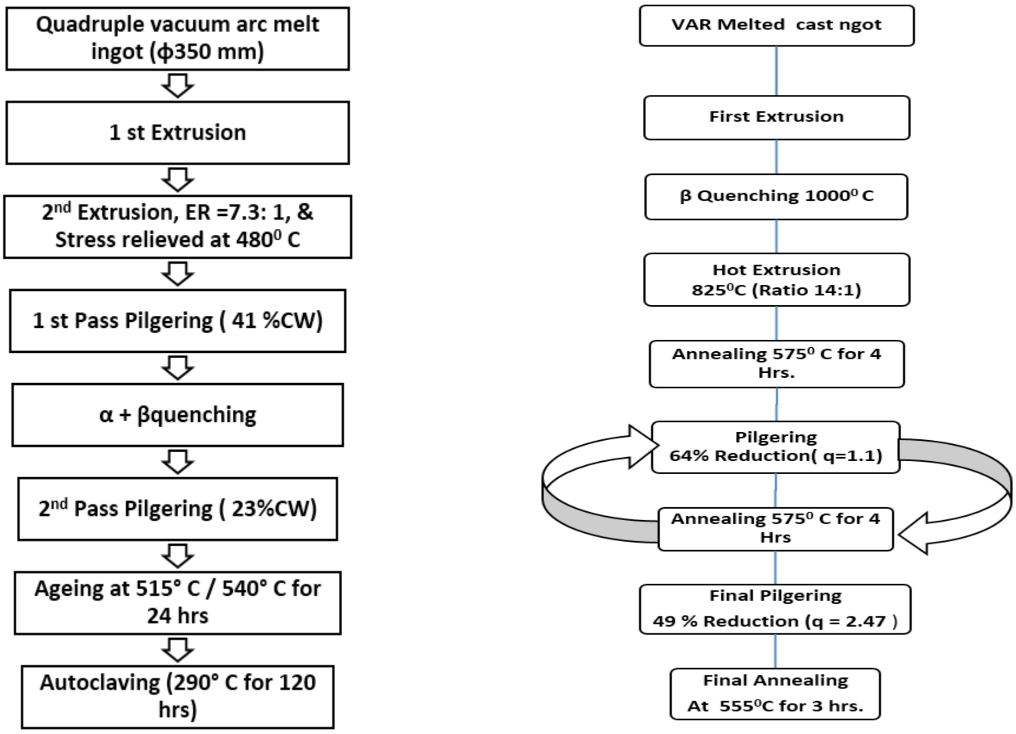

(a) **(b)**

Figure 2.13 Flow sheet for manufacture of (a) Zr-2.5% Nb and (b) Zr-1% Nb alloy tubes

2.4 Fabrication of Zr-4 dissolver assembly

Tubes of different sizes are the major components required for the fabrication of the dissolver vessel and generally manufactured through cold pilgering. The dissolver assembly consists of several other parts such as elbow joints, flanges, nozzles etc. and these parts are manufactured through machining. The fabricated parts were welded using tungsten inert gas and electron beam welding techniques. Various sizes of Zr-4 tubes for the fabrication of dissolver assembly for nuclear fuel reprocessing plant are manufactured at Nuclear Fuel Complex, Hyderabad by multiple pilgering and annealing stages [15, 26].The flow chart employed for the production of Zr-4 tubes for dissolver assembly is shown in Figure 2.14 and all the Zr-4 tubes are manufactured by this process at NFC.

Zr-4 dissolver has been made up of 46 components (Tables 2.7 and 2.8).The dissolver is a U shaped tubular structure with flange openings at the top and drain outlets at the bottom, as shown in Figure 2.15. The main component of the assembly is a cylindrical tube of Ø 114 x 6 mm thick. Two vertical limbs of the U-tubular structure are connected to a horizontal member of Ø 114 x 6 mm thick tube, and 21 numbers of nozzles were welded to these two vertical members for different applications, viz., charging the load, filling the acid, inlet & outlet for the water jacket, temperature and pressure monitoring ports. All the major welds were done by electron beam (EB) welding and rest of the welds were done by TIG welding, due to limiting factors caused by their geometrical configuration. All the weld joints based on the weld configuration were qualified prior to the actual welds. These weld joints were tested by radiography test, liquid penetrant test, testing of weld microstructure of weld & parent material, and corrosion test on weld specimens. During the actual fabrication, the major welds were tested radiographically. Due to the geometrical configuration, the remaining welds were examined using only liquid penetrant test and were allowed for further fabrication. After fabricating the total assembly, it was subjected to helium leak test with an acceptance criterion of $<1x10^{-08}$ std.cc/s and was qualified [67].

The outer jacket for the dissolver was fabricated using Zr-4 sheet, which is rolled to form a tube and was longitudinally TIG welded. After fabrication, the entire dissolver assembly was cleaned and autoclaved at 520°C at the pressure of 10 kg/cm^2 to form a continuous black oxide layer. This oxide layer (50 micron thickness) helps in improving hot acid corrosion resistance of dissolver assembly [24].

Table 2.7: Tubes used for the fabrication of dissolver assembly and final heat-treatment

Size OD x wall thickness (mm)	12 x 2	21 x 2.5	28 x 3	41 x 6	52 x 9	114 x 6	20.8 x 2.5	114 x 6
Heat Treatment	Re-crystallized							

Table 2.8: Overview of the fabrication of various components of dissolver assembly

	Tubes for main body, other connections, thermo-well etc.(OD x wall thickness)	Elbow connector for interconnection	Nozzles (mm OD)	Flanges (OD x ID x T)
Sizes	12 x 2 mm 21 x 2.5 mm 28 x 3 mm 41 x 6 mm 52 x 9 mm 114 x 6 mm 20.8 x 2.5 mm 114 x 6 mm	Square Rod 140 mm and 114 mm milled hole to make right angle connector	13. 7 mm 21.3 mm 22 mm 23 mm 26.7 mm 28 mm 50 mm	200 x 117 x 10 mm 200 x 10 mm #127 x 118 x 6 mm
Process	**Cold pilgeredtubes**	**Machined from hot extruded slab**	**Solid swaged rod**	**Hot/ cold rolled stripes**

Tube 127mm OD x 118mm ID pipe required for cooling jacket for the limb was fabricated from cold rolled sheet by roll forming and TIG welding method.

2.5 Welding of Zirconium alloys

Welding of various Zirconium alloy components was one of the most critical operations in the fabrication of the dissolver assembly. Zirconium alloys have shown excellent weldability.

The following fusion welding methods were used for the fabrication Zirconium dissolverassembly.

- TIG (tungsten inert gas)
- EBW (Electron Beam Welding)

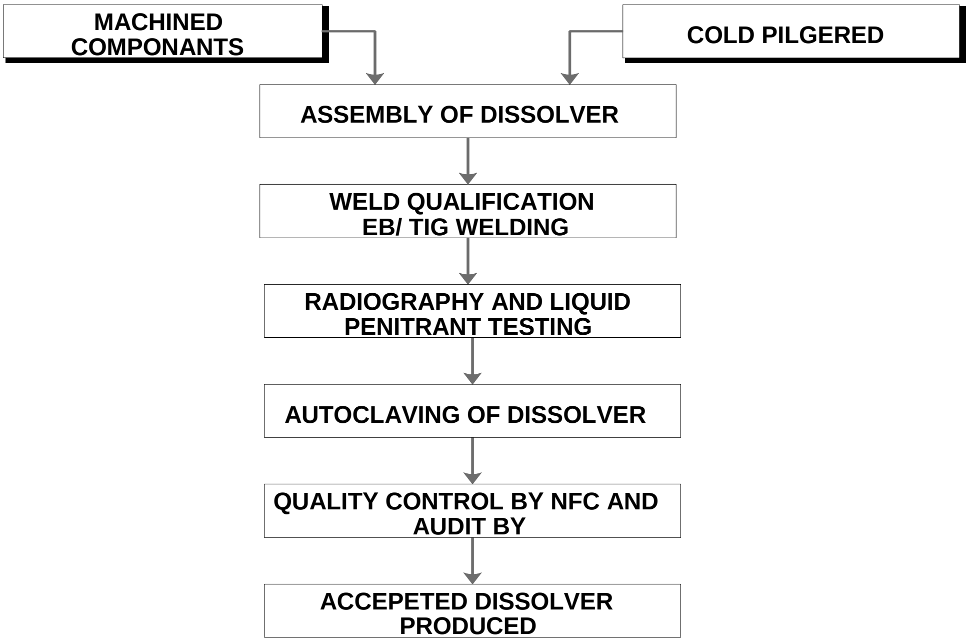

Figure 2.14: Process flow sheet for the fabrication of dissolver assembly

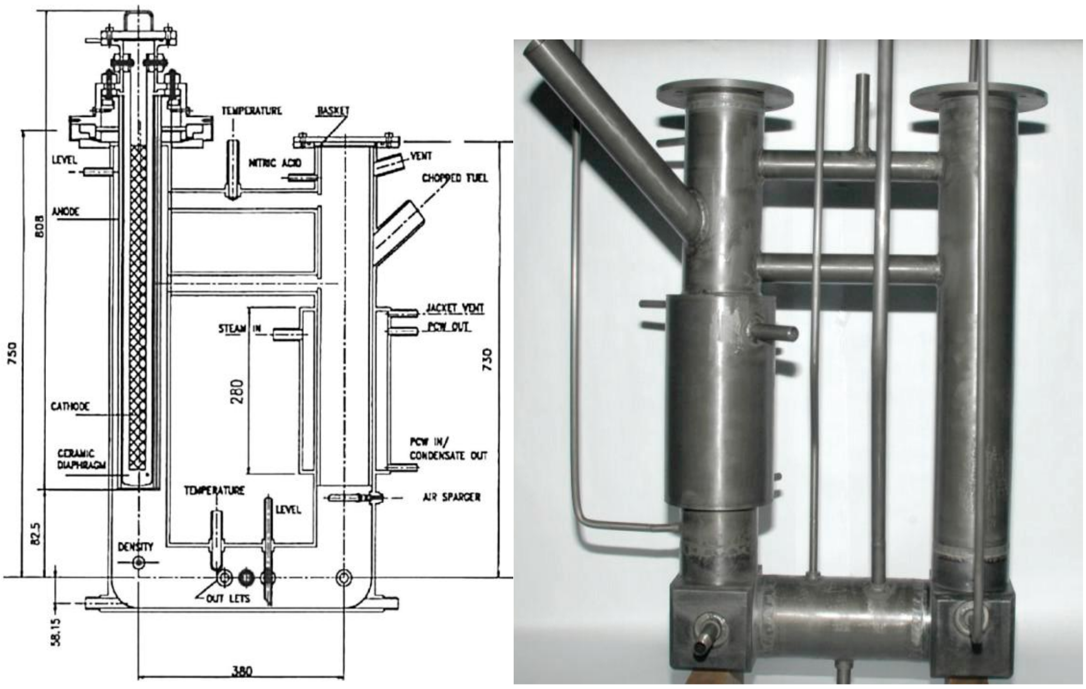

Figure 2.15: Schematic and fabricated Zr-4 dissolver assembly

During welding,microstructual changes occur in the fusion and HAZ of the material, resulting in changes in its mechanical properties. The fusion zone is that part of the material which has been heated in excess of the melting temperature while the HAZ corresponds to the area where the combination of time and temperature has been such that a change in the microstructure of the material takes place. The amount of heat injected by the welding process plays an important role. Processes like laser and electron beam welding give a highly concentrated and limited amount of heat, resulting in a small HAZ. TIG welding provides a lower heat input and consequently results in a larger HAZ. The corrosion behaviour of Zr-4 is very sensitive to its microstructure which is a result of chemical composition and thermal treatment (due to the welding process) [67-69].

2.5.1 Optimization of welding parameters (EB and TIG)

The welding parameters (EB and TIG) were optimised with respect to welding current, arc voltage, arc length and argon flow-rate, argon composition and welding speed (Table 2.9). This was ascertained by carrying out process and weld qualification test before making all the welds on the dissolver as shown in Figure 2.16. EB welding in the vacuum environment of < $2x10^{-4}$ mbar pressure is the best-suitedwelding procedure for this alloy. In this case, only a negligible amount of oxygen, nitrogen or hydrogen inclusions would be present in weld pool and heat affected zone.

Figure 2.16: EB Welding trials for optimization of process parameters.

Table 2.9: Optimised parameters of TIG and EB welding

Welding parameter	**TIG welding**	**EB welding**
Speed	300 mm/min	1000 mm/min
Current	60 A	24 mA
Voltage	----	45 kV
Gas flow	Torch – 8 IGPM (50% Argon and 50% Helium)	----
Vacuum	----	5×10^{-4}mbar

2.6 Materials studied

Zirconium alloys like Zr-2, Zr-4, Zr-2.5%Nb and Zr-1%Nb are being manufactured on industrial scale at the production facility at NFC, Hyderabad, these materials were studied to evaluate their properties. Apart from the above Zirconium alloys, pure Zirconium (unalloyed) was also manufactured specially.

2.7 Characterization of materials

Characterization of materials for study of microstructural changes during thermo-mechanical processing was carried out using Optical Microscopy (OM), Scanning Electron Microscopy (SEM), Energy-dispersive X-ray spectroscopy (EDS), X-ray diffraction (XRD) and Electron Backscatter Diffraction (EBSD) methods. Based on themomechanically processed Zirconium alloys, the experimental matrix was chosen for the evaluation of microstructure, mechanical properties and corrosion resistance (Table 2.10).

2.7.1 Optical microscopy (OM)

The optical microscope is the oldest and the most commonly used instrument for characterization of a variety of materials from micron to sub-micron level. The optical microscope is the conventional and the most familiar device for magnifying a small specimen that cannot be viewed by naked eye. Optical microscopy is a simple lens system consisting of an objective lens with a short focal length (few mm), which creates an image of the object in the intermediate image plane. This image in turn can be viewed with another lens, the eye-piece, which can provide further magnification [70-72]. Conventional optical microscopy still maintains its position as the easiest, fastest and the most widely used method of micro-characterization tools.

Table 2.10 Properties evaluation and Corrosion Studies carried out on different thermo-mechanically processed Zirconium alloys

Sl No	**Material**	**Evaluation of mechanical and microstructural properties**				**Corrosion Studies**			
		Hardness	Mech.	OM	SEM	Practice C	Loop Exp.	SEM	Anodic Pol.
1	Zr Cast (Pure Zr)	√	√	√	√	√	√	√	
2	Zr -2 Cast	√	√	√	√	√	√	√	√
3	Zr-2 Extruded	√		√	√				
4	Zr- 2 Tube	√	√	√	√	√	√	√	
6	Zr -4 Cast	√	√	√	√	√	√	√	√
7	Zr-4 Extruded	√		√	√				
8	Zr-4 Forged	√		√	√				
9	Zr- 4 sheet	√	√	√	√	√	√	√	√
10	Zr- 4 Fuel Tube	√	√	√	√	√	√	√	√
12	Zr- 4 Calendria tube	√	√		√				
13	Zr- 2.5 % Nb Cast	√	√	√	√	√	√	√	√
14	Zr-2.5 % Nb Extruded	√		√	√				
15	Zr- 2.5 % Nb Forged	√			√				
16	Zr-2.5 % Nb Coolant Tube	√	√	√	√	√	√	√	√
17	Zr- 1 % Nb Cast	√			√	√	√	√	
18	Zr- 1 % Nb Extruded	√			√				
19	Zr- 1 % Nb tube		√		√	√	√	√	

Detailed characterization of the Zirconium alloy sample and the microstructural features was carried out by optical microscopy. The microstructural characterization was done by examination of the cross-sections of as cast and product samples under an optical microscope. Optical microscopy consists of studying back–reflected light from polished (and often chemically etched) surfaces of metal samples. By using polarized light, after anodization of the polished surface, it is often possible to clearly distinguish between regions of different crystallographic orientation. The size, shape, and location of individual grains or groups of grains can be determined, but the crystallographic orientation of the individual grains is not determined directly. The specimen was ground and polished using standard metallographic procedure, the polished surface of the specimen was chemically etched using a solution containing HF (10 vol. %), HNO_3 (45 vol. %), and Lactic Acid (45 vol. %) [71, 72]. The optical microscope (Olympus, Japan) model was used for the characterization in the thesis.

2.7.2 Scanning electron microscopy (SEM)

Scanning electron microscope (SEM) is one of the most advanced imaging tools for microstructural analysis wherein the images of the specimen are formed by scanning with a high-energy electron beam. The interaction of electrons with the atoms of the specimen produces signals which provide information mainly about the specimen's surface topography and composition. The electron beam is thermionically emitted from an electron gun fitted with a tungsten filament cathode or lanthanum hexaboride (LaB6) cathode. The accelerated electron beam of energy around 0.2 to 40 keV is focused by one or two condenser lenses to a spot of about 0.4 to 5 nm in diameter. The accelerated electron beam (primary electron beam) interacts with the surface of the specimen and the electrons lose their energy by repeated random scattering and absorption within a teardrop-shaped volume of the specimen known as the interaction volume. Secondary electron (SE), back scattered electron (BSE) and absorbed electrons are produced due to energy exchange between the electron beam and the specimen, each of which can be detected by specialized detectors. Various types of electronic amplifiers are used to amplify the signals and are displayed as variations in brightness on a cathode ray tube (CRT). The raster scanning of the CRT display is synchronised with that of the beam on the specimen in the microscope, and the resulting image is therefore, a distribution map of the intensity of the signal being emitted from the scanned area of the specimen. The image can be captured by photography from a high-resolution cathode ray tube, but in modern technology it can be digitally captured and displayed on a computer monitor and saved in a computer's hard disk [77].

In SEM an electron beam impinges upon the surface of a sample, and informationis obtained from the backscattered electrons as well as the emitted X–ray photons. In modern scanning electron microscopes, the spatial resolution may be as good as ~10 nm. SEM a quantitative technique that reveals grain size, grain boundary character, grain orientation, texture, and phase identity from the polished surface of metallurgical, ceramic, and geological samples. Depending on the scanning electron microscope used, the technique enables analysis of up to cm–sized samples with grains varying in size from the nm to mm range. SEM has been used for detailed characterization of the near surface layers. The samples were examined in SEM in secondary electron mode.

In the present thesis SEM was used to characterize:

1. Zirconium alloys specimens at different conditions such as as-cast ingot, hot extruded, pilgered and final annealed
2. Zirconium alloys specimens exposed corrosive environment study (Practice "C" and loop study)

For characterizing the Zirconium based alloys at different thermo-mechanical processing stages (as cast, β quenched and extruded and final product), metallographic sample preparation of the specimens is required. The samples to be tested were cold mounted with epoxy resin and the mounted samples were prepared according to ASTM E3-11standard [53] and polished up to 0.3 μm using diamond paste. To reveal the microstructure, the final polished samples were etched using a solution consisting of HF (10 vol. %), HNO3 (45 vol. %), and Lactic Acid (45 vol. %). Care was taken to minimize the polishing and grinding duration, in order to avoid unnecessary material removal and smearing of small pores during the polishing. The sample for was cleaned with acetone in a ultrasonic cleaner to remove loose contaminations. The etched samples were analyzed using SEM (LEO VP-450).

2.7.2.1 Energy-dispersive X-ray spectroscopy (EDS)

Energy dispersive X-ray spectroscopy (EDS), is an analytical technique used for the elemental analysis or chemical characterization of a sample. It relies on an interaction of some source of X-ray excitation and a sample. Interaction of the primary beam with atoms in the sample causes shell transitions which result in the emission of an X-ray. The emitted X-ray has an energy characteristic of the parent element. Detection and measurement of the energy permits elemental analysis EDS can provide rapid qualitative, or with adequate standards, quantitative analysis of elemental composition with a sampling depth of 1-2 microns. X-rays may also be used to form maps or line profiles, showing the elemental distribution in a sample surface.

The Scanning Electron Microscope is equipped with an Energy Dispersive Spectrometer (EDS). SEM/EDS provides chemical analysis of the field of view or spot analyses of minute particles. More than 90 elements can be detected with our low-atomic number detector using the SEM/EDS method. This micro-chemical analysis is also a non-destructive test.

In the present thesis SEM attached with energy dispersive X-ray spectroscopy (EDS) was used to characterize the Zr-2 and Zr-4 pilgered and annealed tubes for microstructural and elemental composition analyses for second phase particles. SEM-EDS used in the present thesis is of FEI, Helios NanoLab600i make. The sample for prepared for SEM analysis were used in EDS.

2.7.3 X-ray diffraction **analysis** *(XRD)*

X-ray diffraction (XRD) is a rapid and non-destructive analytical technique used for phase identification of a crystalline material and can provide detailed information about the crystallographic structure of naturally occurring and synthetic materials. XRD is based on the constructive interference of monochromatic X-rays and a crystalline material. The X-rays are generated by a cathode ray tube, filtered to produce monochromatic radiation, collimated to concentrate and directed towards the specimen. A constructive interference (and a diffracted ray) is produced by the interaction of the incident rays with the specimen by satisfying Bragg's Law ($n\lambda=2d\sin\theta$). This law relates the wavelength of electromagnetic radiation (λ) with the diffraction angle (θ) and the lattice spacing (d) in a crystalline specimen. The diffracted X-rays are then detected, processed and counted. By scanning the specimen over a range of 2θ values, all possible diffraction directions of the lattice could be obtained due to the random orientation of the powdered material. Conversion of the diffraction peaks to d-spacing allows the identification of the crystalline materials because each material has a set of unique d-spacing. Typically, this is achieved by the comparison of d-spacing with standard reference patterns [73-76].

Important information that can be obtained from the XRD analysis are:

(1) Identification of crystalline phases and orientation,

(2). Determination of structural properties: Lattice parameters (10-4Å), strain, grain size, expitaxy, phase composition, preferred orientation, order-disorder transformation and thermal expansion),

(3) Measurement of thickness of thin films and multi-layers and

(4) Determination of atomic arrangement.

In the present work XRD studies were carried out for unalloyed Zirconium, Zr-2, Zr-4 and Zr-2.5%Nb alloys was carried out for different thermomechanical processes such as i) as-cast ingot, ii) hot extruded and iii) final pilgered and annealed condition.

The XRD patterns obtained were compared with the standard JCPDF database and available literature. The XRD scans were recorded using Rigaku Dmax 2000 with Cu Ka radiation (λ= 0.154nm or 1.54A˚) as the X-ray source (40 kV and 30mA with Ni filter). Samples were tested in the 2θ angle range 30°–140°, at scan steps of 0.05°2θ/step and scan speed of 1°2θ/min. Monochromatic $K\alpha_1$ was obtained (with K_β peak separation) using the diffracted beam from a crystal monochromator. The $K\alpha_2$ stripping was carried out by using software (assuming $K\alpha_2$/ $K\alpha_1$ intensity ratio as 0.5), smoothening was carried out by Savitzket Golay’s method, and back- ground correction by the Sonnevelt–Visser method.

specimens for product like as cast ingots, extruded/forged , β quenched , pilgered and cold rolled for the XRD scan are prepared by hot mounting on the resin substrate (200ºC & 4200 Ksi). Due to smaller wall thickness in some cases, composite samples are prepared. In this sample, a number of cut pieces (with identical orientation) are stacked together to form a large surface area of 15mm by 10mm for exposure to the X-Ray beam. Surface of the sample is made flat by successive metallographic polishing and finally chemical polishing with 45 % HNO3, 5 % HF, and 50 % H_2O to dissolve around 0.05mm thickness of the sample is carried out to ensure that no deformation layer due to mechanical grinding/polishing exist. These specimens were metallographic ally polished up to 600 grit emery paper. Specimens were immediately cleaned with 45% HNO_3 & 10% HF solution.

Following experimental and processing parameters were used:

Table 2.11 Experimental and processing parameters for XRD

Experimental and processing parameters for XRD	
Scan speed	1 degree/minute
Smoothening:	Savitzket Golay’s method; smoothening points-5
Background Correction	Sonnevelt–Visser’s method –maximum width of peak- 2.0; minimum peak height - 50
$K_{\alpha 2}$ Stripping intensity ratio	0.5

2.7.4 *Electron Backscatter Diffraction (EBSD)*

EBSD is a technique based on measurement of local crystallographic orientation. EBSD measures the orientation of very small volumes of material at specific points on the surface of a sample by using electron diffraction in an electron microscope. Since this technique provides orientation information at a sub-micron spatial location, it enables to relate the crystal orientation to the microstructure. The orientation of a single point in a sample can be distinguished, by EBSD and fast automated orientation analysis is possible, by which orientation maps can be constructed with increasing spatial resolution, in most modern systems as small as 0.05μm. The specimens for EBSD are positioned in a SEM in such a way that a small angle is formed between the incident beam and the surface of the sample. This reduces the path of the electrons that are backscattered in the specimen when the electron beam hits the sample, and increases their chances to be detected. The electron backscatter pattern (or so-called Kikuchi pattern) produced in this way is detected by a phosphor screen, and is the fundamental principle of EBSD. The Kikuchi pattern is unique according to the crystal structure and its orientation with respect to a reference frame. Special algorithms have been developed to solve Kikuchi patterns, which allows determining the crystal structure and the orientation of each point. Figure 2.17 illustrates the main components of an EBSD acquisition system [73-75].

Modern computer systems allow the scanning of millimeter scale areas and automatic storing of the crystallographic orientation of millions of points. In modern systems each point can be stored at a rate as high as 400/s. Speed, spatial resolution, and accuracy depend on several factors such as specimen geometry, material, algorithm parameters, microscope voltage/current, and surface preparation. In EBSD measurements, the statistical distribution of orientation data is often aimed to quantify the orientation distribution within a specific region of the microstructure.

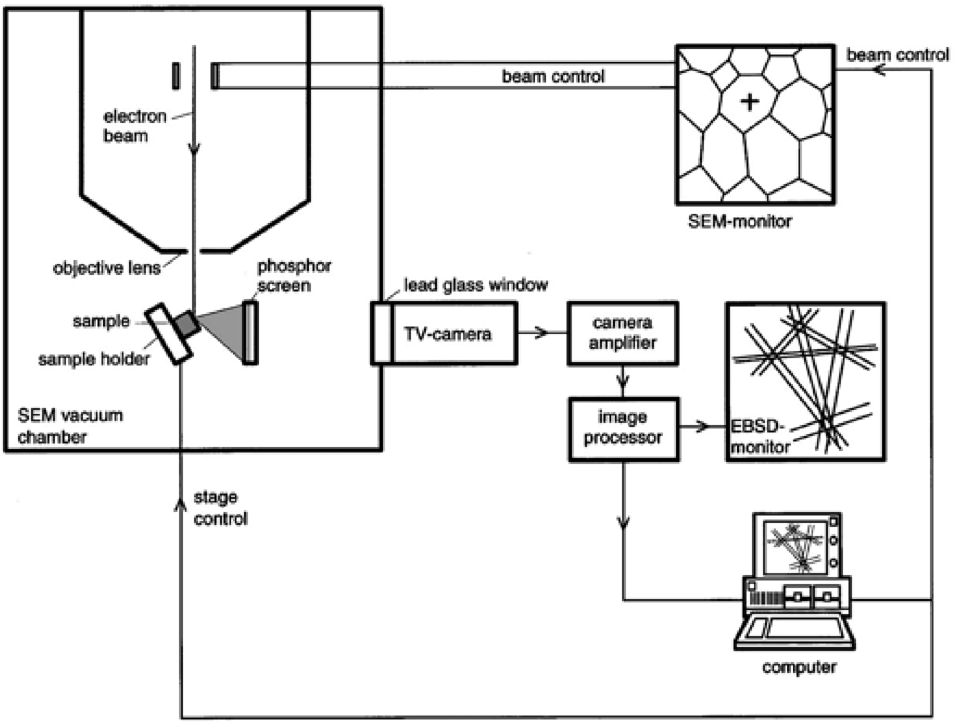

Figure 2.17: Schematic arrangements of all the components of an EBSD with acquisition system.

The EBSD samples were prepared carefully as Zirconium alloys are soft and ductile and prone to formation of mechanical twins during sectioning, mounting, grinding and polishing. Copious water-cooling was used with long grinding periods, and always fresh SiC paper was used for polishing. Samples were etched and ultrasonically cleaned.

2 . 8 Mechanical properties evaluation

The mechanical properties of Zirconium alloys have been carried out at room temperature. As these properties are quite sensitive to specimen history, i.e. Thermo-mechanical processing steps. Even small variation in fabrication procedure can affect the mechanical properties. Impurities such as oxygen, nitrogen and hydrogen can significantly affect the mechanical properties. Although Zirconium is a high-melting-point metal, with respect to its mechanical properties its behaviour is more closely similar to that of metal with much lower melting temperature. Thus its elastic modulus is quite low, and its strength diminishes rapidly with increasing temperature. The mechanical properties of Zirconium alloys are reasonably good at room temperature and at elevated temperature. It is important that mechanical strength tests are carried out on a large number of specimens subjected todifferent thermal treatments.

2.8.1 Tensile testing

Tensile testing is the fundamental testing procedure in which the sample is subjected to controlled tensile load, until its failure. The results of the test are used for material selection and its behaviour under different loading condition. Properties that are directly measured via a tensile test are ultimate tensile strength and maximum elongation. From these measurements, properties like young's modulus, yield strength and strain hardening characteristic can be determined. The tensile test for all the specimens was carried out using INSTRON universal testing machine. The output parameters such as Yield Strength (YS) and Ultimate Tensile Strength (UTS) for all the Zirconium alloys were determined and recorded. Tensile strain was measured using an extensometer attached directly to the specimen gauge length.

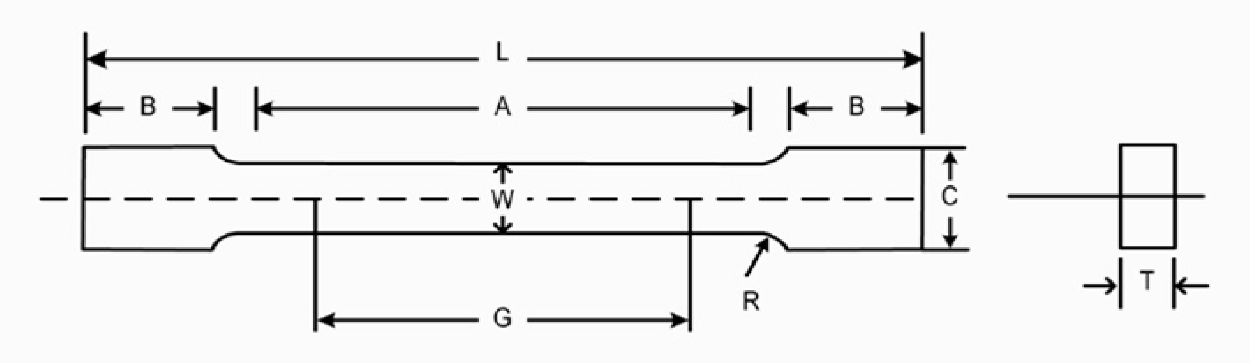

G-Gauge Length	W- Width	T-thickness	R- radius of fillet	L- Overall length.	A-Length of the reduced section	B- Length of grip section	C- width of grip section b
25.0∓0.1 mm	6.0∓0.1 mm	4.0∓0.1mm	6 mm	100 mm	32 mm	30 mm	10 mm

Figure 2.18 Dimensional details of tensile test specimen 0.8 mm sheet

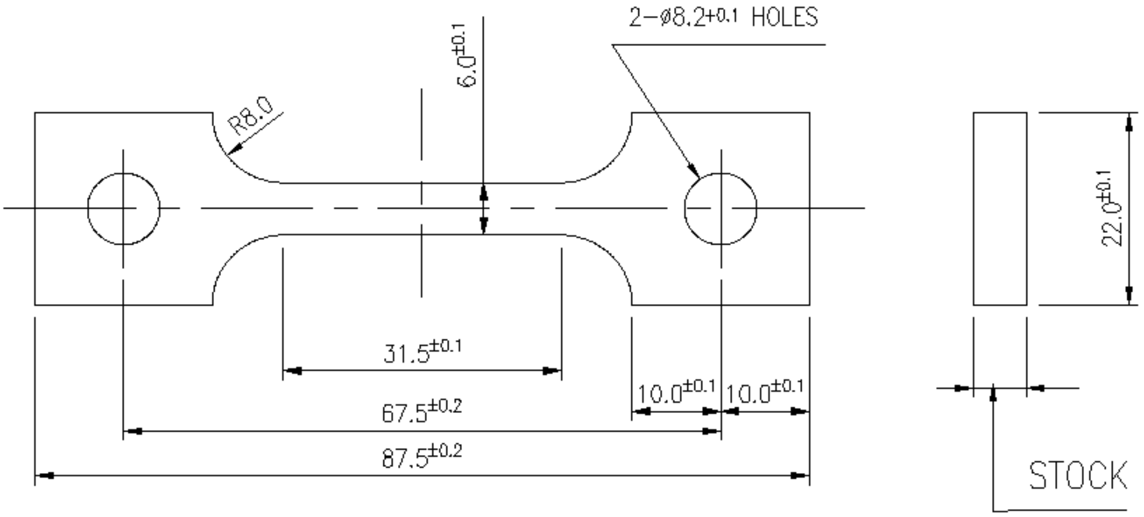

Figure 2. 19: Dimensional details of tensile test specimen 4mm from as cast ingot, extruded/forged billets, hot rolled sheet and coolant tubes (all dimensions are in mm).

Mechanical testing specimens required for tensile testing were prepared as per ASTM-E8/E8M-11 [55] test procedure (Standard test method for tension testing of metallic materials). Standard dog-bone shaped tensile testing specimen of 4 mm thick with standard gauge length of 25.4 mm was prepared from as-cast ingot and extruded billet as shown in Figure 2.19, and cold rolled sheet as shown in Figure 2.18. In order to evaluate the mechanical properties of pilgered tubes and tubes in annealed conditions, “Instron make” universal tensile testing machine was used for tensile testing. For tube testing, the gauge length 50 mm was taken. The accuracy of measurements was ± 5 %. The strain rate applied was 0.7 ± 0.3 % per min up to the yield strength. Beyond the yield strength, the crosshead speed was increased to 5 ± 2 % per min

Tensile test machine used for testing Zirconium alloys samples at NFC is the closed-loop servo-hydraulic system shown schematically in Figure 2.20. Applied force or load is measured by a load cell and elongation of the specimen is obtained by an extensometer attached. The extensometers include LVDTs (linear variable differential transformers), strain gauges, and non-contact laser devices. The test specimen is attached to the loading/strain system by appropriate standard grips as per ASTM Standard E8/E8M commendations. Grips and load-bearing components are made of high strength-creep resistant alloys such as 17-4 PH stainless steel. Strain rate on the specimen during the test can be important. Normally strain rates are in the range $3x10^{-5}s^{-1}$ (slow) to $1x10^{-3}s^{-1}$ (fast). For the Zirconium alloy samples tested at NFC, tensile strain was measured ±0.000l accuracy, using an extensometer attached directly to the specimen gauge length.

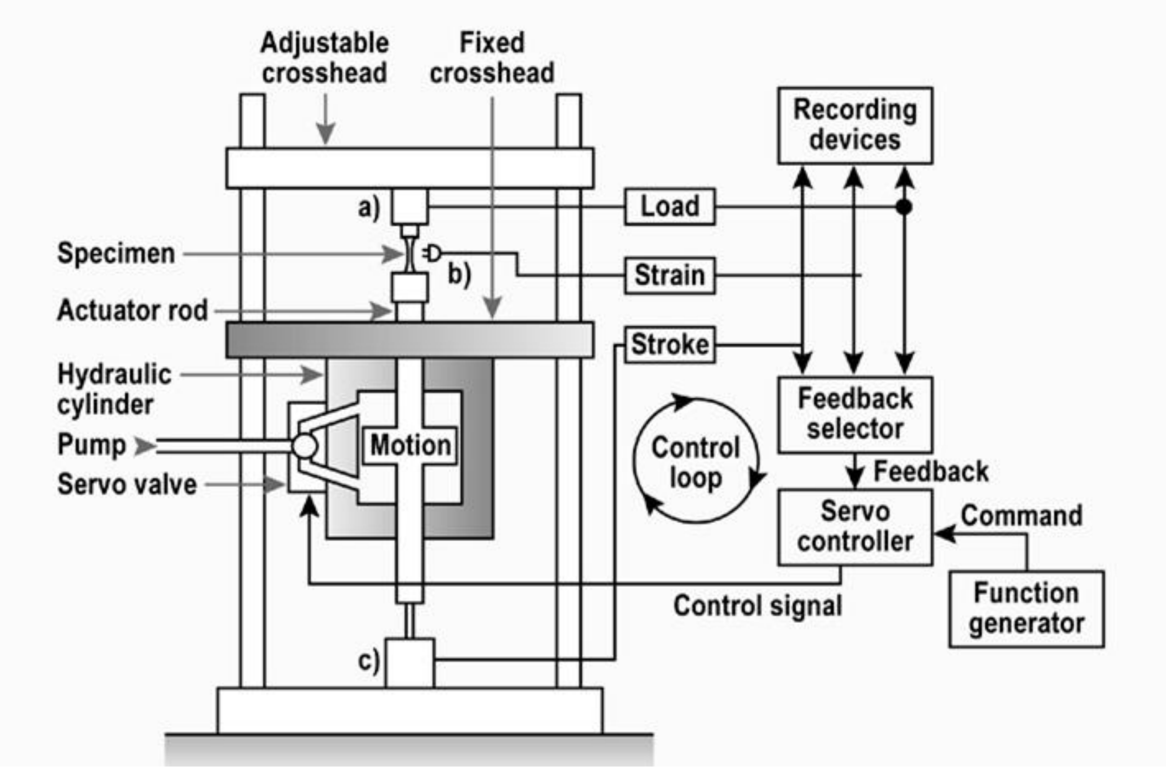

Figure 2.20: Schematic diagram showing closed-loop servo-hydraulic testing system where three sensors are employed: (a) load cell, (b) extensometer, and (c) LVDT.

2.8.2 Hardness Measurement

The Vickers hardness test method consists of indenting the test material with a diamond indenter, in the form of a right pyramid with a square base and an angle of 136° between opposite faces, which is subjected to a load of 1 to 100 kgf. The full load is applied for 10 to 15 second. The two diagonals of the indentation left out on the surface of the material after removal of the load are measured using a microscope and their average value calculated. In the present study, microhardness of various Zirconium alloys with different thermomechnical processes was determined with a load of 200 g applied for 15 s on various regions using

METATECH microhardness tester. The testing body was a four side diamond-pyramid which locks in an angle of 136°. A quadrangle impression is made by the plastic deformation caused by the diamond indenter. With a videographic system, the diagonal marks of the quadrangle and the area of the sloping surfaces of the indentation is calculated automatically, which gives Vickers hardness value.

2.9 Corrosion studies

To evaluate the extent of corrosion on various alloys and thermo mechanical processing, the corrosion studies were carried out by two different methods:

- ASTM Practice C: The corrosion tests were conducted asper ASTM standard 262A practice C [54].
- Long Term Studies: To Study long term corrosion behaviour in boiling nitric acid environment.

ASTM 262A Practice C test

Specimens of pure Zirconium and Zr-2, Zr-4, Zr-2.5%Nb and Zr-1%Nb in as-cast , extruded, forged, pilgerd tubes and rolled and annealed condition were evaluated for their corrosion resistance in boiling concentrated nitric acid solution.

Sample Preparation

The dimensions of corrosion test specimens used for pure Zirconium and Zr-2, Zr-4, Zr-2.5%Nb and Zr-1%Nb in as-cast-ingots, extruded billets and forged rods are given in the Table 2.11. From pilgered tubes and rolled sheets the sample with 0.4 mm and 0.8 mm thickness were used. These specimens were polished up to 600 grade SiC paper, degreased, washed and dried. The surface area of the specimens was measured within ±1% and the initial weight was determined with a precision of 0.2 mg. For products like fuel tube, sheet; the as-produced materials were tested. For Zr-2 and Zr-2.5%Nb alloy tubes, autoclaved black adherent oxide layer was not removed and kept intact for comparison with un-oxidized products like Zr-4 tube and sheet sample.

Table 2.12: Weight and dimensions of the Specimens used for practice C

SAMPLE	Wt. (gms)	L (mm)	b (mm)	h (mm)
Zr cast	7.3636	20.19	19.45	3.03
Zr-2 cast	8.6772	19.79	19.46	3.58
Zr-2 tube	4.6763	*H = 19.84*	*OD =14.27*	*ID =12.40*
Zr-4 cast	9.3862	19.66	19.17	3.99
Zr-4 tube	2.5412	*H = 19.89*	*OD =15.21*	*ID =14.24*
Zr-4 CR Sheet	3.2028	20.45	19.78	1.50
Zr-1% Nb cast	9.0168	20.77	18.62	3.74
Zr-1% Nb tube	0.7604	*H = 21.40*	*OD =4.56*	*ID =3.52*
Zr-2.5%Nb tube	10.9447	19.79	19.49	4.50
Zr -2.5%Nb cast	9.1280	22.91	19.05	3.05

Immersion ASTM 262 A Practice "C" Corrosion testing experimental setup

The corrosion tests were conducted as per ASTM standard practice C. These specimens were degreased in acetone and dried in hot air, and weighed before immersing them into the test solution of boiling 11.5 M nitric acid. The experimental setup used for the present study is shown in Figure 2.21. The specimen was suspended into the test solution with the help of a Teflon thread. A cold-finger condenser was used to reflux nitric acid vapors into the test solution. The ratio of solution volume to specimen surface area was about 50ml/cm^2. The samples were exposed to boiling 11.5 M HNO_3 solutions for five periods of 48 h. To observe the changes in the appearance and to measure the changes in the weight, the specimen was removed after every 48 hours, and fresh test solution was used for each period. After the each period (tests), the coupons were washed, dried and re-weighed and the corrosion rate was calculated from surface area, weight-loss, density and exposure time. Necessary care was taken to avoid the formation of crevices on the specimen. SEM analyses were carried out to observe respectively the changes in the surface morphology and the oxide phases present [23].

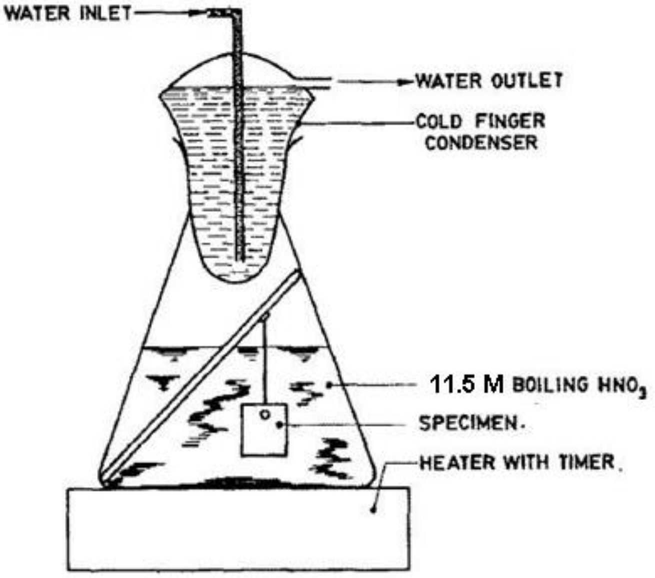

Figure 2.21: Experimental setup for corrosion tests (boiling nitric acid medium)

2.9.1 Long Term Corrosion Studies

Long term corrosion studies were conducted to study long-term corrosion behavior in boiling nitric acid environment. Specimens of pure Zirconium and Zr-2, Zr-4, Zr-2.5%Nb and Zr-1%Nb in as-cast-ingot, extruded, forged, pilgered tubes and rolled and annealed condition were evaluated for their lon-term corrosion resistance in boiling concentrated nitric acid solution for 1000h exposure period.

Sample Preparation

Sample preparation was carried out as per the sample preparation procedure mentioned for ASTM 262A Practice C.

Long term Corrosion testing experimental setup

Long term corrosion studies were conducted to study long term corrosion behavior in boiling nitric acid environment in experimental setups shown in Figure 2.22. A high temperature, high-concentration Zr-4 test facility of 10 liters capacity was designed and fabricated at NFC and commissioned at IGCAR. Since dissolution is carried out under boiling conditions, in this test facility provisions were made to expose Zr-4 test samples in liquid, vapour and condensate conditions for long durations. At the top portion of the system, an inner vessel was made of Zr-4 to collect condensed nitric acid. The condensed nitric acid was collected and automatically removed to the bottom portion through a siphon pipe, and renewed at regular intervals. The samples were held in the liquid phase using polytetrafluoro ethylene (PTFE) thread. Specimensfor Zr-4 in as-cast, extruded, pilgered and autoclaved conditions were used to evaluate their corrosion resistance in concentrated nitric acid solution. In corrosion test, a specimen used was shown in Figure 2.22 in the form of as-cast ingot, pilgered tubes and in autoclaved conditions. These samples were exposed to boiling 11.5 M nitric acid for 1000 h. The change in weight loss, before and after the exposure period was used to calculate the corrosion rate [23].

Figure 2.22: High temperature high concentration experimental setup for corrosion tests in boiling nitric acid medium. (11.5 M HNO_3).

Table 2.13 weight and dimensions of the Specimens used for long term corrosion testing. Zr-2 tube and Zr - 2.5%Nb tube are autoclaved tubes.

SAMPLE	Wt. (gms)	L (mm)	b (mm)	h (mm)
Zr cast (A)	7.4586	20.78	19.16	3.00
Zr-2 cast (B)	9.1288	20.17	20.05	3.56
Zr-2 tube	4.6425	*H = 19.64*	*OD =14.27*	*ID =12.56*
Zr-4 cast	9.9637	20.64	19.51	3.93
Zr-4 tube	2.6534	*H = 20.72*	*OD =15.20*	*ID =13.85*
Zr-4 CR Sheet	3.2028	19.30	17.92	1.49
Zr-1% Nb cast	9.1661	20.90	19.24	3.63
Zr-1% Nb tube	0.7300	*H = 20.54*	*OD =4.45*	*ID =3.59*
Zr -2.5%Nb tube	12.2642	22.16	19.38	4.54
Zr -2.5%Nb cast	9.1660	21.08	19.24	3.64

2.9.2 Surface film analysis

The surface morphology of the specimens subjected to ASTM 262A Practice “C” after Corrosion and Long term Corrosion testing were examined in a scanning electron microscope (SEM) and the passive film formed was analyzed using LASER Raman Spectroscopy (LRS) and XPS.

Raman spectroscopy

Raman spectroscopy is a relatively easy and non-contact method to probe the inelastic scattering of light from a sample surface at room temperature and ambient pressure [76]. Raman spectroscopy involves molecular and crystal lattice vibrations and is therefore, sensitive to the composition, bonding, chemical environment, phase and crystalline structure of the material in any physical form: gases, liquids, solutions, and crystalline or amorphous solids [76]. The Raman phenomenon is a consequence of the interaction of materials with a monochromatic photon beam (laser), most of which are absorbed, reflected or transmitted by the sample. However, a small fraction of photons are scattered. During this interaction, some energy is transmitted to elementary particles of which materials are constituted (electrons, ions etc.). This causes their transition from ground energy levels to ‘virtual’ excited states. These excited states are highly unstable and the particles decay instantaneously to the ground state by one of the following three different processes, as shown in Figure 2.23, (a) Rayleigh scattering (elastic scattering) b) Stokes and (c) Anti-Stokes Raman photons (inelastic scattering). Rayleigh scattering the emission of a photon of the same energy allows the molecule to relax to its ground vibrational state. Rayleigh scattering, therefore, bears no information on vibrational energy levels of the sample. Emission of a photon with energy either below or above that of Rayleigh photons generates a set of frequency shifted ‘Raman’ photons. The energy difference of the Stokes and anti-Stokes Raman photons with respect to the excitation energy gives information about molecular vibrational levels. These photons are collected by a detector and transformed to electrical signals and finally to the corresponding Raman spectrum. Usually, Stokes bands which are more intense than anti-stokes bands are called “Raman spectrum” of the sample. The Rayleigh band is filtered out before reaching the detector [76].

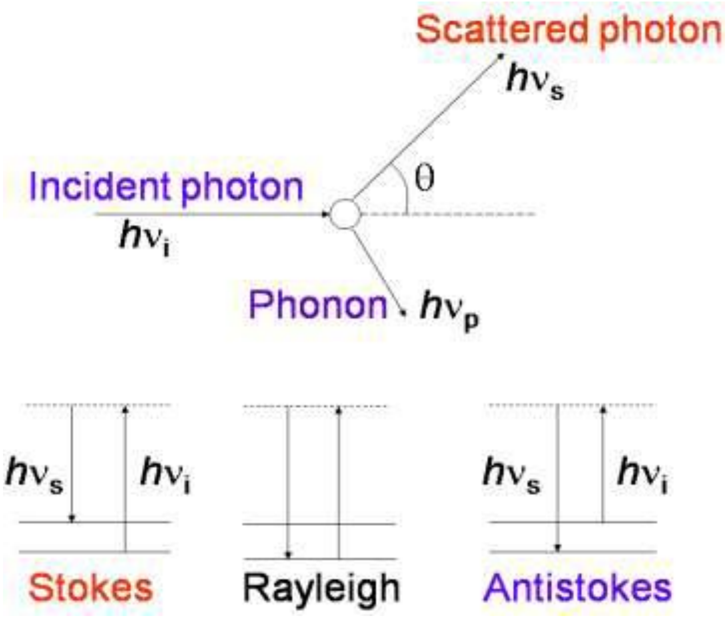

Figure 2.23: Energy level diagrams showing the states involved in Raman signal.

Raman imaging is an extension of Raman microspectroscopy. One key benefit of Raman imaging is that the powerful Raman spectral information can be presented in a visual format and which can be more easily understood. Raman imaging combines Raman spectroscopy with digital imaging technology in order to visualize chemical composition and molecular structure of materials to produce molecular chemical images of materials. Typically, image contrast reveals the distribution of molecular composition based on the "fingerprint" Raman spectral identification. Raman spectroscopy is also considered as a bulk technique because the optical penetration depth of the visible lasers typically used as excitation sources is too long to have a large collection of volumes [80]. Typically, image contrast reveals the distribution of molecular composition based on the "fingerprint" Raman spectral identification.

In the present thesis, Raman spectral analysis of the surface of the Zr-4 pilgered tube and autoclaved Zr-4 exposed to the boiling liquid phase of 11.5 M nitric acid for 1000 h was characterized by LASER Raman Spectroscopy (LRS). HR800 (Jobin Yvon) Raman spectrometer equipped with 1800 grooves/mm holographic grating was used. The samples were placed under an Olympus optical microscope mounted at the entrance of the Raman spectrograph. Argon ion laser of wavelength 488 nm was used as an excitation source. The laser spot size of 3 µm diameter was focused on the sample surface using a 50X (NA = 0.75) objective. The laser power at the sample was ~10 mW. The slit width of the monochromator was 400 µm. The back scattered Raman spectra were recorded using a super cooled charge coupled device (CCD) detector, over the range 80 -800 cm^{-1} with 5 s exposure time and 20 CCD accumulations. All the spectra were baseline corrected [48].

X-ray photoelectron spectroscopy (XPS) analysis

XPS is a surface chemical analysis technique that can be used to analyze the surface chemistry of a material in its as-received state, or after some treatment. XPS is a surface-sensitive quantitative spectroscopic technique that measures the elemental composition at the parts per thousand range, empirical formula, chemical state and electronic state of the elements that exist within a material. XPS spectra are obtained by irradiating a material with a beam of X-rays, while simultaneously measuring the kinetic energy and number of electrons that escape from the top 0 to 10 nm of the material being analyzed. XPS requires high vacuum ($P \sim 10^{-8}$ millibar) or ultra-high vacuum (UHV; $P < 10^{-9}$ millibar) conditions [47]. A schematic arrangement of all the components of XPS is shown in Figure 2.24. The origin of passivity of final pilgered and subsequently annealed Zr-4 sample exposed to boiling 11.5 M HNO_3 for 1000 h was determined by analyzing the surface film by XPS. Depth profile of the passive film was carried out by sputtering at intervals of 0 (as received), 30, 60, 180, 300, 420 and 540 s.

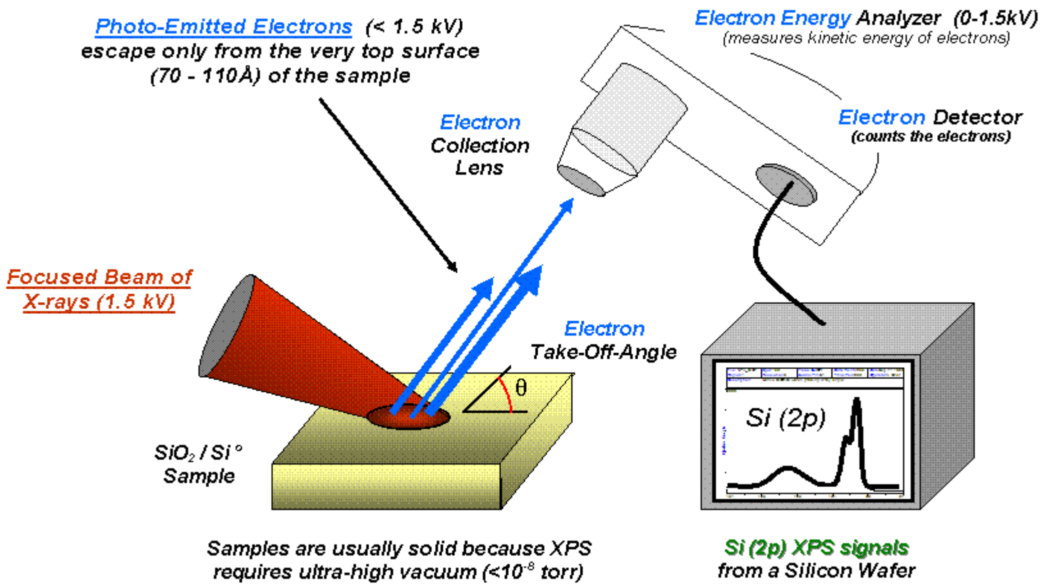

Figure 2.24: Schematic arrangements of all the components of XPS

2.9.3 *Electrochemical characterization*

Three-electrode corrosion cell setup used to carry out the open circuit potential and the potentiodynamic polarization experiments to study the passivation behavior of Zirconium based alloys in 11.5 M nitric acid at room temperature has been described. Potentiodynamic polarization behavior of Zr-4 samples in 11.5 M nitric acid Zr-4 pilgerred tube and Zr-4 autoclaved tube of exposed surface area of 1 cm^2 was used working electrode, Ag/AgCl (3M KCl) as reference and platinum as counter electrode respectively, were used to characterize the electrochemical behavior. Except the autoclaved Zr-4 sample, the surface of pilgered tube was ground up to 1200 grit SiC paper and both the samples were cleaned with acetone, washed in distilled water and air dried to promote reproducible surfaces for the electrochemical studies. In all the electrochemical measurements, the potential was referred with respect to Ag/AgCl (3M KCl) reference electrode. The open circuit potential (OCP), and potentiodynamic polarization behavior of the samples were evaluated in 11.5 M HNO_3 in the temperature range 20-22 °C (hereinafter referred as room temperature), in an aerated condition using a potentiostat [44, 48]. The OCP was monitored for 7200 seconds prior to the tests and a stable OCP value was obtained for all the conditions. After measuring OCP, potentiodynamic polarization tests were performed from 200 mV below OCP to transpassive potential or 2.5 V, at the scanning rate of 0.166 mV/s.

CHAPTER III

EVOLUTION OF MICROSTRUCTURE AND MECHANICAL PROPERTIES AT DIFFERENT STAGES OF THERMO-MECHANICAL TREATMENTS FOR ZIRCONIUM ALLOYS

3.1. Introduction

In this chapter, emphasize is given to the importance of the microstructure evolution and mechanical properties at different stages of thermo-mechanical treatments during processing Zirconium alloys viz; Zr-2, Zr-4, Zr-1%Nb and Zr-2.5%Nb. The evolution of microstructure at different stages of production of Zirconium products was characterized using Optical Microscopy (OM), Scanning Electron Microscopy (SEM), SEM-EDX, XRD and Electron Backscatter Diffraction (EBSD). The results of mechanical properties like yield strength (YS), ultimate tensile strength (UTS) and microhardness of various Zirconium based alloys in as-cast and final product condition are discussed. The results are correlated with the initial and final microstructure of the individual alloys.

3.2. Results and Discussion

Thermo Mechanical Processing (TMP) steps during the fabrication of Zirconium alloys plays the important role in determination of final microstructure and mechanical properties. The impact of thermo-mechanical treatment of the manufacturing process steps that affect the microstructure are as follows [77-79]:

- β-quenching
- Hot rolling or extrusion (especially temperatures)
- Degree of cold rolling or rocking
- Intermediate annealing temperatures
- Final annealing temperature (degree of recrystallization)

Microstructure evaluation for these alloys has been carried out at important stages of manufacturing route, which form the basis for determining the requirement of various thermo-mechanical steps to optimize mechanical properties and corrosion behavior.

3.3. Microstructural Evaluation:

The desirable and technologically important properties of Zirconium and its alloys, such as mechanical strength, toughness, creep, hydrogen pick-up and corrosion resistance are essentially controlled by the morphology and microstructure of precipitated particles of second phase. Like any metal, a pure metal of Zr exhibits poor engineering properties. To improve properties of Zirconium and its alloys; the metallurgical procedures include i) addition of elements with significant solubility and ii) heat treatments producing new phases. The enhance solubility of alloying elements in the α- and β-phases is an important criteria to develope the heat treatments and to control microstructure to enhance mechanical properties and corrosion resistance [20, 27]. The performance of zircaloy depends upon the grain size, crystallographic texture, nature and distribution of precipitates, microstructure and its grain morphology. The evolution of the microstructural features associated with the type and the level of thermomechanical processing ought to be optimized to meet the stringent requirement of excellent physical properties, mechanical properties and close dimensional tolerances [26, 27]. It is desirable that the microstructure obtained after the thermomechanical processing treatment should not change under the operating environment with geometrical integrity. The microstructures evolution developed in the various Zirconium alloys have been characterized through OM, SEM and EBSD at the different stages viz., (i) As cast ingot (ii) after extrusion of β quenched billets and (iii) after final cold work. These are described in details in the following paragraphs. Characterization of the material microstructure in relation to the material performance may elucidate the mechanisms behind the material performance [78-80]. The microstructure of Zirconium alloys depends on heat treatment. Generally in the recrystallized condition it consists of equiaxed grains (α-phase) with second phase particles (SPP) found both in the grain boundaries and inside the grains. In Zirconium alloys transformed from the β-phase the microstructure consists of Widmannstätten type α –plates and the SPP are found between the plates. The Zirconium material microstructure is dictated by the material property requirements for a specific component and its operation conditions. This knowledge may be used during selection of material and to modify the manufacturing process to get optimum material performance. It is also important to study the microstructural changes to get a better mechanistic understanding of the corrosion process during various thermomechanical operations.

3.3.1 Microstructure evaluation for unalloyed Zirconium

The optical and SEM micrographs for as cast ingots for unalloyed Zirconium are given in the Figure 3.1a and 3.1b, respectively. Unalloyed Zirconium products are not being manufactured at Nuclear Fuel Complex, Hyderabad, hence the product analysis was not carried out. The unalloyed Zirconium was taken as reference material for comparison of different properties with other Zirconium alloys.

The as-cast microstructure of single phase unalloyed Zirconium shows (Figure 3.1) very large grains (several millimeters) of the ‘as-cast’ dendritic structure was observed along with second phase particles at interdendritic region and consists of alpha and beta phases parallel plate martensitic morphology. Unalloyed Zirconium microstructure has a single phase structure composed of h.c.p. alpha with a distribution of fine intermetallic mainly from the impurity elements. The microstructure of cast ingot comprises α and β phases parallel plate martensitic morphology (HCP). The h.c.p alpha stringers (bright phase) make up the majority of the microstructure and surrounded by a more or less continuous network of bcc β (dark phase). Most of these α stringers are made up of a series of equiaxed and recrystallized α .

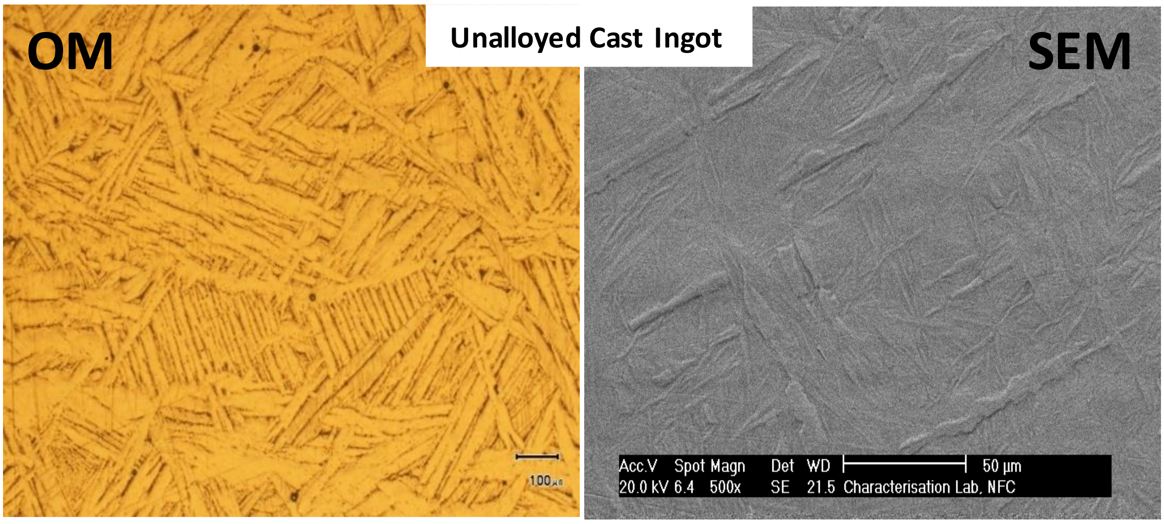

Figure 3.1: Microstructure evaluation for unalloyed as-cast ingot, (a) Optical and (b) SEM

3.3.2 Microstructure evaluation of Zr-2 and Zr-4

The optical and SEM micrographs for Zr-2 and Zr-4 at the different stages of production i.e. as-cast ingots, extruded and final tubes are shown in the Figure 3.2 and 3.3, respectively.

3.3.2.1 Microstructure for as cast ingots

The Zr-2 and Zr-4 are single phase alloys of HCP α Zirconium with finely dispersed intermetallic precipitates within grains. At as-cast ingot stage, the microstructure consists of a fast cooled structure of widmanstatten structure with parallel plate morphology. The as-cast ingot microstructure of Zr-2 and Zr-4 shows {Figure 3.2 (a) and 3.3 (a)} very large grains (several millimeters) of the ‘as-cast’ dendritic structure along with second phase particles at the interdendritic region. The microstructures of Zirconium and its alloys have been studied by several authors [26, 27, 29]. The general microstructures identified for Zr-2 and Zr-4 include the following secondary structures [81]:

- Lenticular α: coarse, plate like structures with irregular and jagged boundaries formed by slow cooling,
- Parallel plate α :Widmanstätten α structures formed on the plane of pre-existing β,

- Basketweave α : nonparallel Widmanstätten α structures resulting from the random precipitation of α plates on a number of planes in one β grain, and
- Martensite α': needle like structures formed by diffusionless transformation.

In Zr-2, tin, iron, chromium and nickel are used as alloying elements with their concentration less than 2% to enhance mechanical strength and corrosion resistance in steam and hot water environment. Zirconium is characterized by two allotropic phases i.e. α phase {hexagonal closed pack (HCP) structure}, is stable below 807 ^{o}C, while the β phase {body centered cubic (BCC)} is stable above 875^{o}C. However, in Zr-2 the stable β temperature ranges are at above 977 ^{o}C, α + β between 877 and 977 ^{o}C, α + β+ χ in the temperature ranges of 807 and 877 ^{o}C and α+ χ below 807 ^{o}C [27]. This results into decomposition of bcc β phase to hcp α phase and the intermetallic χ phase with their overlapping temperatures depending on the thermo mechanical treatments and temperatures [26, 29]. In the pure binary systems, the $ZrFe_2$ and $ZrCr_2$ are Laves phases with cubic or hexagonal structure, and the hard intermetallic phase of χ is the generally known as secondary phase precipitates (SPP) and alongwith the impurities exhibits strong influence on the kinetics of the phase transformation. The $Zr_2(Ni, Fe)$ and $Zr(Fe, Cr)_2$ are the SPP precipitates that make it brittle. Zr-2 is heat treated in an argon environment at 800 °C and quenched in mercury to avoid the formation of brittle hydride [82, 83]. Similarly, in Zr-4 tin, iron, chromium as well as oxygen are added as the main alloying elements that lead to a two-phase microstructure. Small precipitates of α phase Fe and Cr of stable intermetallic phase are also present in Zr-4, upon cooling from the β -range during platelet growth. $Zr(Fe,Cr)_2$ intermetallic particles is the most often observed second phase in Zr-4 ingot. The Sn and O are distributed in solid solution in the matrix as they exhibit greater solubility in the α-phase.

In Zirconium and its alloys the coexistence region of α and β phases are determine by the alloying elements and the intermetallic compounds are formed by diffusion of the alloying elements iron, chromium and nickel from the base Zr matrix. In α -phase, solubilities are very low: 120 ppm for Fe and 200 ppm for Cr at the maximum solubility temperature. Tin and oxygen (1200 ppm) stabilise the α phase, while iron and chromium stabilize the β phase. In addition iron, chromium and nickel act as β-eutectoids, as these elements have a eutectoid decomposition in β phase [84, 85]. Sn is the major alloying element in both Zr-2, and Zr-4 and it is present in solid solution. The solubility of the alloying elements such as chromium and iron in Zirconium is very low and hence these form second phase particles together with Zirconium [26, 27, 57].

Zr-2 and Zr-4 ingot is manufactured by Vacuum Arc Remelting (VAR) in water-cooled copper crucibles by melting into molten pool and subsequent progressive solidification with very high amount of heat transfer. During melting, the ingot is composed of a liquid metal pool (melt pool), a mushy zone and solidified ingot. All the alloying elements are in the molten state in the molten pool are mixed. Segregation at the microscopic level takes place in the mushy zone, where both liquid and solid phases exist. During solidification, ingots are composed of randomly oriented equiaxed grains of few cm. At the bottom and periphery of the ingot, grains are slightly larger and more specifically oriented in columnar grains pattern. The inner ingot microstructure is more equiaxed [26].

3.3.2.2 Microstructure after First Extrusion and β quenching

The optical and SEM micrographs of Zr-2 and Zr-4 alloys after the first extrusion to the billet of size Ø150 mm and β quenching are given in the Figure 3.2 (b) and 3.3(b) respectively. In the β-quenching process, the product of the logs/billets are homogenised, thereby decreasing the micro segregation of the alloying elements and in some cases to establish the optimum size and distribution of SPPs to improve the corrosion performance as well as the mechanical properties of the final product. The most critical parameters in β-quenching are: heat up rate, time at temperature to achieve uniform temperature distribution, cool down process and quenching rate. The β quenching or processing in Zircaloy generally consists of three different steps:

(i) α to β phase transformation by furnace heating, resulting to hcp structure (α phase) changes its to bcc structure (β phase),

(ii) a homogenisation treatment of β phase for dissolution of the second phase precipitates and

(iii) β to α phase transformation by cooling (β quenching) the specimen [86, 87].

After extrusion and β quenching, the microstructure indicates the first breakage of the as-cast structure. Extrusion is first stage of metal working operation, wherein dendritic cast structure of the ingot is broken down. Zr-2 and Zr-4 are extruded at a temperature close to 850°C. The extruded structure consists of equiaxed and recrystallized alpha grains with a clear bimodal distribution in grain size with grain morphology-larger elongated grains and smaller equiaxed grains. Larger elongated grains are found to have a higher average misorientation, higher overall dislocation density and they contain a greater amount of intermetallic precipitates. Extrusion parameters such as extrusion ratio, extrusion temperature and billet grain size have been proved to exert a profound influence on the development of microstructure in Zirconium alloys.

After completion of hot working processes like forging, extrusion, hot rolling, etc., the workpiece is heated to 1040°C ± 10°C and soaked for half an hour (not less than 20 minutes and not more than 45 minutes) and then quenched in water. Homogenization in the β phase leads to the complete dissolution of all the second phase particles but gives rise to significant grain growth. After 30 minutes at 1050°C, grain size may reach several millimeters. During the water quench, the β grains transform into a needles by bainitic transformation due to the slow cooling rate of the large ingots involved. The β-eutectoid elements are repelled by the transformation front and precipitate at the boundaries of those needles. This β quench is a reference state for further processing. β quenching leads to grain refinement of the as-cast structure. Large grains are broken down into smaller grains. The β quenching also gives

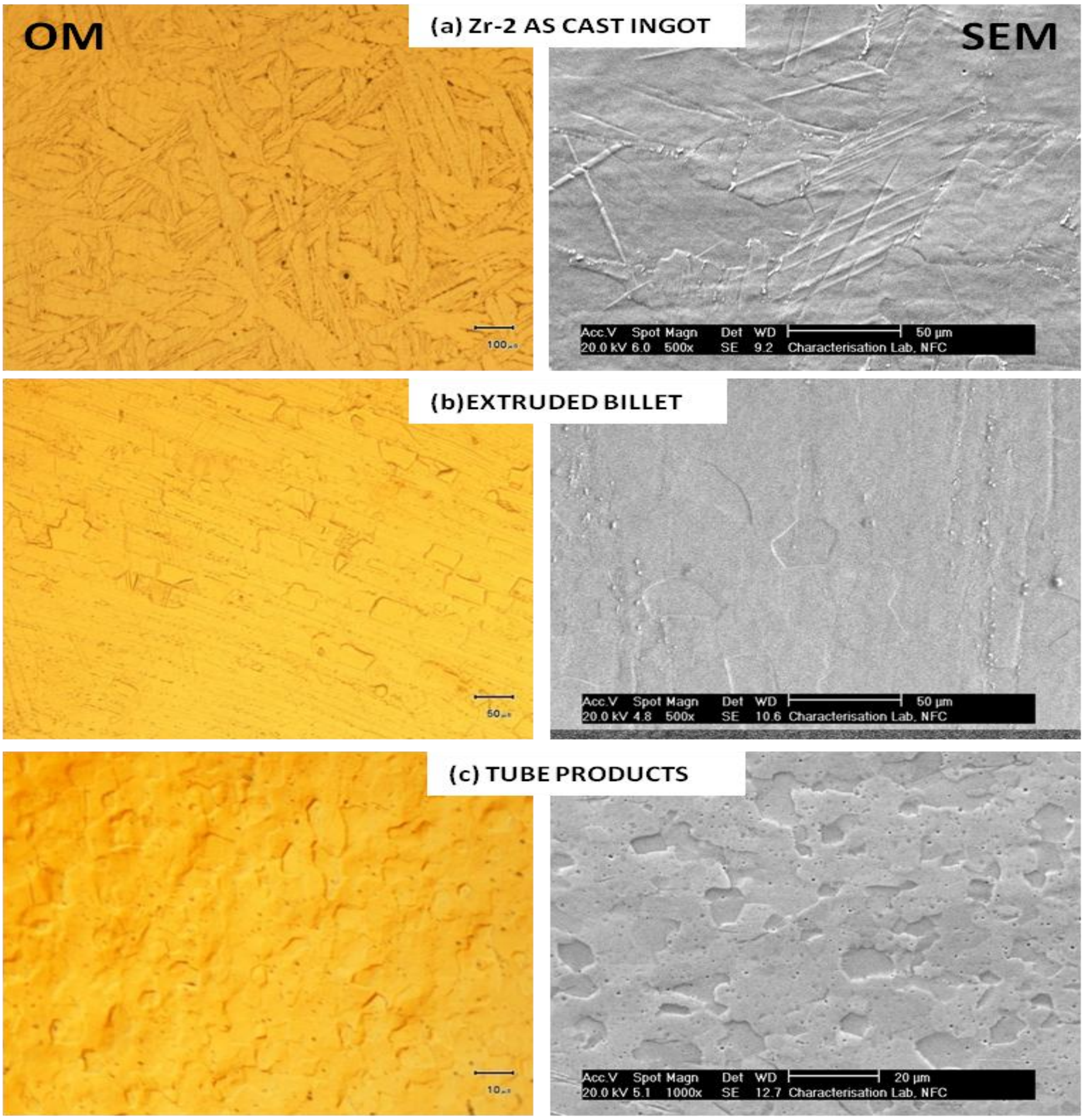

Figure 3.2: Optical and SEM Microstructure evaluation for Zr-2 a) as-cast ingot indicate dendritic cast structure and the presence of precipitated small intermetallic second phase particles (Fe, Cr, Ni, Si, C), Second Phase Particle (SPPs at grain boundaries). b) Extruded Billet Extruded indicate presence banded structure elongated in the extrusion direction and dynamic recrystallization c) Final Zr-2 tube product indicate the presenceof elongated grains in working direction.

Widmanstatten basket weave morphology and a randomized texture (although often referred to as acicular) microstructure in which various α-variants develop on crystallographically equivalent lattice planes from the β- phase [56,59,87,88]. In Zr alloys, two different Widmanstatten morphologies have been observed in Zr-4 that depending to a difference in the kinetics of the nucleation process of β to α phase transformation: basket-weave structures are observed when the nucleation process occurs in volume, whereas parallel-plate structure develops preferentially when nucleation sites are situated on the prior β grain boundaries [87, 89].

Hot extruded microstructure exhibited larger elongated grain size of about 20-30 μm along the extrusion direction and smaller equiaxed grain size of 5-10 μm as shown Figure 3.2 (b) and 3.3(b) for Zr-2 and Zr-4 alloys respectively (optical microstructure) and for EBSD microstructure Zr-4 alloy in Figure 3.4 (c). Moreover, the Zr (Fe, Cr)$_2$ intermetallic particles were randomly distributed in the hot extruded condition as shown Figure 3.2 (b) and 3.3(b) for Zr-2 and Zr-4 alloys respectively (SEM microstructure). These phases may have precipitates due to the low cooling rate after extrusion. In general, large grains of the 'as cast' structure get refined during the process of β-quenching that subsequently leads to Widmanstätten morphology. During hot extrusion, bimodal distributions in grain size and in grain morphology evolved [11, 78]. Thereby, they exhibited larger elongated grains in association with smaller equiaxed grains. Detail of microtextural analysis of the grains in Zr-2 and Zr-4 alloys indicated that [78];

- Elongated larger grains had higher misorientation and contain more dislocation density.
- Larger grains exhibited more intermetallics precipitates.
- Larger grains were more textured.

In zirconium alloys, the corrosion resistance of Zr-2 depends on the second phase particle size and structure. The increasing second phase particle increases the oxide thickness with increasing second phase particle diameter and increasing number of particles with the hexagonal close packed structure. On the other hand, Zr-4 corrosion depends on iron content in the matrix. The corrosion resistance increased with increasing matrix iron content [85]. It is evident that the microstructural changes along with the formation of intermetallic particles can greatly influence corrosion resistance, creep, hydride precipitation and reorientation, etc. [78]. Hence it is essential to evolve an efficient processing flow sheet that results in components with suitable microstructure with high corrosion resistance required for long term tolerances in aggressive nitric acid of reprocessing environments.

3.3.2.3 Microstructure after final pilgering and final annealing

In the case of Zr-2 tubes are annealed and the grains are equiaxed in the final condition as shown in Figure 3.2 (c). Final Zr-2 tube product indicate the presence of elongated grains in working direction. Zr-4 pilgered tubes exhibited elongated grain structure on the longitudinal surface of the tube as shown in Figure3.3 (c). Pilgering is a process in which the tube size is reduced with the help of to and fro movement of either half ring or full ring tapered grooved dies with a stationery mandrel on the inside of the tube. During the process, the outer diameter (OD) and Wall Thickness (WT) are simultaneously reduced. The process is ideally suited for cold working of Zirconium alloys as a texture in the finished product can be effectively controlled.

The pilgered Zr-4 is distinguished by two distinct microstructural features i. e.: fragmenting/deforming and non-fragmenting/ non-deforming grains. The former had higher stored energy of cold work and easily distinguished from the grain size refinement. On the other hand, the non-fragmented grains, provided significant growth inhibition or pinning to the recrystallized grains and did not contribute directly to recrystallization. A combination of these two mechanisms defined the recrystallization behavior of pilgered Zr-4 [90, 91]. After each pilgering step, an intermediate annealing is performed to restore the material ductility or further cold working. Mostly the grains were fragmented due to the ‘heterogeneous deformation’ of the pilgering process [8]. The average grain size after pilgering is about 10-20 μm. After pilgering, the $Zr(Fe,Cr)_2$ intermetallic particles were uniformly distributed. The final annealed microstructure of Zr-4 tube is a re-crystallized equiaxed microstructure with a grain size of 5-10 μm. It has been reported that the final annealed microstructure consisted of evenly distributed fine $Zr\ (Fe,Cr)_2$ intermetallic particles within the grains [8].Similarly, in Zr-4 it is also reported that the pilgering processing steps modified the microstructure in the following sequence:

Widmanstätten structure (β-quenched) → bimodal grain size/shape (hot extruded) → initial grain growth (during first annealing) → heterogeneous deformation (first pilgered) → fully recrystallized (second annealed) → heterogeneous deformation (second pilgered) → partially recrystallized (third annealed) → heterogeneous deformation (third pilgered) → partially recrystallized (final annealed).

The evolutions of the texture were related to grain size of larger grains, having a stronger contribution towards textural evolution. Furthermore, the process involving pilgering operations results into heterogeneous deformation along with grains fragmentation and some grains/orientations were unaffected. During the intermediate annealing steps, complete or partial recrystallization occurs and the resultant larger recrystallized grains had a strong influence on the developments of crystallographic texture [92].

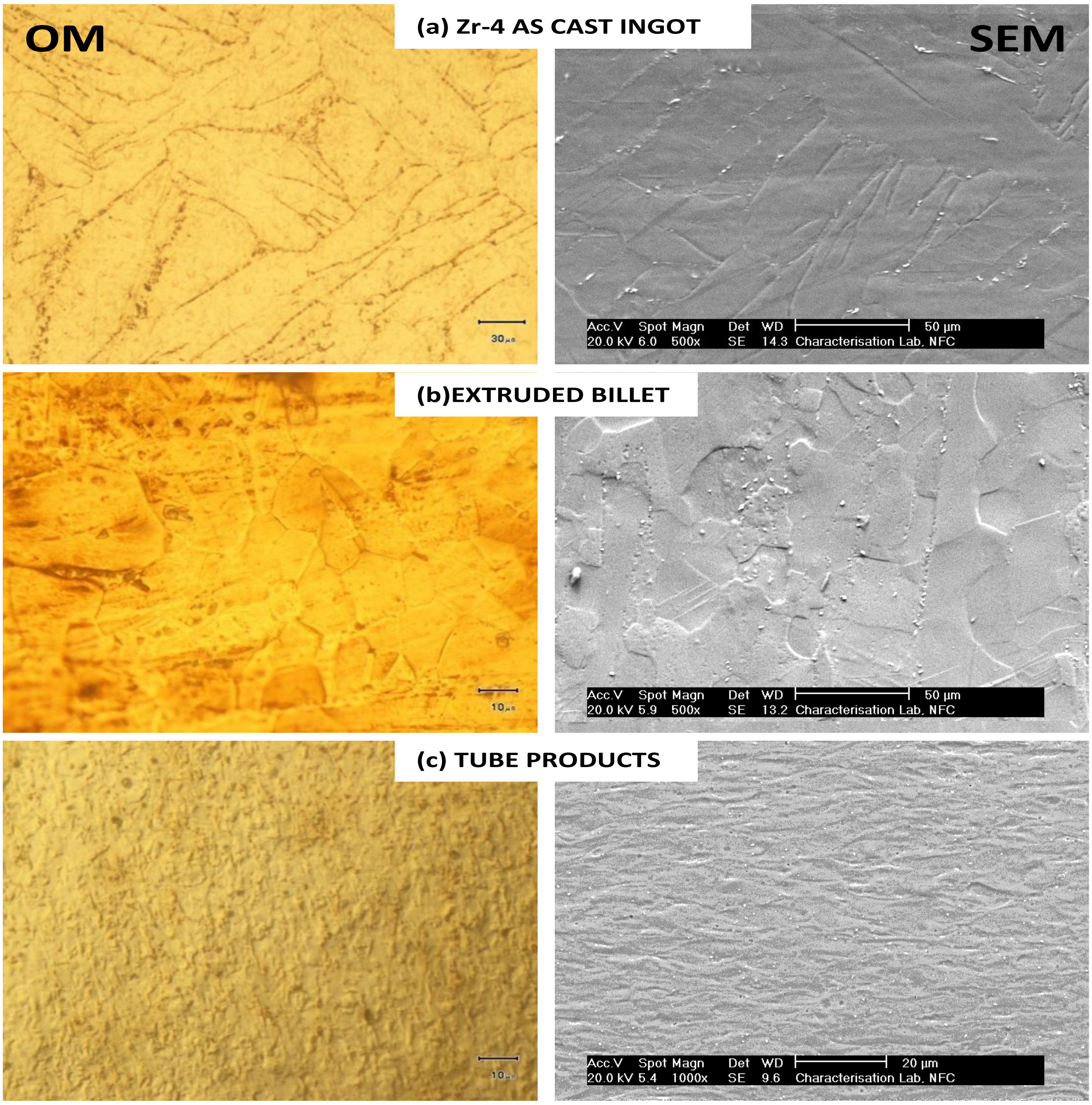

Figure 3.3: Optical and SEM Microstructure evaluation for Zr-4 a) as-cast ingot indicate dendritic cast structure and the presence of precipitated small intermetallic second phase particles (Fe, Cr, Ni, Si, C), Second Phase Particle (SPPs at grain boundaries). b) Extruded Billet, Extruded Billet indicates presence banded structure elongated in the extrusion direction and dynamic recrystallization. c) Final tube product 4 tubes indicate the presenceof elongated grains in working direction and annealed sheet is showing recrystallized bright elongated areas.

3.3.2.4 Microstructural evolution by SEM-EDS

The behavior of Zr alloys is also strongly dependent on secondary phases appearing during the fabrication process. The structure and the morphology of these secondary phases that precipitates in Zirconium alloys as well as the concentration and distribution of the alloying elements present in zirconium alloys have significant effects on corrosion resistance and mechanical behavior. However, volume fraction of thses second phase precipitates are small (few nanometers for the smallest) to allow the use of standard methods for phase determination. Hence, Zr-2 and Zr-4 pilgered and annealed tubes sample have been successfully investigated for microstructural and elemental composition analyses for second phase particles by Energy Dispersive Spectroscopy (EDS) spectrum and with the help of corresponding electron diffraction pattern on ‘FEI, Helios NanoLab600i’ make SEM attached with energy dispersive X-ray spectroscopy (EDS).

In the present thesis SEM attached with energy dispersive X-ray spectroscopy (EDS) was used to characterize the Zr-2 and Zr-4 pilgered and annealed tubes for microstructural and elemental composition analyses for second phase particles. SEM-EDS used in the present thesis is of ‘FEI, Helios NanoLab600i’ make. The sample for prepared for SEM analysis were used in EDS. Magnified SEM images and the corresponding EDX spectra for Zr-2 and Zr-4 tubes are shown in Figure 3.4 and 3.5 respectively.

The EDS spectrum of secondary phase particles for Zr-2, 80000x mangnification reveals that sizes of secondary phase particles for Fe, Cr and Ni is about 300 nm and was found to possess the concentration alloying elements Cr (0.39 and 0.52 wt%) , Fe (3.97 and 3.68 wt%), Ni (4.34 and 4.23 wt%) and Sn (2.53 and 3.18 wt%). It clearly indicated that SPP’s are rich Fe, Cr and Ni compared to the bulk material composition.

Table 3.1: Zr-2 base material and SPP compositions carried out by EDS. secondary phase composition (Zr and SPP’s with $Zr(Fe,Cr,Ni)_2$ stoichiometry).

Phases	Bulk Material		Secondary phase precipitates			
	Spot 2		Spot 1 (SPP)		Spot 3 (SPP)	
Element	Weight %	Atomic %	Weight %	Atomic %	Weight %	Atomic %
ZrL	97.88	97.19	88.38	84.72	88.77	84.84
SnL	0.73	0.56	3.18	2.35	2.53	1.86
CrK	0.31	0.54	0.52	0.88	0.39	0.65
FeK	0.56	0.91	3.68	5.76	3.97	6.20
NiK	0.52	0.80	4.23	6.30	4.34	6.45

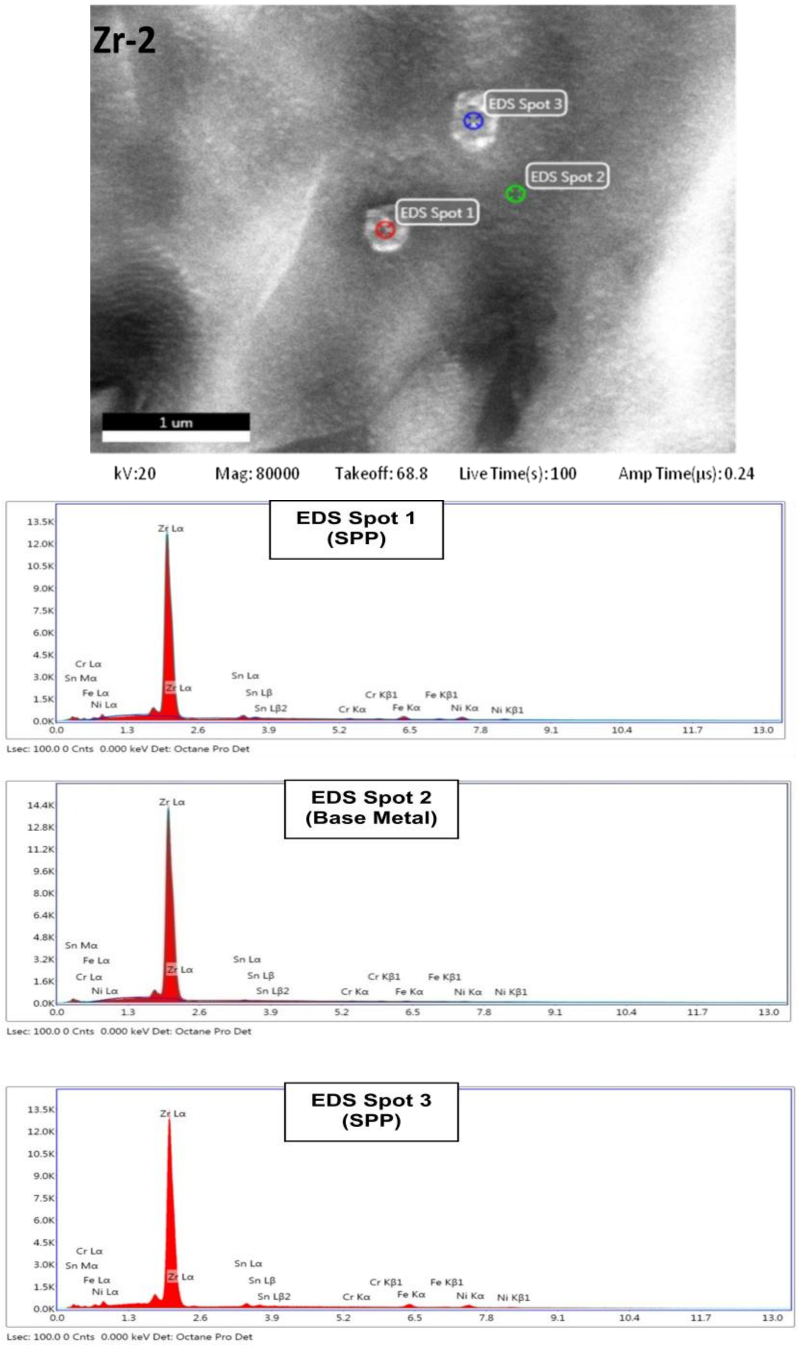

	Spot 2 (Base Material)		Spot 1 (SPP)		Spot 3 (SPP)	
Element	Weight %	Atomic %	Weight %	Atomic %	Weight %	Atomic %
ZrL	97.88	97.19	88.38	84.72	88.77	84.84
SnL	0.73	0.56	3.18	2.35	2.53	1.86
CrK	0.31	0.54	0.52	0.88	0.39	0.65
FeK	0.56	0.91	3.68	5.76	3.97	6.20
NiK	0.52	0.80	4.23	6.30	4.34	6.45

Figure 3.4 EDS elemental analysis for Zr-2 tube on base metal precipitated small intermetallic second phase particles (Fe, Cr, Ni). Second phase particles indicate the presenceof higher concentration of Fe, Cr, Ni compared to base material Zr-2.

In Zr-2, the partitioning of Fe between the two types of intermetallic phases leads to a more complex relationship between nominal composition and precipitate composition, giving a broad range of Fe/Cr ratio in Zr(Cr,Fe)$_2$, and Fe/Ni ratio in Zr$_2$(Fe,Ni) .

Similarly, the EDS spectrum of secondary phase particles for Zr-4, at 80000x mangnification reveals that sizes of secondary phase particles for Fe, and Cr are about 300 nm and was found to possess the concentration alloying elements Cr (4.63 wt%) , Fe (8.82 wt%). It clearly indicated that SPP's are rich Fe,and Cr compared to the bulk material composition is shown in Table 3.2.

Table 3.2: Zr-2 base material and SPP compositions carried out by EDS. secondary phase composition (Zr and SPP's with Zr(Fe,Cr)$_2$ stoichiometry).

Phases	Bulk Material		Secondary phase precipitates	
	Spot 2		Spot 1	
Element	Weight %	Atomic %	Weight %	Atomic %
ZrL	98.27	98.35	85.79	78.78
SnL	1.38	1.06	0.76	0.54
CrK	0.13	0.23	4.63	7.46
FeK	0.22	0.35	8.82	13.23

The orthorhombic Zr$_3$Fe phase which appears in the binary Zr-Fe diagram is found only in Zr-4 with very high Fe/Cr ratios, probably because its formation is too sluggish compared to the formation of the Zr(Cr,Fe)$_2$ precipitates. As a result, upon cooling from the β-phase the Zr(Cr,Fe)$_2$ precipitates form first and consume the available Fe. The phase compositions and content play a vital role on the mechanical properties of the extruded tubes.

The behavior of Zirconium alloys is also strongly dependent on secondary phases appearing during the fabrication process. The structure and the morphology of these secondary phases that precipitates in Zr alloys as well as the concentration and distribution of the alloying elements present in zirconium alloys have significant effects on corrosion resistance but also on mechanical behavior of these alloys.

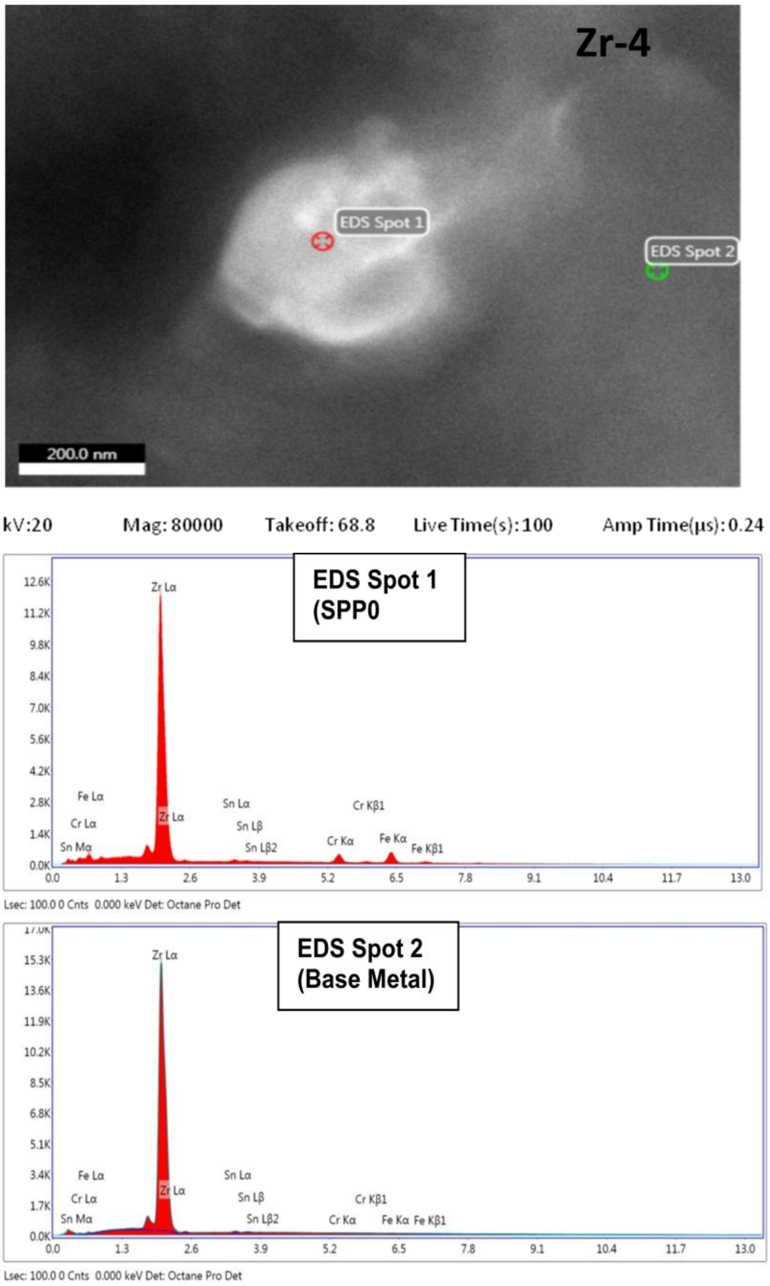

	Spot 2(Base Material)		Spot 1 (SPP)	
Element	Weight %	Atomic %	Weight %	Atomic %
ZrL	98.27	98.35	85.79	78.78
SnL	1.38	1.06	0.76	0.54
CrK	0.13	0.23	4.63	7.46
FeK	0.22	0.35	8.82	13.23

Figure 3.5 EDS elemental analysis for Zr-4 tube on base metal precipitated small intermetallic second phase particles (Fe, Cr). Secondary phase particles indicate the presenceof higher concentration of Fe, Cr, compared to base material Zr-4.

3.3.2.4 Microstructural evolution by EBSD

EBSD maps from Zr-4 tube sections are presented in figure 3.4, clearly indicates the changes in microstructure during pilgering and annealing operations. EBSD maps indicates that as-cast Zr-4 ingot has dendritic cast structure and with the presence of small intermetallic second phase particles (Fe, Cr, Ni, Si, C), Second Phase Particle (SPPs at grain boundaries). Similarly, β quenched microstructure consists of Widmannstatten type α-plates. Hot extruded microstructure of extruded billets & slabs indicates presence of banded structure and dynamic recrystlisation. Cold worked pilgered structure is elongated in deformation direction; cold work followed by annealing shows bright elongated structure along the working direction. The microstructural changes at different stages of thermomechanical process have been indicated in the EBSD images (Figure 3.4):

Stage I: The fragmented region gradually increases by the TMP steps from as cast ingot to hot extrusion {Figure 3.4(a) - (c)}. The qualitative changes in the microstructures are clearly evident.

Stage II: after the 1st annealing, the microstructure appears with low confidence index regions were replaced by fine recrystallized grains and with grain coarsening {Figure 3.4(d)}.

Stage III: Pilgering and final annealing, changes in the microstructures with smaller grain sizes are noticeable. Finer and smaller grains formed in stage II appeared to have coarsened. However, the overall microstructural changes affecting the degree of and the grain size as seen in a typical EBSD image {Figure 3.4(h)}.

The microstructure of Zirconium alloys depends on heat treatment. Generally in the recrystallized condition, it consists of equiaxed grains (α-phase) with second phase particles (SPP) found both in the grain boundaries and inside the grains. In Zirconium alloys transformed from the β-phase the microstructure consists of widmannstätten type α-plates. In the present work, the SPP are found between the plates.

The cold working steps and intermediate recrystallizations allow further control of the precipitate size distribution. The as-cold worked samples were given a stress-relief annealing heat treatment (560 ^{o}C for 1 h) to evaluate the recrystallization behaviour. It appears the particle size were essentially unchanged. However, after β-quenching the shape changed from an irregular plate features {Figure 3.4 (b) to Figure 3.4(d)} to spheroidal {Figure 3.4(e-h)}. The SPP particles appearprimarily at lathe and grain boundaries in the as-β-quenched material, but intermediate processing to the final size annealing resulted in a uniform distribution in the matrix {Figure 3.4(d-h)}. After each cold working step of plate or tube material, an annealing treatment is mandatory to restore ductility. It is usually performed in the range of 530-600°C to obtain the fully recrystallized material (RX). The resultant microstructure is an equiaxed Zr grains with the precipitates located at the α-grain boundaries (they are obtained there not by intergranular precipitation, but because they pin the grain boundaries during grain growth) and within the grains. These different heat treatments contribute to the control of the cumulative annealing parameter. For better mechanical properties of the final product, the temperature of the last annealing treatment can be reduced to avoid complete recrystallization. This is the stress-relieved (SR) state, characterized by elongated grains and a high density of dislocations, and thus achieving a greater mechanical strength. The final annealing affects the degree of recrystallization and the grain size (typically between 2 and 4 μm). In most cases, the TMP of fabrication routes for zircaloy has been developed to obtain good corrosion resistance. Annealing related transformations in Zr alloys in the past demonstrated abrupt changes in the mechanical properties in Zr-2 associated with the fine recrystallized grains. In Zr-4 recovery and recrystallization showed strong heterogeneity in the deformed microstructures and also heterogeneous nucleation from the heavily fragmented grains. Thereby, a complete recrystallization, without significant grain coarsening, established an optimum combination of strength and ductility in these alloys [93, 94].

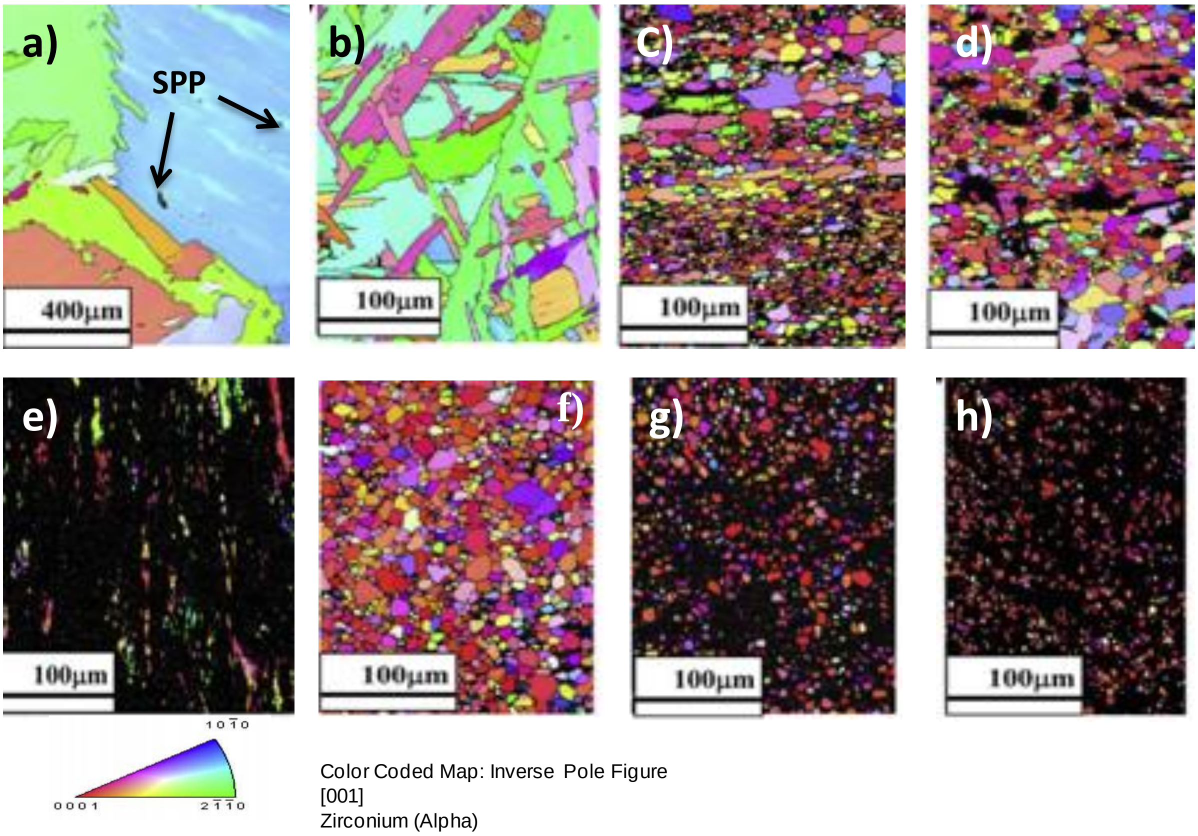

Figure 3.6: EBSD microstructure evaluation of Zr-4 during the thermomechanical process shown (a) as cast ingot (b) β quenched (c) hot extruded (d) first annealing (e) 1stpilgering (f) Second annealing (g) 2nd pilgering (h) final annealing.

3.3.2.5 Microstructure after welding for Zr-4 tube

Welding is usually required for Zircaloy used for various nuclear applications. The welding by fusion welding processes includes gas tungsten arc welding, electron beam welding and resistance welding and it require strict control of the welding atmosphere as Zirconium and its alloying elements are highly reactive with oxygen and nitrogen. In addition, the fusion welding processes may introduce defects due to coarse inhomogeneous microstructure resulting from high heat-input fusion processes that can deteriorate the mechanical properties of the weld. Most of the these associated problems are attributed to the melting/solidification and/or high thermal effect related to fusion welding process of solid-state joining processes with desirable low heat input. Electron beam welding (EBW) has some advantageous features over the other welding techniques. In this joining process, the weld joints are produced by coalescence of the materials with heat from a high energy electron beam. Since the process is carried out in a vacuum and the beam are focused on a small area, materials can be joined in a short duration and resulting to the long-range flow of heat and voids, cracks and oxidation can be minimized.

Dissolver assembly for reprocessing is fabricated by the welding operation. The microstructure of the weld region of TIG and EB welded Zr-4 samples is shown in Figure 3.5. The welds exhibits a transformed equiaxial homogeneous grain structure or acicular a grains surrounded by prior β grain boundaries (Widmanstatten or basketweave structure). The weldments features are known to influence the service performance of welded structures.

Depending on the welding process used, it influences the distributions, size, the morphology of the structural elements of macro and micro segregation, microstructure (phase structure and morphology), inclusions depending on impurities, porosity, secondary precipitates, etc. During welding by TIG or EB processes the material is heated to melting temperatures, wherein the base material passes from a granular structure of α-phase to β-phase and then into liquid. Once it is cooled, the welded zone exhibits a granular structure acicular "needle-like" α grain surrounded with a primary β phase grain boundaries which is also an α Widmanstätten structure. In general, the structures obtained after welding are the result of the interaction between the associated thermal cycle of the cooling process involved and the characteristics of the material (i.e., the chemical composition and prior thermomechanical treatment). Also, the thermal cycle effect is a function of the maximum temperature attained, the time at high temperature and the cooling rate. Thereby, the micro structural feature must take into account these factors.

The weld region of TIG welded Zr-4 sample exhibited coarse acicular α structure in comparison to the fine acicular structure of EB welded sample. This is attributed to the slower cooling and solidification of TIG welds in comparison with EB welds. The welds exhibited a transformed grain structure or acicular α grains surrounded by prior β grain boundaries (Widmanstatten or basketweave structure).

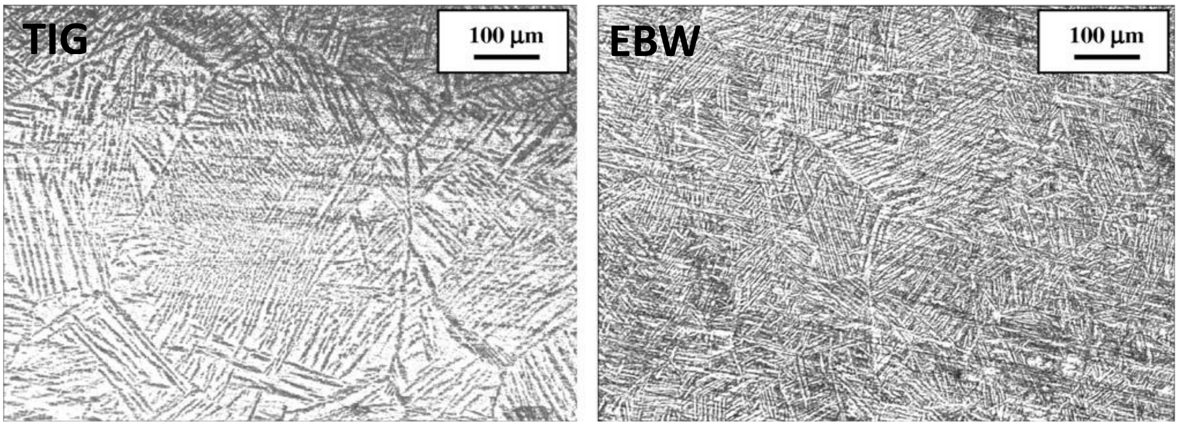

Figure 3.7: Microstructure from the weld region of TIG weld and EB weld of Zr-4 sample

3.3.3 Microstructure evaluation for Zr-2.5%Nb alloy

The fabrication of Zr-2.5%Nb tubes involves a large number of thermo-mechanical treatments and the final microstructure thus developed determines the properties of these tubes [83-85]. In Zirconium, alloying with Nb improves its mechanical, corrosion and irradiation stability properties. Among this, the Zr-2.5%Nb alloy is one of the most important alloy of Zr-Nb series used as pressure tubes material in PHWRs. The life of the pressure tubes is expected to serve for more than 30 years in the severe reactor environment. In Zr-2.5%Nb alloys microstructure, texture and the phase transformation evolution are complex processes. Depending on annealing treatment, soaking temperature and cooling rate, the β phase can be transformed into a variety of microstructures viz., allotriomorph α, Widmanstatten alpha with parallel plates or basket weave structure, martensitic microstructure, and omega phase. In addition, in Zr-2.5%Nb alloy the grain boundaries nucleate and grow preferentially along the high angle grain boundaries of parent β phase. In low undercooling, the first phase to form is β-Zr (BCC structure) to α-Zr (HCP structure) transformation. In moderate or higher undercooling Widmanstatten side plates form either by nucleating at grain boundaries or by branching out from grain boundaries. The β/α interface tend to propagate toward the Burgers related β grains leading to the development of periodic protrusions with morphological instability [95, 96].

The evolutions of microstructure in Zr-2.5Nb alloy tube as a function of thermo-mechanical treatment and during their fabrication are investigated in the present work. The specific detail of the evolution of microstructure during their fabrication has been presented in this section. The optical and SEM micrographs of Zr-2.5%Nb and Zr-1%Nb alloys at the different stages of production i.e. as-cast ingots, extruded and final tubes are given in Figure 3.6 and 3.7.

3.3.3.1 Microstructure for as cast ingots Zr-2.5%Nb

The Zr-2.5%Nb is mostly used in the extruded and cold-worked condition for pressure tubes in PHW reactors. The desirable properties of this material are associated mostly with the formation of fine elongated grain structure and the crystallographic texture produced during the extrusion stage. In standard Zr-2.5%Nb pressure tubes, the texture comprises a predominantly of transverse distribution of the basal plane normal and along with a weak component in the tube axis. During Zr-2.5%Nb pressure tubes manufacturing route by TMP, the process steps of cold-working and stress-relieved fuel cladding (i.e., the repetitive cold-working and intermediate annealing after extrusion, resulting to the high ratio of wall reduction to diameter reduction on final pass) leads to the formation of basal plane normal closer to the radial direction. The useful properties of this Zr-2.5%Nb alloy that are technologically important such as delayed hydride cracking and irradiation induced deformation, are mostly controlled by the phases and texture evolution [96, 97]. During the different TMP stages of fabrication of Zr-2.5%Nb alloy pressure tube, the formation of the hot-extruded texture is done through the cold deformation and intermediate annealing stages, generating the final texture of the finished tube similar to the parent hot-extruded texture. Thereby, optimization of texture is essential step involve in the TMP sequence.

The as-cast microstructure of alloys Zr-2.5% Nb shows {Figure 3.6(a)} very large grains (several millimeters of size) of the 'as-cast' dendritic structure was observed along with second phase particles at the inter dendritic region. The Zr-2.5%Nb and Zr-1%Nb are two phase alloys and these alloys consists of primary phase as α-Zirconium (HCP) secondary phase as β-Zirconium (BCC). At ingot stage the microstructure consists of fast cooled martensitic parallel plate morphology. These alloys consist of primary phase as a Zirconium (HCP) and secondary phase as β-Zirconium (BCC). During the thermo-mechanical processing the β–Zirconium transform to β-niobium as a stable phase. In the case of Zr-2.5%Nb at ingot stage the microstructure consists of fast cooled martensitic parallel plate morphology. The correlation between the extrusion conditions {extrusion-temperature (650-850^{o}C), preheat time (0.5 – 3.0 h), extrusion ratio/geometry (4:1, 10:1) and billet microstructure (fine, coarse)} is also reported [97]. The bulk textures of the extrusions, in general, comprised of three predominantly components namely [98]:

1. A radial component developed by crystallographic rotation of the α phase due to pyramidal slip, prism and basal slip similar to the textures produces by cold working at lower temperatures.
2. A transverse component associated with the texture developed in the α phase, by bodily rotation of the α phase within the β phase at higher temperatures.
3. An axial component developed at high temperatures and associated with the texture developed in the β phase and the α/β phase transformation. It is therefore associated with a significant volume fraction of β-Zr, present during extrusion.

3.3.3.2 Microstructure after First Extrusion and β quenching Zr-2.5%Nb alloys

The optical and SEM micrographs after first extrusion and β quenching of Zr-2.5%Nb alloys for Ø 230 mm billet are given in Figure 3.6 (b) and shows the microstructure obtained after the first breakage of the as-cast structure as in all the Zr-2.5%Nb alloy [86, 99].

Extrusion is first stage of metal working operation, wherein dendritic cast structure of the ingot has to be broken down. Zr-2.5%Nb alloy is extruded at a temperature close to 950°C. The extruded billet microstructure normally shows coarse α widmanstatten type of microstructure in which β phase. The β-quenched structure in Zr-2.5%Nb extruded tubes is consists of lath as well as plate martensites in which three distinct types of morphologies exist. These are large primary martensite plates which are occasionally internally twinned, fine secondary martensite plates arranged in self-accommodating groups and martensite laths stacked almost parallel within the packets [26, 27].

For Zr-2.5%Nb, (Ø230 mm billet) after β-quenching stage shows the microstructure consisting of martensitic (α’) basket weave morphology as illustrated in Figure 3.6. After extrusion, the alpha grains are elongated with a network of the second phase (β) around the grain boundary [85]. During the further processing, the phase is further gets deformed with higher aspect ratio. The secondary β-Zirconium phase present as continuous grain boundary with about 20 wt % Nb gets transformed to β-Nb, which is broken but enriched in Nb upto 80 wt %. A typical microstructure of the extruded Zr-2.5%Nb consists of about 90% α Zr and ~10% β Zr. Nb content is partitioned between the phases such that the predominant α phase has α Nb content less than 1 wt%, while the β-phase contains ~20wt% Nb. The volume fraction of the β phase is higher and the niobium content is less. During hot extrusion, the α and β phases dynamically recrystallizes and gives rise to thin and platelet-like shaped α grains that are mostly elongated in the axial direction and flattened in the radial direction. The β phase is sandwiched between α stringers. Extrusion elongates grain microstructures.

Fragmentation of the β stringers also occurred due to the heavy cold deformation and high presence of dislocation density within the α stringers. During annealing treatment, recrystallization of the two phases occurs. Additionally, in several regions continuous stingers of β phase gets globalized. It is found that optimum annealing treatment (550°C ~ for 6 hours) retains the elongated morphology of the two phases produced in the hot extrusion step. Furthermore, in the Zr-2.5%Nb alloy the starting single-phase martensitic structure is provided by β-quenching, which are transformed during the hot extrusion with the evolution of various textural developments. Normally, after the hot extrusion temperature, the β volume fraction is larger; so the large plates are those which nucleated at early stages of hot extrusion. During cooling from the hot extrusion temperature, Zr-rich β transforms to α+Nb-rich β Nb. By two-stage pilgering and annealing steps, the texture of the hot-extruded Zr-2.5Nb alloy could be reverse back [85]. Hence, hot extrusion is a complex process involving deformation, recrystallization (static and dynamic) and possible phase transformation leading to complex hot extruded microstructure which is difficult to define properly due to development a clear bimodal distribution in grain size and in grain morphology with larger elongated grains in association with smaller equiaxed grains. In general, deformation (both hot extrusion, as well as pilgering) strengthened the material properties, while annealing enhanced grain coarsening by the way of recovery/recrystallization to optimize mechanical properties.

3.3.3.3 Microstructure after final pilgering

The microstructure of Zr-2.5%Nb tube in stress relieved condition is shown in Figure 3.6 (c) showing α-Zr grains and fine β-Nb phase at α grain boundary. Due to the high amount of deformation, the microstructure could not be revealed clearly. However lamellar structure of the phase is still retained. The TEM micrograph also revealed the presence of high dislocation density after this operation [26, 27, 28].

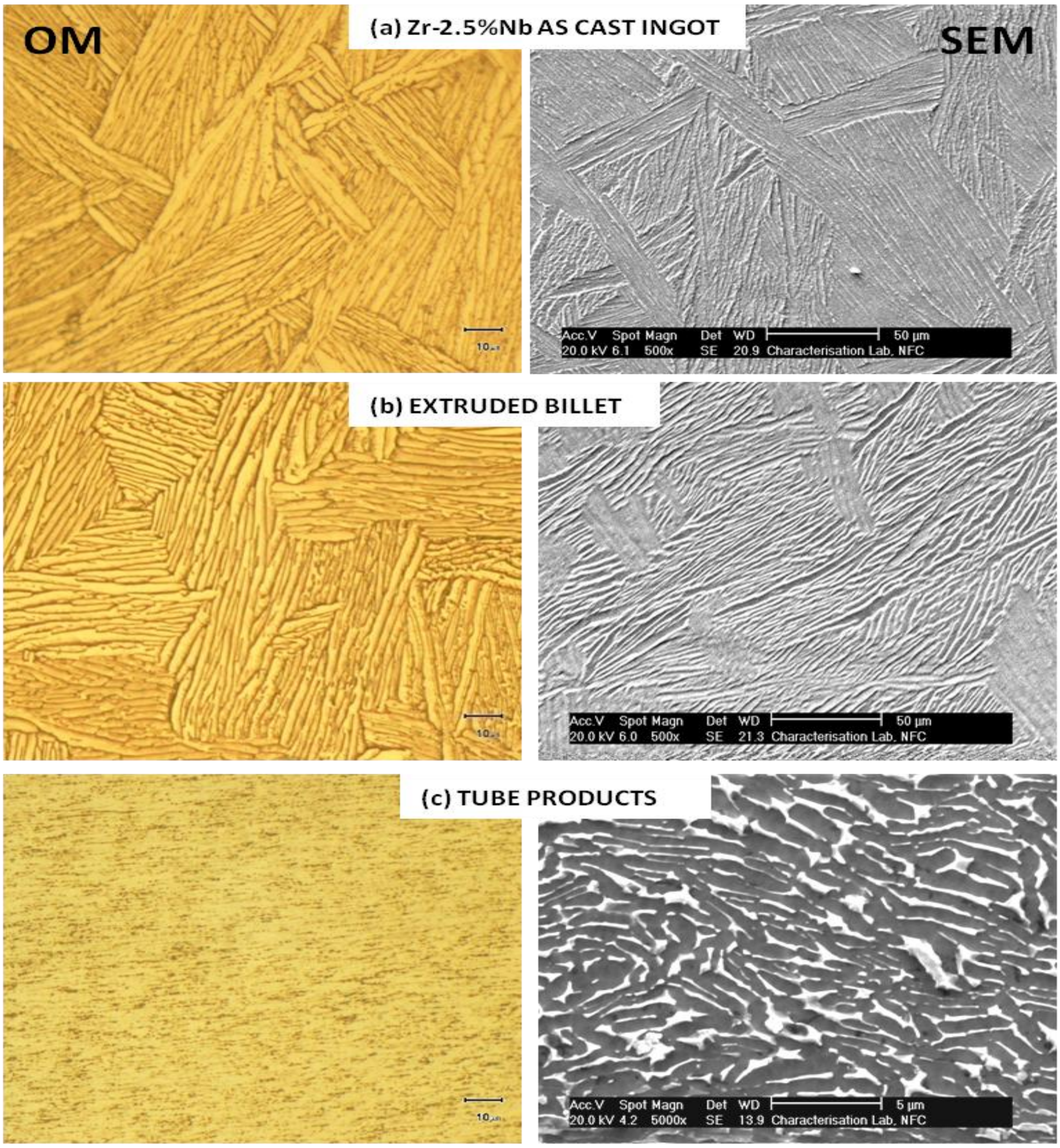

Figure 3.8: Optical and SEM Microstructure evaluation for Zr-2.5%Nb a) as-cast ingot indicate dendritic cast structure and the microstructure consists of fast cooled martensitic parallel plate morphology. b) Extruded Billet, Extruded Billet indicates presence banded structure elongated in extrusion direction and dynamic recrystallization. c) Final tube product. Microstructure of Zr2.5%Nb Tube in stress relived condition showing α-Zr grains and fine β-Nb phase at α grain boundary.

3.3.4 Microstructure evaluation for Zr-1%Nb alloy

3.3.4.1 Microstructure after as-cast ingots Zr-1%Nb alloy

The microstructure of as cast Zr-1%Nb alloy ingot is similar to that of Zr-2.5%Nb alloy ingot because of only marginal difference in chemical composition. A large grains (several millimeters) of the ‘as-cast’ dendritic structure was observed along with second phase particles at the inter-dendritic region, as shown in Figure 3.7(a) [100, 101]. The Zr-1%Nb alloy is composed of two phases microstructure: α-Zr (hexagonally close packed) and β-Zr (body-centered cubic) like Zr-2.5%Nb alloy. Thereby, the microstructure of the Zr-Nb alloys are different from those other commonly used Zirconium-based alloys. In addition, in these alloys, the shape, size and size distributions of the β-Zr phase may significantly differ depending on the TMP and heat treatment. The matrix phase (α, hcp) consists of equiaxed with spherical second phase particles (β, bcc) distributed inside as well as at the grain boundaries of the matrix phase. In comparison, the Zr-2.5%Nb alloy has duplex microstructure of α and β-phases in which the distribution depends on the prior thermo-mechanical treatment. However, in the Zr-1%Nb alloy, the β-phase is distributed as fine spherical particles within α matrix. Similarly, the zircaloys also have a microstructure similar to the Zr-1%Nb alloy but essentially with a single phase microstructure in which intermetallic precipitates are distributed within the α matrix [102]. Furthermore, in the Zr-1%Nb alloy, the β-Zr phase is distributed as fine spherical particles within the α-Zr matrix. Zircaloy alloys also shows microstructure similar to the Zr-1%Nb alloy, but they essentially exhibit a single-phase microstructure in which intermetallic precipitates are distributed within the α-Zr matrix. In Zr-1%Nb alloy, therefore, the size, size distribution and composition of the β-Zr phase are expected to vary with aging time, TMP treatment and temperature [85, 102].

3.3.4.2 Microstructure after First Extrusion and β quenching Zr-1%Nb alloy

Extruded Zr-1%Nb alloy shows metastable Zr rich β phase present at the interface of the extruded α lamellaes. In subsequent annealing treatments these Zr rich β phase transforms into bands of Nb rich fine β precipitates. As has been mentioned earlier, annealing treatments have been carried out both above and below the monotectoid temperature, Tm ~ 610^0C. At T>Tm, the precipitating phase will correspond to the βI phase which during equilibrium cooling can transform into the βII phase through the monotectoid reaction βI = α + βII. In the

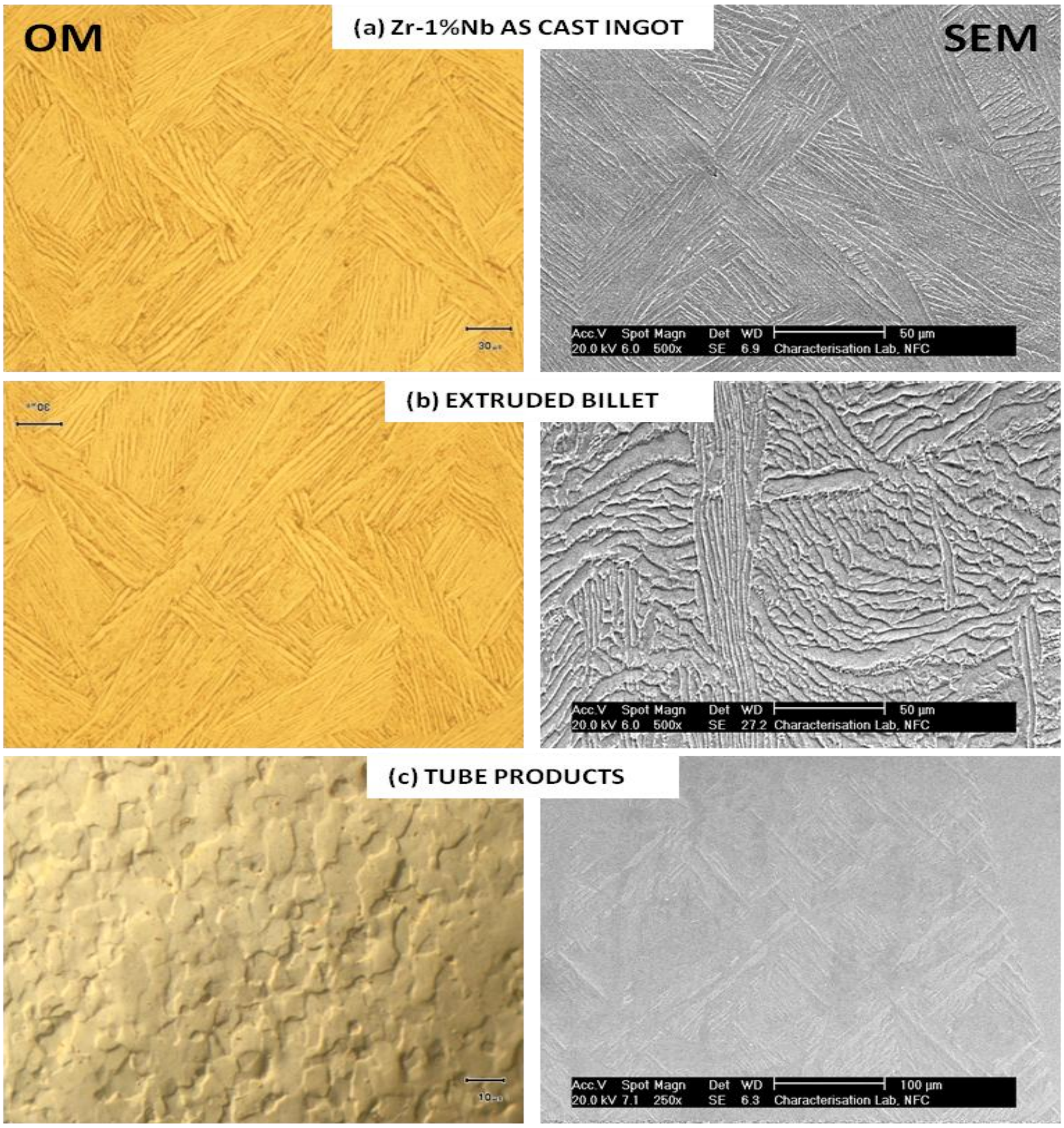

Figure 3.9: Optical and SEM Microstructure evaluation for Zr-1%Nb alloy a) as-cast ingot indicate dendritic cast structure and the microstructure consists of fast cooled martensitic parallel plate morphology. b) Extruded Billet indicate presence banded structure elongated in extrusion direction and dynamic recrystallization. c) Zr-1%Nb fuel tubes are cold -worked and annealed and shows fully recrystalised microstructure.

case of Z-1%Nb, β quenching leads to the formation of the lath martensites. Extruded billet indicates presence banded structure elongated in the extrusion direction and dynamic recrystallization (figure 3.7(b)).In Zr-Nb alloy systems, the various sequences of phase transformations possible in the alloys includes the following:

1. The martensitic transformation from the β (bcc) to the α (hcp) phase in alloys containing 0 to 7 % Nb,

2. The β to ω (hexagonal) transformation in alloys containing 7 to 17 wt% Nb during β quenching (athermal ω) or isothermal holding (ω precipitation),
3. The precipitation of α from the supersaturated β phase,
4. Phase separation, β → β1 (Zr rich) + βII (Nb rich), that can initiate by a spinodal decomposition in a suitable temperature and composition regime, and a monotectoid reaction, βI →α + βII (at 510 ºC and 20 % Nb) [103].

3.3.4.3 Microstructure after final pilgering and final annealing for Zr-1%Nb alloy

Zr-1%Nb alloy tubes are cold-worked and intermittently annealed before further processing. Final Zr-1%Nb fuel tubes are cold-worked & annealed and shows fully recrystallized microstructure. In case of Zr-1%Nb, annealing at 580°C for 1 h showed a fully recrystallized microstructure {Figure 3.7(c)}. Precipitate size and volume fraction was considerably less and the precipitate distribution was not uniform. The precipitates were of the β phase. On increasing the annealing time to 4 hours at 580°C, the bimodal grain size distribution (as seen in the case of 1 hour) was retained in the microstructure. Precipitate volume fraction increased substantially, the precipitate size distribution was bimodal and the distribution was not uniform. The precipitate composition, morphology and volume fraction depended strongly on the composition of the alloy and annealing temperature. The composition range and the precipitates distribution suggested (1) the continuous nucleation of β phase close to β_I during the cooling process and (2) the enrichment of β precipitates with Nb. The preferential nucleation of metastable βI is attributed to the smaller activation energy requirement in comparison to the β_{II} phase [103]. The presence of bimodal precipitate size distribution supported the continuous nucleation process where large and small precipitates may be distributed inside the grains and some precipitation of particles at the grain boundary. The monotectoid reaction in the Zr-Nb phase diagram plays a major role in the evolution of β precipitates in Zr-Nb based alloy. The extent of recrystallization has been found to be an important parameter in deciding the mechanical properties [91, 92]. However, the nucleation process of β precipitates in the $\alpha^{'}$ matrix of composition Zr-1%Nb involves (1) segregation of Nb atoms and (2) transformation of crystal structure from hcp to bcc [104].

3.4 XRD analysis

X-ray diffraction studies were conducted for phase identification and analysis by using a monochromatic copper K, radiation in conjunction with the XRD scans were recorded using Rigaku Dmax 2000 with Cu Ka radiation (λ= 0.154nm or 1.54A°) as the X-ray source (40 kV and 30mA with Ni filter). Samples were tested in the 2θ angle range 30°–140°, at scan steps of 0.05°2θ/step and scan speed of 1°2θ/min. Monochromatic $K\alpha_1$ was obtained (with K_β peak separation) using the diffracted beam from a crystal monochromator. The $K\alpha_2$ stripping was carried out by using software (assuming $K\alpha_2$/ $K\alpha_1$ intensity ratio as 0.5), smoothening was carried out by Savitzket Golay’s method, and back- ground correction by the Sonnevelt–Visser method.

XRD analysis for unalloyed Zirconium, Zr-2, Zr-4 and Zr-2.5%Nb alloys was carried out for different thermomechanical processes such as i) as-cast ingot, ii) hot extruded and iii) final pilgered and annealed condition.

All the samlpes for unalloyed Zirconium and Zr-4 confirms that the formation of α HCP phase in as-cast, extruded and final pilgered stages, though second phase particles were observed in optical and SEM/EDS analysis, their presence in XRD is not revealed. This could be attributed to low volume fraction of the second phase in these alloys.

Tin is an α stabilizer, and at the concentration of 1.2-1.8 % used in Zircaloys to form intermetallic precipitates. Such precipitates are however not observed, due to kinetic reasons, and, Sn is found in the α phase in solid solution. Tin, has some impact on mechanical properties, by increasing the tensile yield strength, and therefore it is not completely eliminated from the alloys.

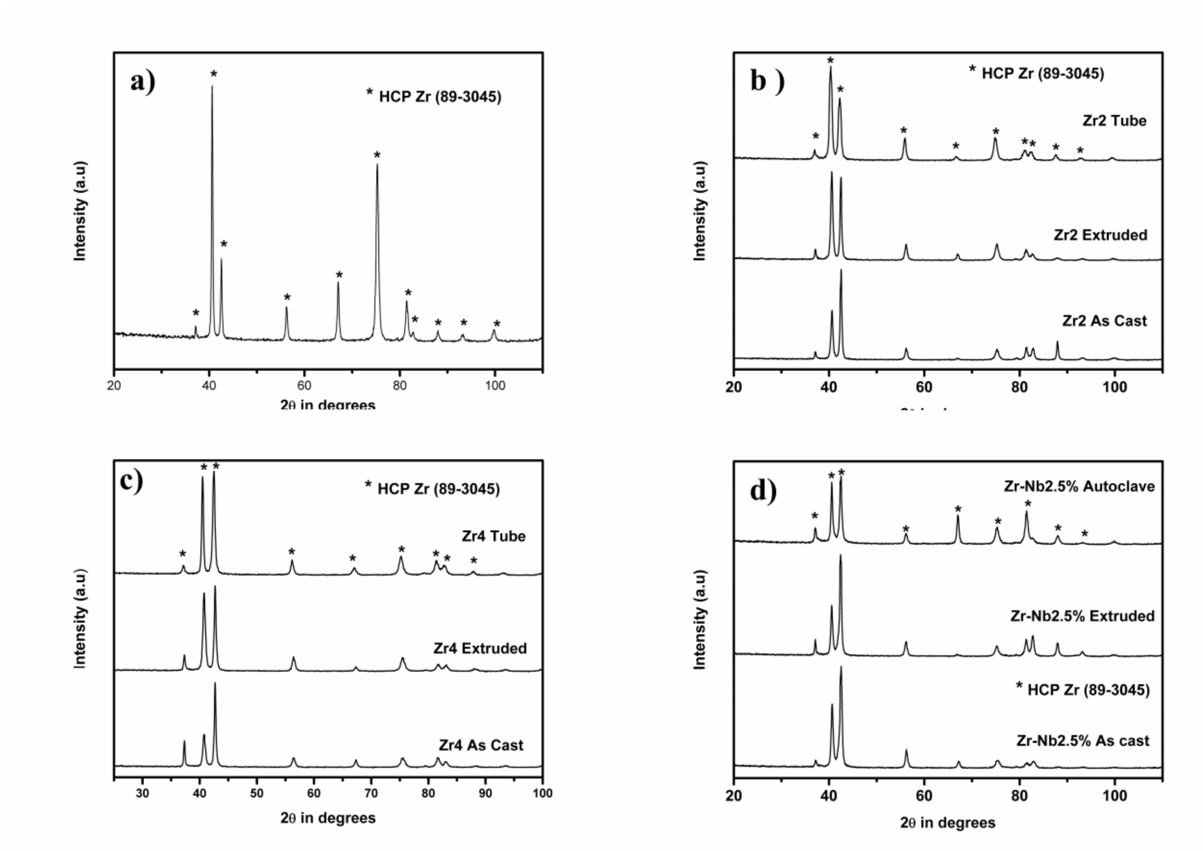

Figure 3.10.: XRD analysis a) Unalloyed Zr b) Zr-2 c) Zr-4 and d) Zr-2.5%Nb alloys during different thermomechanical processes: i) As-cast ingot, ii) Hot extruded and iii) Final pilgered and annealed condition. All the samples confirms that the formation of α HCP phase in as-cast, extruded and final pilgered stages, though second phase particles were observed in optical and SEM/EDS analysis, their presence in XRD is not revealed. This could be attributed to low volume fraction of the second phase in these alloys.

For the Zr-Cr and Zr-Ni binary alloys, the stable forms of the second-phase precipitates are Zr_2Ni or $ZrCr_2$. These phases are observed in the Zircaloys, with Fe substituting for the corresponding transition metal. In Zr-4, the partitioning intermetallic phases leads to formation of second-phase precipitates are $Zr(Cr,Fe)_2$ and Zr_3Fe. In Zr-2 alloys, the partitioning of Fe between the two types of intermetallic phases leads to a more complex relationship between nominal composition and precipitate composition, giving a broad range of Fe/Cr ratio in $Zr(Cr,Fe)_2$, and Fe/Ni ratio in $Zr_2(Fe,Ni)$.

The as-cast Zr-4 ingot indicates presence of small intermetallic second phase particles (Fe, Cr, Ni, Si, C), Second Phase Particle (SPPs at grain boundaries). Precipitation after β-quenching is rapid and the coarsening rate of those precipitates controls their sizes in the final microstructure.The final anneal controls the microstructure of the product. The alloying elements in solid solution may impact the corrosion and hydriding properties as well as strength of the material, while the SPPs mainly affect the corrosion and hydriding performance. The phase compositions and content play a fatal role on the mechanical properties of the as-extrude and final pilgered tubes.

In case of Zr-2.5%Nb alloy, at ingot stage the microstructure consists of fast cooled martensitic parallel plate morphology. At billet stage after β-quenching the structure consists of martensitic (α') basket weave morphology. After extrusion the alpha grains are elongated with a network of second phase (β) around the grain boundary, due to higher volume fraction of the β phase it is detected in the XRD at this stage. During the further processing the α phase is further gets deformed with higher aspect ratio. The secondary β-Zirconium phase present as continuous grain boundary with about 20 wt % Nb gets transformed to β-Nb, which is broken but enriched in Nb upto 80 wt %. Due to low volume fraction of the β-Nb no peaks are detected in XRD.

3.5 Mechanical properties

Mechanical properties analysis was carried out at different stages of manufacturing to study the effect of various thermomechanical processes evolved during manufacturing. Mechanical properties like tensile strength, % elongation was evaluated at room temperature with different Zirconium alloys at as-cast ingot, extruded & β quench stages and final thermomechanical treatment at finishing cold reduction stage followed by heat-treatment. The evaluation of mechanical properties carried out and has been summarized and shown in Figure 3.11 and 3.12. The mechanical properties of the tubes produced from the unalloyed Zirconium, Zr-2, Zr-4, Zr-1%Nb alloy tubes and Zr-2.5%Nb alloys have been studied at various process steps like as-cast, extruded & β quenched and final tube product. In essence, the variation in the mechanical properties of tubes produced from different process steps and with different alloy type is not found to be significant. Zirconium alloys follow the standard work hardening phenomenon due to cold-working. As percentage cold work is increased, mechanical properties like YS and UTS are also increased but percentage elongation is decreased significantly. However, it is evident that the mechanical properties of zircaloy and its alloys are largely dependent on microstructure and crystallographic texture of the α and β phases and also interactions between them during deformation and heat treatments. In additions, during TMP treatments in the various fabrication steps, the nature of β-phase transformation and the final microstructure, eventually govern the long-term and short-term mechanical properties of the pressure tubes. Thereby, the mechanical properties of the Zr alloys are strongly dependent on several parameters such as alloy composition, texture and metallurgical state. For most of the practical application the properties at 300-400 ^{o}C are most important. Room temperature behavior is used mostly for comparison [77, 105]. However, it can be noticed that as-cast ingot samples are showing slightly lesser mechanical properties and ductility compared to final product and extruded & β quenched. The rest of the properties for Zr-2.5%Nb alloys are better than tubes produced from Zr-2, Zr-4 and Zr-1%Nb alloys due to the addition of a higher quantity of alloying element. The mechanical properties are considerably related to microstructural and textural properties [6,85,91]. At room temperature, in the annealed state, oxygen-free Zr has low yield strength (i.e. about 150MPa). However, the yield strength can be increased by solution strengthening by addition of oxygen, tin, or niobium. Tin is known to cause only a small increase in tensile strength, but substantially improve creep strength, Nb increases both the yield and creep strength. Zircaloys have yield strengths in the range of 250-300MPa and the Zr-2.5% Nb alloy, show the marginally higher strength of about 300-400 MPa. As observed in other alloy metals, reduction in grain size is also used to obtain higher strength. For all those materials, the ductility remains high, above 15%. Furthermore, in Zr and its alloys additional strength is obtained by cold working, with increasing yield strength above 400-500MPa. After the TMP treatments, this is followed by a stress-relieving heat treatment to restore ductility without significant reduction in strength by relaxing the internal stresses. Also, the texture evolution itself can increase alloy strength by changing the Schmid factor for slip or twinning [105].

In Figure 3.11, the as-cast unalloyed Zirconium, Zr-2, Zr-4 Zr-2.5%Nb and Zr-1%Nb ingot exhibit YS of about 210, 250, 300, 335 & 230 MPa, UTS of about 330, 470, 442, 517 & 380 MPa and percentage of elongation values 24, 22, 19, 8.5 & 21.5% respectively. The lower mechanical properties of as-cast ingot were attributed to the course dendritic cast structure.

For the hot extruded Zr-2, Zr-4 Zr-2.5%Nb and Zr-1%Nb the YS was about 340, 336, 418 & 351MPa and UTS was about 470,471, 517 & 483 MPa and percentage of elongation was 14, 25 , 18 & 19%. The slight increase in mechanical properties could be attributed to the bimodal microstructure obtained by hot extrusion.

For final pass pilgered and heat-treated condition, for Zr-2, Zr-4, Zr-2.5%Nb and Zr-1%Nb YS and UTS increased significantly as shown in Figure 3.11. Interestingly, similar YS values for 325, 483, 504 & 310 MPa; UTS 521, 621, 736 & 393 and percentage of elongation was 25, 30, 17 & 32 respectively were observed. The improved mechanical properties are related to grain size refinement and work hardening during the pilgering process. The most important parameters that influence the mechanical properties in Zirconium and its alloys are the dual phase microstructure associated with the volume fraction of primary α, closely related to the partitioning effect of alloying elements such as Nb, O and Fe in α and β phases. Similarly, the properties of the fabricated tube (i.e., crystallographic texture, mechanical properties) are strong functions of the amount of primary a phase (after heat treatment) present in the alloy, which in turn is dependent on the soaking temperature in the α + β phase field. In Zr-Nb alloys, the Nb content in β phase significantly increases the strength by solute strengthening the effect. At lower concentration of Nb in β Zr, deformation mode was predominantly slip, while at higher Nb concentration (>40%) solute strengthening increasingly blocked dislocation slip leading to twinning [106]. Twinning is sometimes cited as the cause for the peak/drop and this deformation mechanism is initiated only after several percents of plastic strains, in both axial and circumferential directions of a tube [107].

3.5.1 Hardness testing

Hardness testing was performed for various Zirconium alloys and unalloyed Zirconium in "FEI" microhardness tester. Hardness was evaluated as a function of different important stages of production. Hardness studies of at the different tremomomechanical processing states were also carried out and the results are presented in the Figure 3.12 [67].

As-cast-ingots for pure Zirconium, Zr-2 , Zr-4, Zr-2.5% Nb and Zr1% Nb are composed of randomly oriented equiaxed grains of few centimeters and are having a hardness value of 114, 147, 145, 187 & 157 VHN respectively. Unalloyed Zirconium shows the lowest value as no alloying elements are added and Zr-2.5%Nb alloy has the highest value attributed to niobium metal and parallel plate martensitic morphology. As-cast Zr-2, Zr-4 and Zr-1%Nb hardness values are in moderate ranges.

Extruded and β quenched billets of Zr-2, Zr-4, Zr-2.5%Nb and Zr-1%Nb are showing hardness value of 161, 156, 190 & 179 VHN respectively. The hardness is higher compared to as-cast ingot for all the alloys, in case of Zr-2 and Zr-4 attributed to Widmannstätten type α-plates. Alloy Zr-2.5%Nb shows a basket weave martesite (hcp) structure.

Finally cold worked and fully annealed Zr-2 shows lower hardness value 188 HV compared to 258 HV in Zr-4, indicating that the stress relieved treatment at lower temperature exhibit higher strength. The Zirconium alloys tubing is usually fabricated in two conditions: fully recrystallized (final anneal at 560°C) or cold work stress relieved (if the final anneal is at 480° C). Initially due to cold working hardness increased in both the alloys. In the alloys, precipitation, recovery and recrystallization process take place during the annealing process.

Final pass Zr-1%Nb tubes are cold-worked and annealed as per the requirement that shows hardness value of 210 HV with fully recrystalised microstructure. Final tube of Zr-2.5%Nb is showing hardness value of 248 HV. This higher value is due to cold worked and stress relieved condition and presence of considerable amount of dislocation density and α-Zr grains and fine β-Nb phase at α grain boundary.

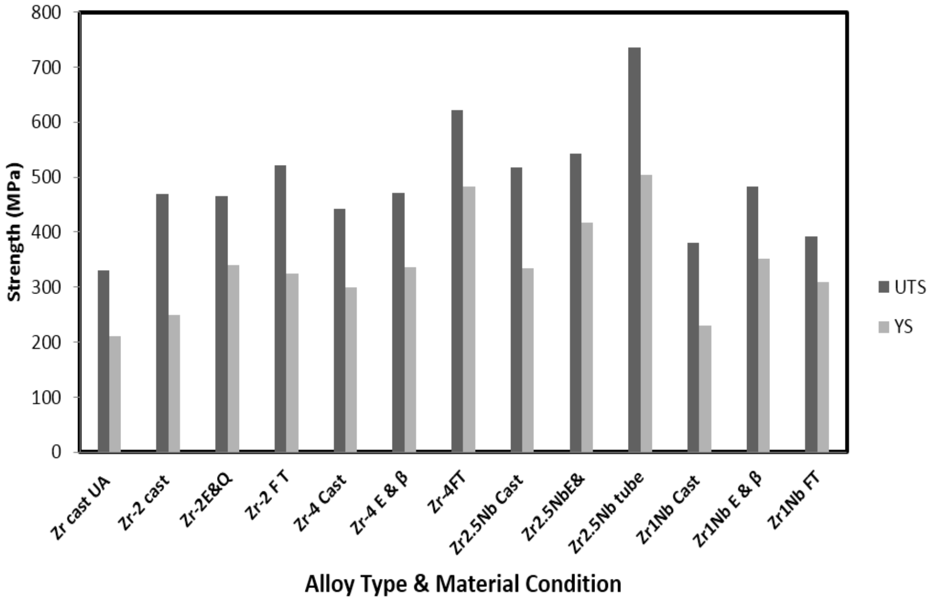

Figure 3.11: Effect of material condition on mechanical properties of Zirconium and its alloys.

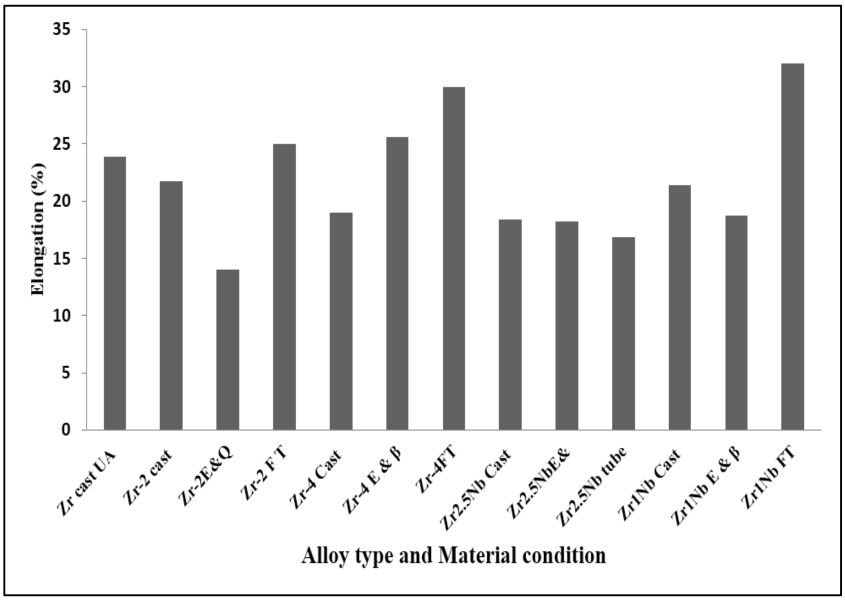

Figure 3.12: Effect of material condition on mechanical properties of Zirconium and its alloys.

3.5.2 Hardness testing in Weld Region

The weld region of the TIG welded Zr-4 exhibited a hardness value of 387 VHN, while the hardness of the base metal was only 183 VHN. The weld region of the EB welded Zr-4 showed a hardness value of 197 VHN in the weld region (Figure 3.11). The increase in the hardness in the TIG weld region might be due to increase in oxygen or nitrogen content in the weld region. It has been reported [13] that hardness increased to 10 points by a 140 ppm increase in nitrogen content (for an initial content ranging between 20 and 1000 ppm) or by a 200 ppm increase in oxygen content (for an initial content ranging between 500 and 4000 ppm) [24].

The microstructure of the cast ingot for all the Zirconium alloys is evolved due to directional rapid cooling across the ingot diameter and longitudinally is dendritic type without any sign of alloying element/ impurities segregation with basket-weave or Widmenstratten morphology. In the case of pure Zr-2.5%Nb and Zr-1%Nb alloy, the microstructure is consists of the of fast cooled martensitic parallel plate morphology.

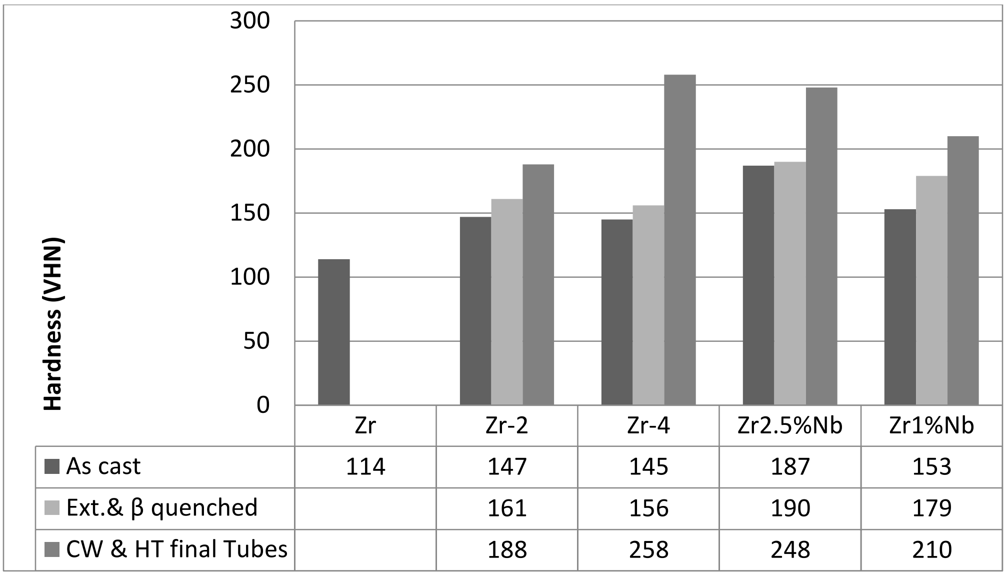

	Zr	Zr-2	Zr-4	Zr2.5%Nb	Zr1%Nb
■ As cast	114	147	145	187	153
■ Ext.& β quenched		161	156	190	179
■ CW & HT final Tubes		188	258	248	210

Figure 3.13: Hardness values for unalloyed Zirconium and Zirconium alloys at different manufacturing stages. (As cast, Extrusion and β quenched and Cold worked and final heat treated)

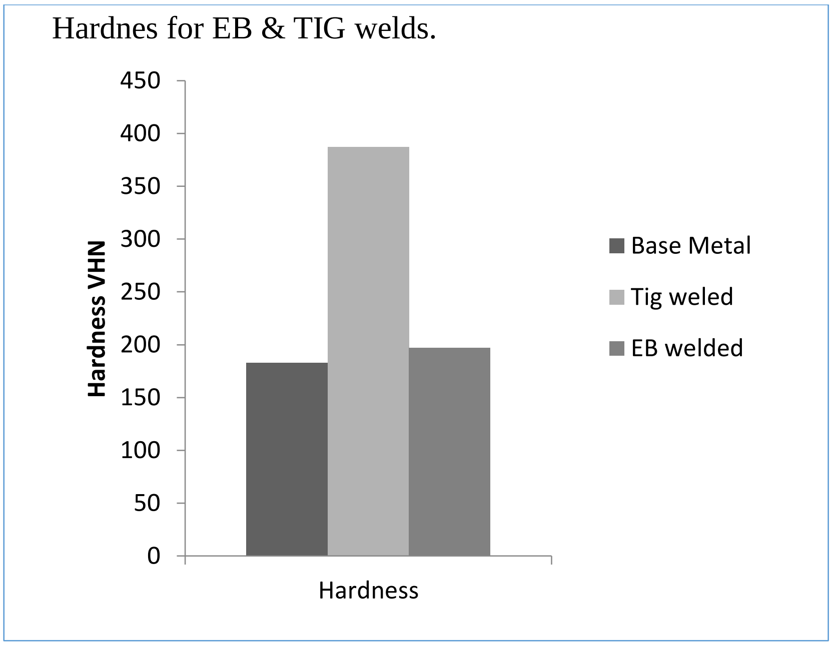

Figure 3.14: Hardness values for Zr-4 in the base metal. TIG welded and EB welded region.

3.6 Conclusions

In this chapter, the methodology used for optimization of manufacturing processes with consideration of microstructural and mechanical properties of various Zirconium alloys and unalloyed Zirconium were highlighted. The effect of thermomechanical processing on the evolution of microstructure behavior has been studied. Mechanical and microstructural properties depend strongly on the composition of the alloy and annealing temperature. The extent of recrystallization has been found to be an important parameter in deciding the mechanical properties. Hot processing maps have been used to identify the optimum processing parameters for Zirconium alloys and the strain rate-temperature domains corresponding to the occurrence of dynamic recovery and recrystallization processes. TMP steps used for the fabrication of Zr components are aimed at obtaining required microstructure. The final microstructure and associated properties, is often a cumulative outcome of series of changes occurring at each stage of processing. Hence, systematic characterizations of the microstructural evolution at the different stage are carried out.

SEM-EDS analysis for Zr-2 tubes show evenly distributed fine second phase particles, and indicate the presence of higher concentration of Fe, Cr and Ni compared to base material. In Zr-2 alloys, the partitioning of Fe between the two types of intermetallic phases leads to a more complex relationship between nominal composition and precipitate composition, giving a broad range of Fe/Cr ratio in $Zr(Cr,Fe)_2$, and Fe/Ni ratio in $Zr_2(Fe,Ni)$. Similarly for Zr-4 tubes show evenly distributed fine $Zr(Fe, Cr)_2$ precipitates and intermetallic particles within the grains with very high Fe/Cr ratios.

EBSD maps clearly show the change in microstructure during pilgering and annealing operations. The as-cast Zr-4 ingot indicates dendritic cast structure and presence of small intermetallic second phase particles (Fe, Cr, Ni, Si, C), Second Phase Particle (SPPs at grain boundaries). Similarly, β quenched microstructure consists of Widmannstatten type α-plates. Hot extruded microstructure of extruded billets and slabs indicates the presence of banded structure and dynamic recrystlisation. Cold worked pilgered structure is elongated in the direction of deformation; Cold work followed by annealing is showing bright elongated structure along the working direction.

In the case of Zr-2.5%Nb at ingot stage the microstructure consists of fast cooled martensitic parallel plate morphology. Extruded Zr-2.5%Nb and Zr-1%Nb alloy show metastable Zr rich β phase is likely to be present at the interface of the extruded α lamellaes. In subsequent annealing treatments, these Zr rich β phase transforms into bands of Nb-rich fine β precipitates. The extent of recrystallization has been found to be an important parameter in deciding the mechanical properties.

- The Zr-2.5Nb and Zr-1%Nb are two phase alloys. These alloys consist of primary phase as a Zirconium (HCP) and secondary phase as β-Zirconium (BCC).
- Cast ingot is having very low mechanical properties and hardness with considerable percentage elongation of 25.6%. Low mechanical properties can be attributed to course dendritic cast grain structure.
- Randomized 'β-quenched' microstructure is having better mechanical properties due to homogenous microstructure.
- Hot extrusion, developed a clear bimodal distribution in grain size and in grain morphology with larger elongated grains in association with smaller equiaxed grains. Elongated larger grains had higher grain average misorientation and more dislocation density. Hence are having more pronounced mechanical properties, the first annealing operation of blanks is carried out 'First annealed' for recovery/recrystallization and also at grain coarsening (an increase in average grain size of 9-12 µm from hot extruded structure). Bimodal grain size distribution remained though the large grains were, in general, less elongated.
- All the pilgering stages produce a 'heterogeneous deformation structure' increasing mechanical properties considerably and decreasing percentage elongation, hence necessitating intermediate annealing before next cold-working operation.

In case of Zr-Nb alloy, the processing steps also modifies microstructure in the following sequence:

Widmanstätten structure (β -quenched) → bimodal grain size/shape (hot extruded) →relative grain growth (first annealing) → heterogeneous deformation (first pilgered) →fully recrystallized (second annealed) →heterogeneous deformation (second pilgered) →partially recrystallized → (third annealed) →heterogeneous deformation (third pilgered) → partially recrystallized (final annealed).

In case of the products, the microstructure is influenced by thermo-mechanical processing (TMP) steps used for the fabrication of Zr components.

- Zr-2, the microstructure is consists of the equiaxed grains, tubes for are as they are in fully annealed condition.
- Zr-4, the microstructure is consists of the elongated grains in working direction for tubes, as they are in stress relieved condition. In the case of cold rolled and annealed sheet annealed are showing recrystallized bright elongated areas.
- Zr-2.5%Nb alloy, tube microstructure is consists of stress relieved condition showing α-Zr grains and fine β-Nb phase at α grain boundary.
- Zr-1%Nb alloy tube microstructure is consists of recrystalised micro-structure.

TIG welded Zr-4 sample exhibited coarse acicular α structure in comparison to the fine acicular structure of EB welded sample. All welds exhibited a transformed grain structure or acicular α grains surrounded by prior β grain boundaries (Widmanstatten or basketweave structure).

TIG welded Zr-4 exhibited a hardness value of 387 VHN, while the hardness of the base metal was only 183 VHN and EB weld is 197 VHN. The increase in the hardness in the TIG weld region is due to increase in oxygen or nitrogen content in the weld region.

CHAPTER IV

CORROSION BEHAVIOR OF ZIRCONIUM ALLOYS IN NITRIC ACID

4.1 Introduction

In the present study of corrosion, investigations were carried out for Zirconium and its alloys like Zr-2, Zr-4, Zr-1%Nb and Zr-2.5%Nb in boiling 11.5 M HNO_3 to simulate dissolver condition in the nuclear reprocessing plant. Like any other valve metals, Zirconium forms stable and strongly adherent ZrO_2 oxide passive film in most aqueous environment protecting it from corrosion process. The passive film form instantly when the metal surface is exposed to air or any environment containing a trace of moisture or oxygen. However, unlike most valve metal passive film, anodic passive oxide film on Zirconium may incorporate anions from the anodizing solutions further enhancing the film stability [77, 108]. The great demand for highly corrosion resistant stable light weight material to be used in nuclear industry, thermal reactors, chemical industries and electrochemical methods of the spent fuel reprocessing by Purex process along with waste minimization makes the corrosion and passivation of Zirconium and its alloys very significant. In addition, Zirconium has superior corrosion resistance to concentrated HNO_3 at elevated temperature compared to titanium and its alloys; thereby Zirconium and its alloys are being successfully used as a preferred material for chemical plants for handling HNO_3 or spent nuclear fuel reprocessing plants involving aggressive nitric acid media. This chapter describes the corrosion behavior of the Zirconium-based alloys which were subjected to boiling 11.5 M HNO_3 as per ASTM A262 Practice C for 240 h (5 periods of 48 h) and for 1000 h boiling 11.5 M HNO_3 in the Zirconium test loop facility. SEM investigation of these samples surface subjected to ASTM A262 practice C and Zirconium test loop facility had been carried out. Potentiodynamic polarization behavior of Zr-4 tubes in nitric acid at room temperature was also studied. Zr-4, one of the candidate material for dissolver assembly fabrication, was also studied in the different condition [48].

4.2 Results and Discussion:

4.2.1 Potentiodynamic polarization behavior of Zr-4 tubes in nitric acid

The polarization curves recorded for Zr-4 in different conditions of the cast, extruded, pilgered and autoclaved in 11.5 M HNO_3 at room temperature are shown in Figure 4.1. Corrosion parameters such as the corrosion potential, E_{corr} and corrosion current density, I_{corr} were extrapolated and listed in Table 4.1. It is very important to understand fully the characteristic of anodic polarization curves for Zr-4 in HNO_3. The E_{corr} and I_{corr} values were obtained by Tafel method [48]. As observed in Figure 4.1, the polarization curve of the passivity and its breakdown potential of Zr-4 in 11.5 M HNO_3 can be divided into two or three characteristic regions, i.e., primary, secondary and tertiary potential regions as mentioned below:

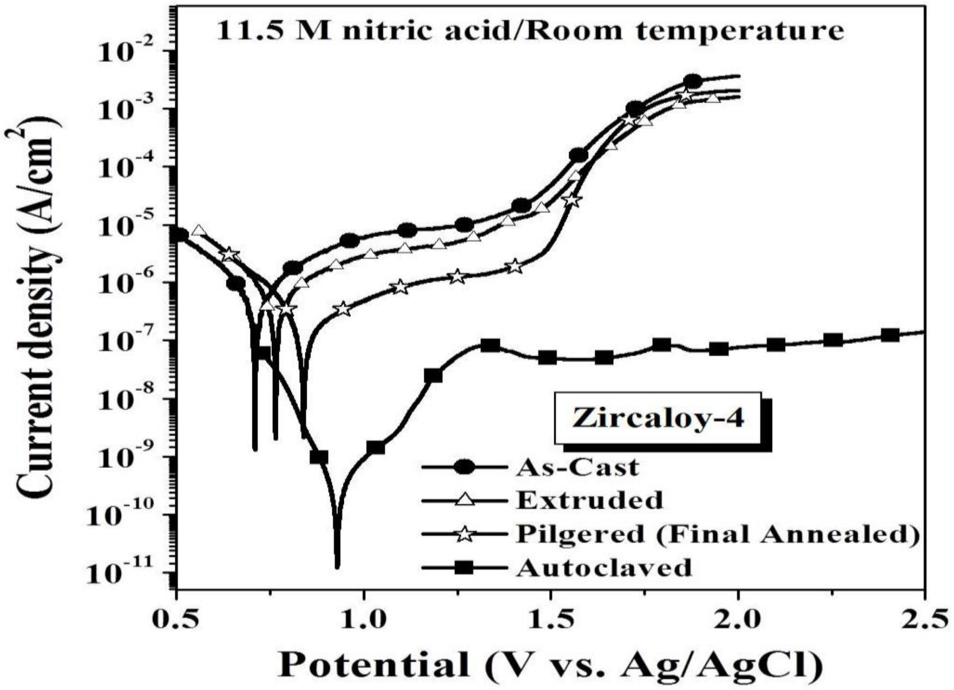

Figure 4.1: Potentiodynamic polarization curves recorded for different theremomechanical treated Zr-4 samples in 11.5 M HNO_3 at room temperature.

(1) In the primary potential region, the passivity is maintained by the ZrO_2 film.

(2) Towards transpassive region, breakdown of the ZrO_2 passive film broke down owing to partial dissolutions of ZrO_2 as ZrO^{2+} and Zr^{4+} at the potential above 1.5V (vs. Ag/AgCl) up to 2V in 11.5 M HNO_3, and

(3) Beyond this region, it is the oxygen evolution stage and the thickening of ZrO_2 film occurred.

However, in autoclaved specimen no tertiary or transpassive potential region is seen in the polarization curve attributing to the enhanced stability of ZrO_2 film. Figure 4.2 shows the schematic illustration depicting the stability and breakdown of the surface films formed on Zirconium in three characteristic potential regions [109].

Table 4.1: Polarization parameters of different theremomechanical treated Zr-4 samples in 11.5 HNO_3 at room temperature, Polarization parameters: corrosion potential E_{corr}, passivation potential E_{pass}, corrosion current density I_{corr}, passive current density $I_{pass}$and Tafel Slope Constantsβa & βc

Material/Electrolyte		E_{corr}	I_{corr}	E_{pass}	I_{pass}l	Tafel Slope Constants	
		V vs. Ag/AgCl	x 10^{-6} A/cm^2	V vs. Ag/AgCl	x 10^{-6} A/cm^2	βa mv/dec	βc mv/dec
As-cast	Nitric	0.71	0.20	0.84	2.3	280	390
Extruded	Nitric	0.76	0.13	0.86	1.24	280	870
Pilgered and Annealed	Nitric	0.84	0.10	0.93	0.296	200	540
Autoclaved	Nitric	0.92	0.00067	1.5	0.0497	-	-

In Zirconium and its alloys, the corrosion behavior depends significantly on the microstructure, which can be modified by thermomechanical treatments. It is evident that the shapes of polarization curves in 11.5 M HNO_3 changed depending on the material condition, i.e., cast, extruded, pilgered and auto-claved.In nitric acid, the Zr-4 pilgered tube sample exhibited spontaneous passivation with the distinct passive region, until the transpassive potential, E_{tp} as shown in Figure 4.1. Passivation of Zr-4 in nitric acid is attributed to the formation of ZrO_2 and the E_{tp} was about 1.5V in nitric acid. To improve the corrosion behavior of Zr-4 pilgered tube further, autoclaving was done and these samples were subjected to potentiodynamic polarization test in nitric. Autoclaving of Zr-4 resulted in the formation of a thick black colored oxide layer of ZrO_2 [48]. The lowest corrosion current values obtained for the autoclaved Zr-4 sample in nitric suggested that the ZrO_2 formed during autoclaving acted as a barrier layer. Though current was fluctuating above E_{corr}, in the passive region, the measured current values were lower than that for pilgered conditions of Zr-4. Interestingly, the increase in current values due to the transpassive behavior was not noticed for the autoclaved Zr-4, until 2.5V. The potentiodynamic polarization results obtained in nitric acid indicated that the highest corrosion resistance is offered by the autoclaved Zr-4 sample when compared to the pilgered conditions of Zr-4. Thus, the corrosion resistance of these materials were evaluated as discussed in the following sections by weight loss measurements, by exposing the samples to boiling liquid nitric acid for 1000 h. In Zirconium alloys, the corrosion resistance in nitric acid is affected by its concentration and temperature of nitric acid as well as applied potential [109]. Though Zirconium alloys show high general corrosion resistance in HNO_3 media, in highly oxidizing spent fuel reprocessing media, certain factors need to be closely investigated. These includes the followings [14, 109]:

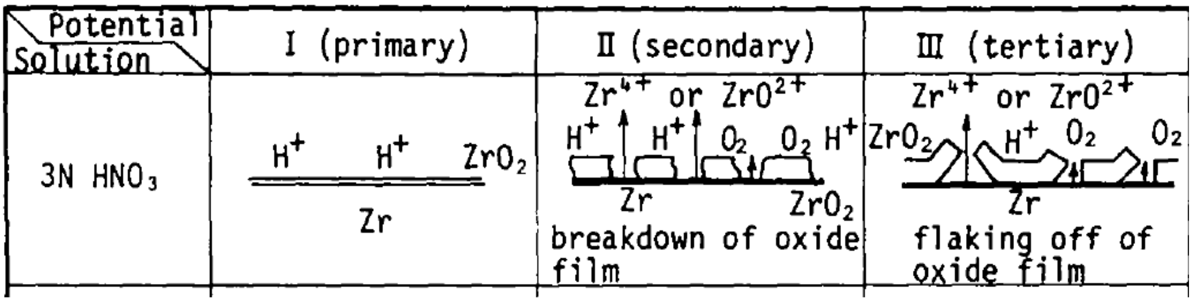

Figure 4.2. Schematic illustration showing the passive films formed on Zirconium in the characteristic potential region in nitric acid [109].

(i) It exhibits passive-transpassive transition regions,

(ii) Shifts in high corrosion potential towards transpassive potential region as concentration increases with higher corrosion,

(iii) Require Zr sponge addition for inhibiting corrosion of Zr vessels in fluoride containing environments, and

(iv) Corrosion fatigue and stress corrosion cracking in heat affected zones (HAZ) of welds observed in laboratory test. Thereby, it is essential to understand the characteristic of polarization curves for Zirconium in HNO_3, and the relationship between passivity and breakdown of passivity to provide understanding to its corrosion resistance behaviors.

4.2.2 ASTM A262 practice "C" and long term loop corrosion test

The average corrosion rates of as-cast-ingot, pilgered tube, cold-rolled sheet and autoclaved tube for unalloyed Zirconium, Zr-2, Zr-4, Zr-2.5%Nb and Zr-1%Nb have taken up for practice "C" and long term corrosion loop have been tabulated in Table 4.2. The corrosion rates clearly indicated that Zirconium and its alloys i.e. Zr-2, Zr-4, Zr-2.5%Nb and Zr-1% Nb show superior corrosion resistance. The high corrosion resistance of Zirconium and its alloys in highly oxidizing nitric acid conditions is due to stable and adherent ZrO_2 film formed on their surface [19, 20].

- The corrosion rates obtained from ASTM A262practice "C" corrosion test for as-cast ingots of unalloyed Zirconium, Zr-2, Zr-4, Zr-1%Nb are 0.005, 0.005, 0.006 and 0.006 mpy respectively and corrosion rates for as-cast Zr-2.5%Nb ingot is 0.1 mpy.
- The corrosion rates obtained from ASTM A262 practice "C" for tubes made out of Zr-2, Zr-4, Zr-2.5%Nb and Zr-1%Nb are 0.04, 0.02, 0.08 and 0.07 respectively, and for autoclaved Zr-4 tube is 0.003 mpy.
- The corrosion rates obtained from long term corrosion loop test for as-cast ingots of unalloyed Zirconium, Zr-2, Zr-4, Zr-1%Nb is 0.005, 0.006, 0.006 and 0.006 mpy respectively, and corrosion rate of as-cast Zr-2.5%Nb ingot is 0.15 mpy.

- The corrosion rates obtained from long term corrosion loop test for tube made out Zr-2, Zr-4, Zr-2.5%Nb and Zr-1%Nb are 0.02, 0.02, 0.001 and 0.07 mpy respectively.

Pilgered tube shows the higher corrosion rates compared to as-cast ingot and autoclaved tube. Pilgered tube exhibited elongated grain structure and evenly distributed fine $Zr(Fe, Cr)_2$ intermetallic particles within the grains and highly cold-worked surface area resulting in marginally higher corrosion rate for the as-cast. As cast ingot with large dendritic microstructure resulted in moderate corrosion rate. Due to the presence of thick black colored barrier oxide layer of ZrO_2, the autoclaved tubes exhibited negligible corrosion rate of 0.003 mpy in boiling nitric acid.

Zirconium and its alloys are often used in handling very corrosive environments as they are regarded as being highly corrosion resistant materials, this can attributed due to the ZrO_2 passive film formed. In particular, in Zr the addition of Nb (i.e. Zr-2.5wt%Nb alloy) shows the absence of a corrosion rate transition, usually observed in the corrosion process of Zircaloy [110].

The kinetics of corrosion process of Zirconium alloys is characterized by two periods named pre-transition and post-transition. A schematic illustration of these pre and post transition kinetics is shown in Figure 4.3 and represented by dashed lines. Subsequently, shown in this graph is the recent view that three stages can be differentiated for Zirconium alloy corrosion processes, [111, 112]:

1. During the early pre-transition the growth regime, the oxides are characterized by the formation of a thin, black, tightly adherent corrosion film that grows thicker and controlled by diffusion.
2. The intermediate stage that lies between the pre and post transition stages and this region comprise a series of successive cubic curves, similar to the initial cubic kinetic curve and

characterized by superposition of various parts of the oxide layer following pretransition growth rate, and

3. The linear post-transition kinetic regime where the corrosion rate increases, porosity is developed in the oxide and loses adherence and the hydrogen uptake increases due to deterioration of the oxide barrier layer.

Figure 4.4 shows typical microstructures of the oxide layer for Zirconium-based cladding materials. In the early stages of the oxide formation by corrosion process, the oxide layers are dense and composed predominantly of grains with tetragonal or cubic structure [113].

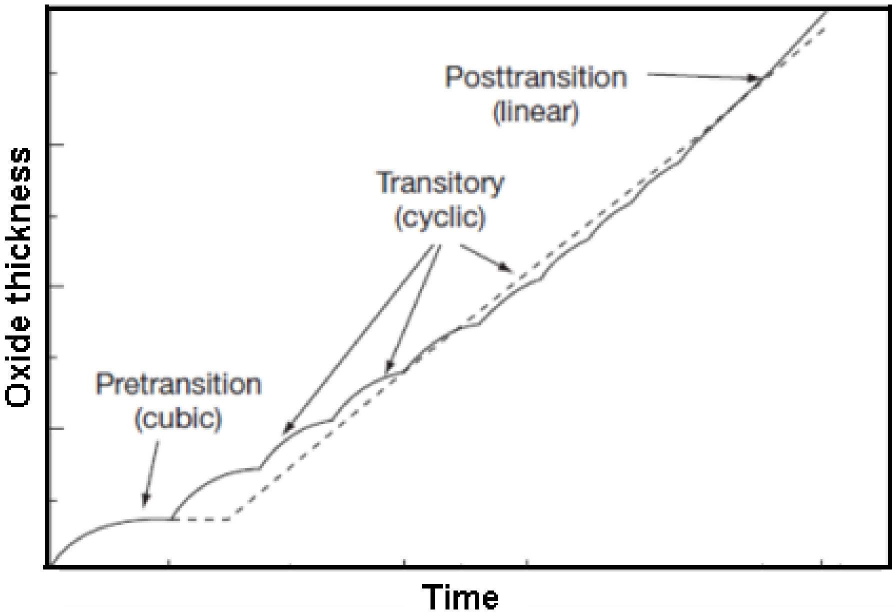

Figure 4.3: Schematic representations of the Zirconium alloys showing the different corrosion kinetics of pretransition, transitory and post transition regions. The dashed lines indicated the pre- and post transition regimes [112].

Gradually, the grains grow into columnar pattern and tend to transform to monoclinic oxide, which constitutes the majority of the oxide formed. The tetragonal phase is often associated with protective nature, and the corrosion rate is known to slow down with oxide thickness, and that depends on the oxidizing species in the layer. Thereby, the corrosion behaviour of Zirconium and Zr-Nb alloys significantly depend on the microstructure, which are modified during the thermomechanical treatments. The α martensitic structures of niobium in the matrix are known to exhibit poor corrosion resistance with the highest corrosion rates. However, none of the investigated alloys shows any of such structure and thereby good corrosion resistance in highly oxidizing nitric acid was prominently observed (Table 4.2). The improve corrosion resistance of Zr-Nb alloys with both α'-martensitic and (α-Zr+ β-Zr) structures are also reported [114]. It is unclear whether the beneficial effect of α-Zr+ β-Zr can improve the oxide stability in nitric acid medium.

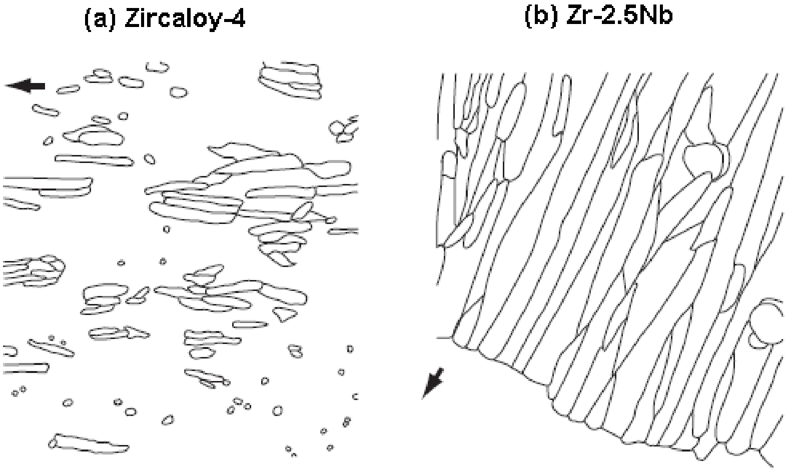

Figure 4.4 The schematic representation of the nature of grain size, shape, and orientation at the oxide/metal interface of (a) Zr-4, and (b) Zr-2.5%Nb alloy oxides. The black arrows indicate oxide growth direction effecting the corrosion process [113].

Table 4.2 corrosion rates of as-cast ingot, pilgered tube and autoclaved tube of Zr, Zr-2, Zr-4, Zr-2.5%Nb and Zr-1%Nb in mpy.

	Pure Zr		**Zr-2**		**Zr-4**		**Zr-2.5%Nb**		**Zr-1%Nb**	
	Loop	Practice C	Loop	Practice C	Loop	Practice C	Loop	Practice C	Loop	Practice C
As cast	0.005 mpy	0.005 mpy	0.006 mpy	0.005 mpy	0.005 mpy	0.006 mpy	0.15 mpy	0.1 mpy	0.006 mpy	0.006 mpy
Tube			0.02 mpy	0.04 mpy	0.02 mpy	0.02 mpy	0.01 mpy	0.08 mpy	0.06 mpy	0.07 mpy
Auto-claved					0.003 mpy	0.003 mpy				

SEM images of corrosion surface morphology for as-cast ingot unalloyed Zirconium, Zr-2, Zr-2, Zr-4, Zr-2.5%Nb and Zr-1%Nb and tubes for Zr-2 Zr-4, Zr-2.5%Nb for ASTM practice C corrosion studies, exposed to boiling 11.5 M HNO3 at room temperature for 240 h are and for long term loop test in boiling 11.5 M nitric acid for 1000 h are shown in Figure 4.5 and Figure 4.6 respectively.

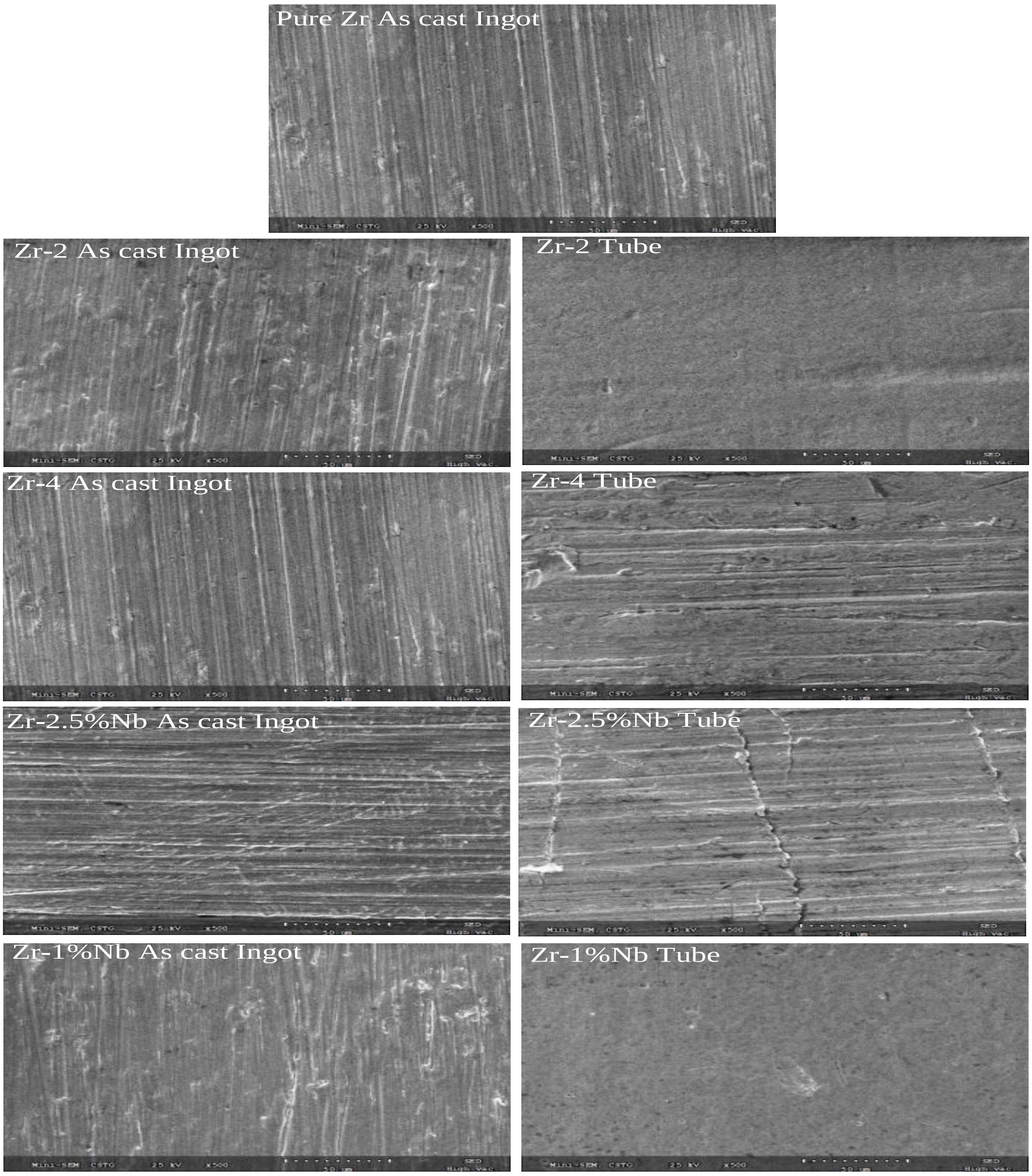

Figure 4.5: SEM images showing corrosion surface morphology for unalloyed Zirconium as cast ingot, Zr-2 as-cast ingot and tube, Zr-4 as cast ingot , Zr-2.5%Nb as cast ingot & tube and Zr-1%Nb as-cast ingot & tube for ASTM practice C corrosion studies , exposed to boiling 11.5 M HNO_3 at room temperature for 240 h.

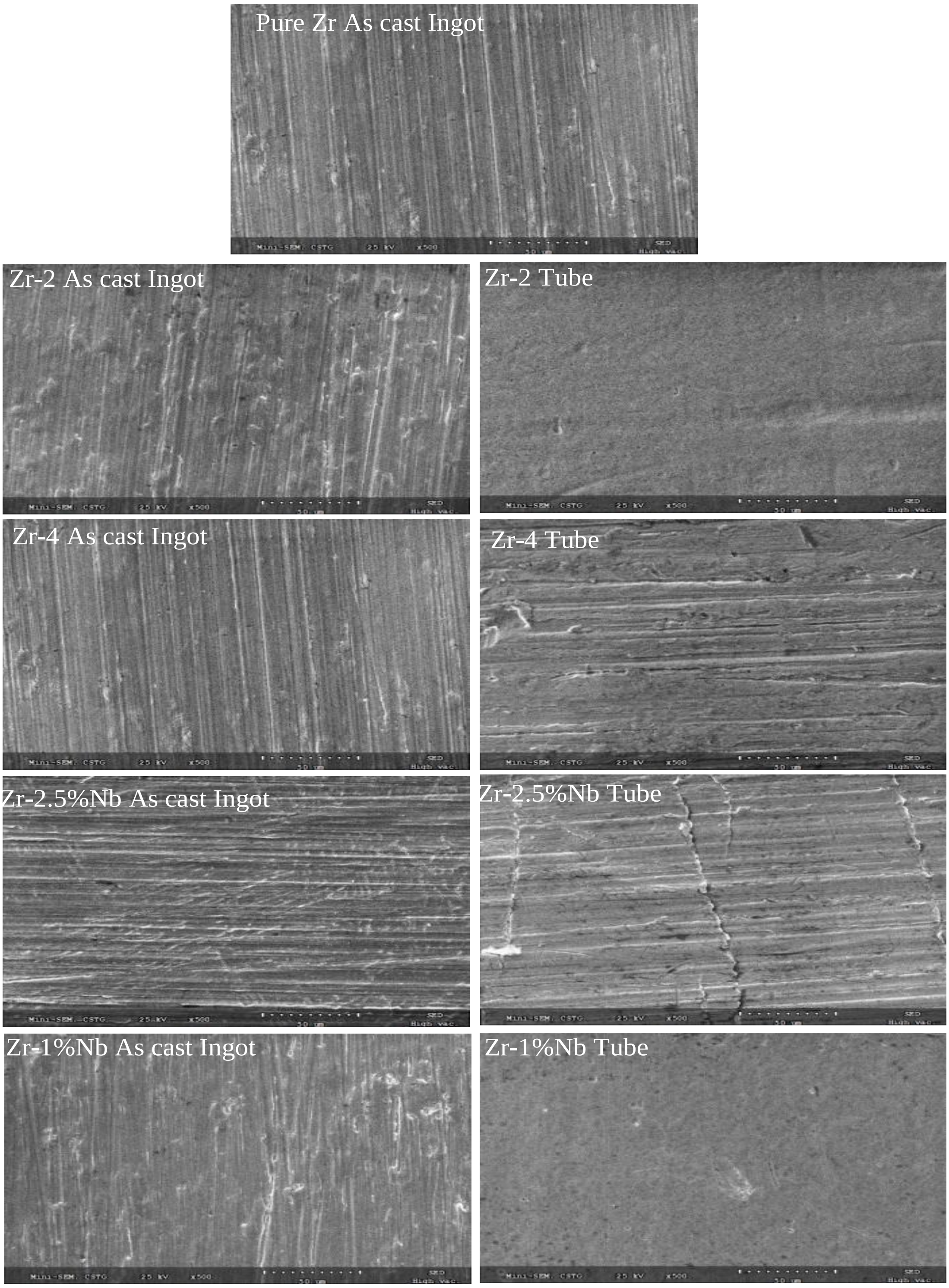

Figure 4.6: SEM images showing corrosion surface morphology for unalloyed Zirconium as cast ingot, Zr-2 as-cast ingot & tube, Zr-4 as-cast ingot, Zr-2.5%Nb as cast ingot & tube and Zr-1%Nb as cast ingot & tube for corrosion loop studies, exposed to boiling 11.5 M HNO_3 at room temperature for 1000 h.

As the corrosion rates are very low in all the samples, unattacked surface morphology was observed in SEM. It can be attributed to smooth and compact surface might have resulted in superior corrosion resistance among all the Zirconium alloys.

4.2.3 Corrosion behavior for EB and TIG welds of Zr-4 tubes in boiling 11.5 M nitric acid

The average corrosion rate for five individual periods in boiling liquid phase of 11.5 M nitric acid for Zr-4-Plate, Zr-4-TIG weld and Zr-4-EB weld samples are shown in Table 4.2. The corrosion rates clearly indicated that Zr-4 shows better corrosion rate in both wrought and welded conditions. The high corrosion resistance of Zirconium and its alloys in highly oxidizing nitric acid condition is due to stable and adherent ZrO_2 film formed on the surface. In the present work a thin and protective black oxide layer film was noticed on the surface of Zr-4 and its welds after completion of the corrosion testing. The corrosion rates of weldments of Zr-4 samples are nearly same, indicating that the corrosion of Zr-4 is not sensitive to weld microstructure. The SEM micrographs of Zr-4 TIG weld and Zr-4 EB weld samples exposed to liquid phases are shown in Figure 4.7. The smooth, compact and highly adherent passive film present over the surface resulted in superior corrosion resistance of Zr-4 and their weldments. The corrosion rates of TIG and EB weldments of Zr-4 samples are nearly same, indicating that the corrosion resistance of Zr-4 in nitric acid is not sensitive to microstructure. It is also not sensitive to changes in concentration, concentration of its own ion in solution, heavy metal ions and the crystal structure of Zirconium [23, 115]. The present results clearly indicates the excellent corrosion resistance of Zr-4 and its weldments in boiling 11.5 M nitric acid medium.

Table 4.3: The average corrosion rate values of Zr-4 EB and TIG welded tubes in comparison to parent material in liquid phase boiling 11.5 M nitric acid for 240 h
(Corrosion rate in mm/y)

Material condition	**Average corrosion rate on in liquid**
Z4-TIG weld	0.0005
Z4-EB weld	0

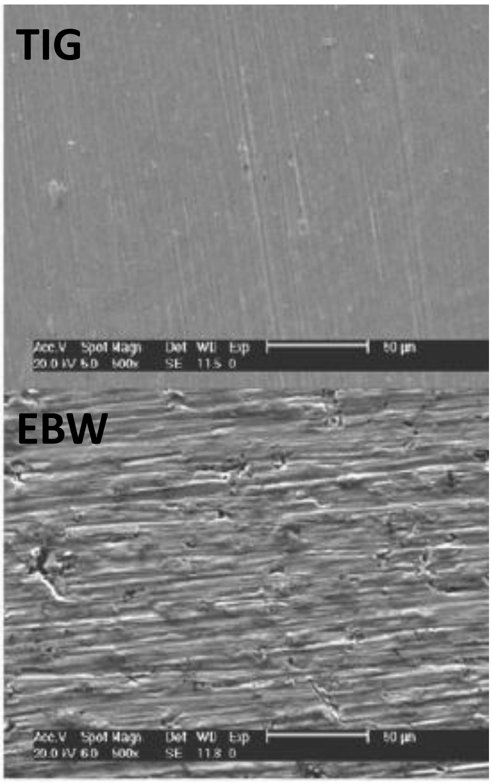

Figure 4.7: SEM micrographs of Zr-4 TIG weld and Zr-4 EB weld exposed to liquid, phases of boiling 11.5 M nitric acid for 240 h.

4.2.4 LRS analysis of Zr-4 exposed to boiling 11.5 M nitric acid

Zirconium has a unique combination of desirable properties that led to its use as a structural material for components in nuclear reactors and spent fuel reprocessing applications. Zirconium and alloys are chosen since it provides desirable mechanical strength and ease in processing characteristics common to other metals, but with a much lower thermal neutron absorption cross-section. Also, very high corrosion resistance of Zirconium in service application in highly oxidizing nitric acid media, which is again related to its surface chemistry of passive oxide film. It is also of interest to identify which forms of oxide exist on Zr-based alloys. In addition, Raman spectroscopy, being an optical technique, can be used to study the surfaces oxide film compositions of Zr materials formed in different aqueous environments. Figure 4.8 shows the LRS spectra of final pilgered and subsequently annealed Zr-4tube and autoclaved Zr-4 samples exposed to boiling liquid phase of for 1000 h. For Zr-4 pilgered tube and autoclaved Zr-4 exposed to boiling 11.5 M nitric acid, a major peak around 175-180 cm^{-1} and minor peaks in the range 338-383 cm^{-1} correspond to monoclinic ZrO_2 phase, are observed and shown in Figure 4.8. Similarly, the peak at 638-643 cm^{-1} and the minor peak at 272 cm^{-1} correspond to the tetragonal ZrO_2 phase [48, 77]. The peak at 479 cm^{-1} can be assigned to both monoclinic and tetragonal phase of ZrO_2.Thereby, the expected peak positions for tetragonal (t), monoclinic (m) and cubic (c) phases of ZrO_2 are shown. However, it should be mentioned that all the peaks corresponding to the monoclinic and tetragonal phases did not appear. The shift in the peak positions also indicated the formation of monoclinic and tetragonal mixed phase of ZrO_2 in the passive films formed in the boiling liquid phase of nitric acid. The formation of mixed phases monoclinic and tetragonal phases of ZrO_2 on Zirconium pilgered tube and autoclaved samples has been confirmed by LRS studies. These oxide films are responsible for the observed high corrosion resistance of Zr-based materials in the boiling nitric acid. The low overall intensities and broad line shapes of the spectra indicate that the oxide layers are thin and/or disordered.

4.2.5 XPS analysis of Zr-4 exposed to boiling 11.5 M nitric acid

In Zr-based materials, the role of alloying elements and their effects on corrosion in various environments is extensively investigated in particular on the role of passive oxide film affecting the corrosion resistance. Zircaloys are nominally single-phase α-Zr which is stabilized by the addition of tin in solid solution. Other elements insoluble in α-Zr (Fe, Cr, Ni) are added to form intermetallic precipitates that strongly influence the corrosion resistance, hydriding, and mechanical properties of the materials in service. The origin of the passivity of final pilgered and subsequently annealed Zr-4 sample exposed to boiling 11.5 M HNO_3 for 1000 h was determined by analyzing the surface film by XPS. Depth profile of the passive film was carried out by sputtering at intervals of 0 (as received), 30, 60, 180, 300, 420 and 540 s. The XPS survey scan of as-received and final sputtering condition of the Zr-4 sample is shown in Figure 4.9 a. Survey scans over a long range were carried out to identify the oxide films of the alloy constituents and possible contamination. Survey scans show the presence of carbon (C 1s), oxygen (O 1s) and Zirconium (Zr 3p, Zr 3d) for the as-received and final sputtered conditions of the Zr-4 sample. The C 1s peak corresponded to an unavoidable contaminant carbon that formed during sample handling. After sputtering for about 30 s, the signal from the carbon did not appear confirming that the carbon was not a part of the passive film of Zr-4. The O 1s peaks appeared throughout the depth profile of the sample, originating from oxygen as metal-O-metal bond. The XPS spectra of as-received and final sputtering for Zr3d of the passive film are shown in Figure 4.9 b. The binding energies 179.3eV and 181.7eV corresponding to the peaks of $Zr3d_{5/2}$ and $Zr3d_{3/2}$ respectively corresponding to the Zr metallic state [48]. The binding energies of 183.4 eV and 185.8eV were assigned to the peaks of ZrO_2 [48]. For the as-received condition of the passive film, no metallic peaks were observed and the presence of Zr was observed only in its respective

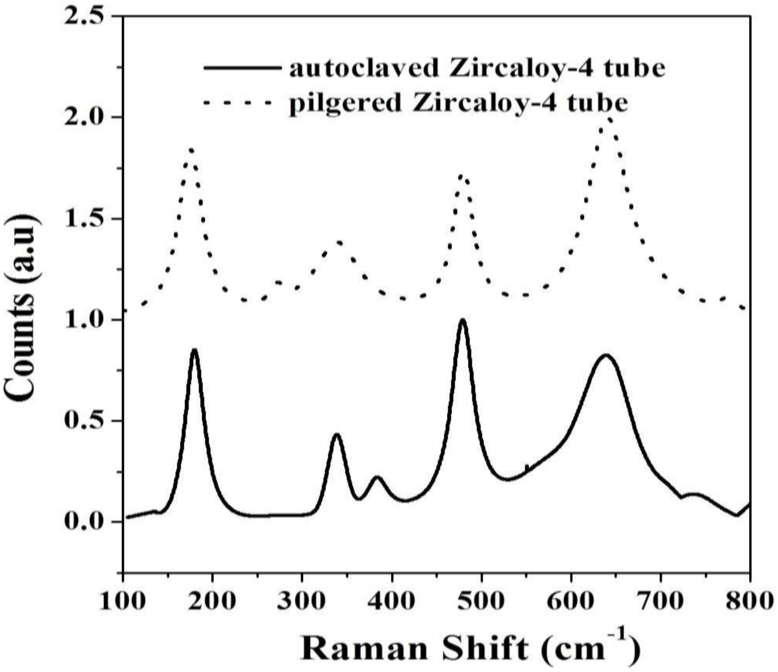

Figure 4.8: LRS spectra of pilgered and autoclaved Zr4 tubes exposed to boiling 11.5 M HNO_3.

oxide state of ZrO_2. In the final sputtered condition of the passive film, both metallic and oxide states of Zr were observed and the metallic states were found to be predominant. The atomic concentration of the oxide species and metallic species of Zr that are present in the passive film of the pilgered Zr-4 with respect to the sputtering time are shown in Figure 4.9c. The XPS depth profile of the passive film of Zr-4 shows decreasing the oxide concentration and increasing the metallic concentration as observed and is shown in Figure 4.9c. The oxide/metal interface region is marked in Figure 4.9c, based on the assumption that the ratio of the concentration of the oxide to metallic species was 4 [48]. Thus, the region from the outer surface of the oxide/metal interface is assumed to be the oxide film. This implies that the passive film formed on pilgered Zr-4 is ≈ 3 nm thick with respect to the sputtering rate of about 0.0166 nm s^{-1} of the standard Ag layer. The XPS analysis confirmed that the origin of the passivity of Zr-4 in boiling 11.5 M nitric acid is due to the formation of thin (≈3 nm) and a protective passive layer of ZrO_2 .Thereby, the corrosion resistance of Zr-4 is attributed to the formation of strong and adherent protective ZrO_2 oxide formation on the surface as evident in the present XPS results. Hence, insignificant corrosion rate, i.e., high corrosion resistance of Zr-4 in both liquid phase and condensate/vapour conditions is due to the formation of the protective ZrO_2 passive oxide film. Furthermore, for Zirconium and its alloys, in nitric acid media three types of phenomena can lower the protective nature of the ZrO_2 passive layer [19, 77]:

(i). The presence of stress or strain: in the process equipment in passive conditions, under U-bend and C-ring tests (i.e., submitted to a stress or strain) electrochemical depassivation of the material occur above 80% HNO_3 and SCC occurs [109];

(ii). Friction or erosion a mechanical degradation, leading to film instability and (iii). The presence of complex fluorides ions in the nitric media increases the dissolution with concentration.

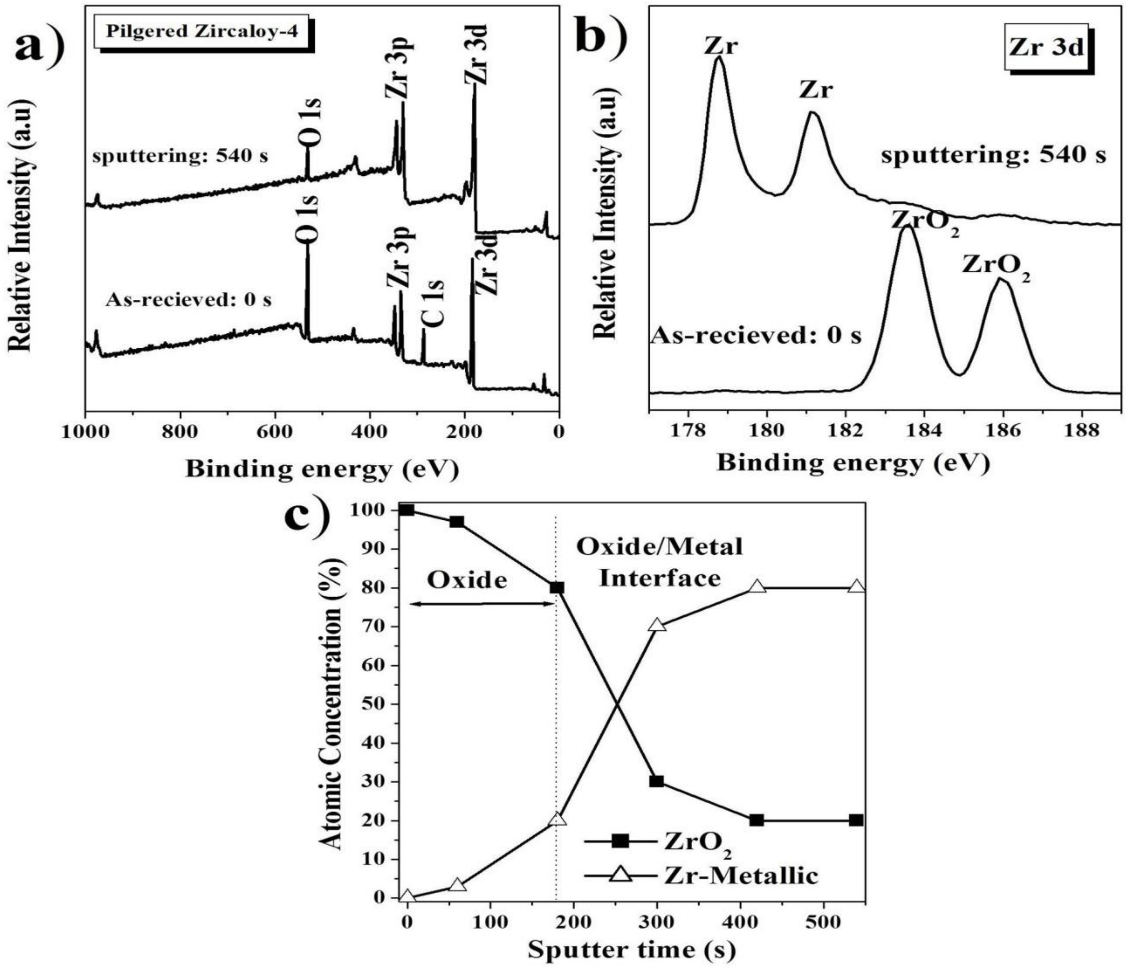

Figure 4.9: : XPS analysis of final pilgered Zr-4 tubes exposed to boiling 11.5 M HNO_3 (a) XPS survey scan for the as-received and final sputtering conditions (b) XPS spectra of Zr $3d_{5/2}$ and Zr $3d_{3/2}$ in the as-received and final sputtering conditions (c) Cumulative atomic concentration of oxide species and metallic.

4.2.6 Nitric Acid Corrosion Issues in Zirconium Alloys

In spent fuel reprocessing plants, nitric media of various concentrations are used in the PUREX process for the separation of fission products, uranium and plutonium. As part of material qualification for developing corrosion resistance materials, extensive studies need to be carried out by selecting the most suitable materials for fabrication of equipment for hostile and highly oxidizing nitric acid applications in spent nuclear fuel reprocessing plants. The constructional materials for the equipment used in reprocessing plants are mainly AISI type

304L stainless steel (SS) along with refractory metals like titanium and Zirconium and its alloys. Unlike titanium, austenitic SS, Zirconium and its alloys have been explored in reprocessing plant because of its superior corrosion resistance and is unaffected by vapour and condensates in boiling nitric acid [33, 39, 40]. However, the primary concern with the use of Zirconium is its susceptibility to corrosion fatigue and SCC in highly concentrated and hot nitric acid conditions.

Zirconium possesses high corrosion resistance in highly oxidizing and corrosive nitric acid conditions attributed to the formation of stable and adherent ZrO_2 film in the surface. However, the chemical and physical state of the material: composition, metallurgical condition, and surface condition and the fabrication process may influence its corrosion resistance. Zirconium and its alloys show corrosion rate typically below 1 mpy up to 70 % HNO_3 and for temperatures up to 260°C [44, 45]. Additionally, Zirconium does not exhibit complicated microstructures like SS. Sheets, tubes and pipes have similar corrosion resistance without intergranular corrosion.

In France, 80 tons of Zirconium and 5500 m of piping were employed in La Hague reprocessing plant for the manufacturing of various components like dissolvers, oxalic mother liquor evaporator and heat exchangers, vitrification dust scrubber, and liquid waste treatment reactors [18, 24, 25]. These components were used in 3 M to 12 M HNO_3 in the presence of oxidising ions Cr (VI), Fe (III), Pu (IV), insoluble platinoids, and sulphides [116]. Furthermore, the corrosion resistance of Zirconium alloys in nitric acid is not affected by concentration, temperature and as well as applied potential. However, concerns associated with the application of zircaloy are cost, fabrication and SCC behaviour. SCC does not occur in Zr in boiling HNO_3 at concentrations less than 70%, whereas SCC is initiated in 6-94% HNO_3 when a potential is applied above the critical potential for SCC, attributed to anisotropic nature of the hcp structure. Thus, crystallographic texture control through rolling process has been established to overcome the SCC susceptibility [118]. In addition, Japanese experience at Rokkasho plant showed that Zr exhibited excellent corrosion resistance and didn’t have the susceptibility to SCC in the simulated dissolver solution at small-scale mock-up test study (up to 50,000 h) [119]. Studies have been carried out to evaluate the corrosion resistance of Zr-2 and Zr-4 in the wrought and welded form in 11.5 M HNO_3.Three-phase corrosion results indicated that Zr-2 exhibits superior corrosion resistance in both wrought and welded condition in comparison with other materials. Similarly, Zr-4 based high-temperature corrosion testing system of 10 litres capacity was made with provisions for testing under liquid, vapour and condensate conditions [119]. The system has been operated for 15000 h with 11.5 M nitric acid. Studies conducted so far indicated corrosion rate values below 1 mpy for Zr-4 samples.

Studies on the prototype dissolver vessel similar to the design of the operating dissolver at CORAL plant was manufactured for long term corrosion evaluation under simulated dissolver conditions (SDS). Zirconium-702 (Commercially pure Zirconium), Zr-4, autoclaved Zr-4, and commercial pure titanium (CP-Ti) exhibited low corrosion rates of 0.003 to 0.009 mils/yr. in the as-received and welded conditions exposed to the boiling liquid phase of the dissolver solution for 2500 h [120]. Thereby insignificant corrosion rates for candidate materials both in as-received and weld conditions of Zirconium-702 and Zr-4 was obtained in liquid and vapour phase of the simulated dissolver environment. Due to the superior corrosion resistance of zircaloy in both wrought and welded conditions; thereby, Zirconium and its alloys are chosen as candidate materials for the construction of the critical equipment, such as fuel dissolvers and nitric acid recovery concentrators.

The advantages of using Zirconium for reprocessing plants though more expensive than type 304L SS,is realized by improved performance (i.e., zero corrosion rates in boiling high nitric acid concentrations) and extended service life of the components. As an example, unlike titanium and type 304L SS, zircoloy is unaffected by vapour and condensates corrosion in boiling nitric acid. Zirconium is lighter (~20%) than stainless steel thus requiring fewer tubes for heat transfer. The corrosion rate of different grades of Zirconium alloys in boiling nitric acid is unaffected by an increase in concentrations, by metallurgical state or by the presence of oxidizing species. Thereby, maintenance and inspection in a highly radioactive reprocessing environment can be minimized or avoided. In view of all the above advantages of its properties, Zirconium alloys are considered as a very suitable candidate material for dissolver and evaporator application in future FBR reprocessing plants [22, 50].

4.3. Conclusions

The key findings drawn from the study of the corrosion behavior on various Zirconium based alloys in 11.5 M HNO_3 are as follows:

- The potentiodynamic polarization results obtained in nitric acid indicated that better corrosion resistance is offered by the autoclaved Zr-4 sample when compared to the pilgered conditions of Zr-4.
- Insignificant corrosion rate was observed between different grades of Zirconium in boiling nitric acid. The effect of the metallurgical state after thermomechanical processing on the corrosion resistance of the Zirconium indicated that the corrosion rate is unaffected by the metallurgical state. Since the corrosion rate of Zirconium and its alloys is negligible, no maintenance and inspection are necessary in a radioactive environment, and extended component plant life can be realized.
- The corrosion rate obtained from ASTM A262 practice C corrosion test for as-cast ingots of unalloyed Zirconium, Zr-2, Zr-4 and Zr-1%Nb is 0.005, 0.005, 0.006 and 0.006 mpy respectively and corrosion rate of as-cast Zr-2.5%Nb ingot is 0.1 mpy.

- The corrosion rate obtained from ASTM A262 practice C for tube Zr-2, Zr-4, Zr-2.5%Nb and Zr-1%Nb are 0.04, 0.02, 0.08 and 0.07 respectively and for autoclaved Zr-4 tube is 0.003 mpy.
- The corrosion rate obtained from long term corrosion loop test for as-cast ingots of unalloyed Zirconium, Zr-2, Zr-4 and Zr-1%Nb is 0.005, 0.006, 0.006 and 0.006 mpy respectively and corrosion rate of as-cast Zr-2.5%Nb ingot is 0.15 mpy.
- The corrosion rate obtained from long term corrosion loop test for tube made out Zr-2, Zir-4, Zr-2.5%Nb and Zr-1%Nb are 0.02, 0.02, 0.001 and 0.07 mpy respectively. These results thereby indicates high corrosion resistance of Zirconium and its alloys in highly oxidizing nitric acid.
- Pilgered tube exhibited elongated grain structure and evenly distributed fine $Zr(Fe, Cr)_2$ intermetallic particles within the grains and highly cold-worked surface area resulting in slightly higher corrosion rate for the as-cast. As cast ingot shows large dendritic microstructure, resulting in moderate corrosion rate. Due to the presence of thick black colored barrier oxide layer of ZrO_2, the autoclaved tubes exhibited negligible corrosion rate of 0.003 mpy in boiling nitric acid.
- In ASTM A262 practice C corrosion test, the Zr-4 EB weld exhibited superior corrosion resistance (0 mpy) compared to TIG welded (0.0005 mpy) condition attributed to the smooth surface resulting in superior corrosion resistance of their weldments.
- The LRS spectra of final pilgered and subsequently annealed Zr-4 tube and autoclaved Zr-4 samples exposed to boiling liquid phase of for 1000 h shows a major peak around 175-180 cm^{-1} and minor peaks in the range 338-383 cm^{-1} correspond to monoclinic ZrO_2 phase. Similarly, the peak at 638-643 cm^{-1} and the minor peak at 272 cm^{-1} correspond to the tetragonal ZrO_2 phase. The peak at 479 cm^{-1} can be assigned to both monoclinic and tetragonal phase of ZrO_2. The shift in the peak positions also indicated the formation of

monoclinic and tetragonal mixed phase of ZrO_2 in the passive films formed in the boiling liquid phase of nitric acid.

- The XPS analysis confirms that the passivity of Zr-4 in boiling 11.5 M nitric acid is due to the formation of thin (≈ 3 nm) and a protective passive layer of ZrO_2.

CHAPTER V

CONCLUSIONS, SUMMARY AND SCOPE FOR FUTURE WORK

This chapter provides important conclusions derived from the results of the microstructural, mechanical properties and corrosion behavior investigations carried out on various Zirconium based alloys under various thermo-mechanical processes. The effect of thermomechanical processing on the evolution of microstructure behavior has been studied. The final microstructure, and associated properties is often a cumulative outcome of series of changes occurring at each stage of processing. Hence, a systematic characterization of the microstructural evolution at different stages were carried out. The detailed characterization of all the Zirconium based alloys for the thesis work are also summarized.

The present thesis dealt with the effect of thermo mechanical processing parameters on the evolution of microstructure, mechanical properties and corrosion behavior of various Zirconium based alloys which will be used as the candidate material for the fabrication of dissolver assembly in the nuclear spent fuel reprocessing plant. The life of the dissolver assembly determines the life of the nuclear spent fuel reprocessing plant, as aggressive conditions prevailing in the reprocessing plant demand structural materials and accessories of the unit operations with good mechanical integrity and thermal stability combined with corrosion resistance to provide high performance and long service life.

The chemical composition and microstructure of a Zirconium alloy are critical factors that ensure its proper functioning in corrosive environment. Microstructure is of crucial importance while choosing a material, which in turn is a function of the material chemistry and the thermo-mechanical manufacturing processes. Thus, proper selection of alloying elements and the manufacturing process conditions are crucial to yield the appropriate microstructure resulting in the required properties. Zirconium with the optimized proportion of alloying elements in combination with an appropriate thermomechanical manufacturing process will provide appropriate microstructure and corrosion resistance in the nitric acidic environment at various concentrations. Zr-2 and Zr-4 are single phase alloys and Zr-2.5%Nb and Zr-1.0%Nb alloy are two phase alloy, and there can be variety of phase transformations product from the high temperature β phase by controlling the β phase composition and cooling rate. Thus, it is possible to generate a range of microstructure by suitable heat treatment methods by varying thermomechanical process parameter. In depth understanding about the mechanisms of microstructural evolution for various Zirconium based alloys and unalloyed Zirconium during different thermomechanical processing steps has been studied. The brief description of the main findings of the thesis is summarized below.

Apart from this, suggestions are provided for additional work to be continued in the near future for further evaluation of the performance of newer Zirconium based alloys and their development for such critical applications like dissolver assembly for the nuclear spent fuel reprocessing plant.

5.1 Conclusions

5.1.1. Microstructural Evaluation and co-relation of mechanical properties

In summary, this study emphasise the importance of various thermo-mechanical treatments required for processing the Zirconium alloys. The optimized microstructure has been correlated with the obtained mechanical and corrosion properties of the Zirconium alloys. The detailed study on the evolution of microstructure and mechanical properties as a function of the different thermomechanical processing steps led to the following important inferences in the present study.

- The microstructure of the as-cast ingots for all the Zirconium alloys, evolved by directional rapid cooling longitudinally and across the ingot diameter, is dendritic type without alloying element/impurities with basket-weave or Widmenstratten morphology. In the case of Zr-2.5% Nb and Zr-1% Nb alloy, the microstructure consists of the of fast cooled martensitic parallel plate morphology. The Zr-2.5%Nb and Zr-1% Nb alloys consist of primary phase as a α-Zirconium (hcp) and secondary phase as β-Zirconium (bcc). Cast ingot shows low mechanical properties and hardness with considerable percentage elongation. Low mechanical properties can be attributed to coarse dendritic cast grain structure.

- Randomized ‘β-quenched’ microstructure reveals better mechanical properties due homogenous microstructure.
- Bimodal distribution in grain size and in grain morphology with larger elongated grains in association with smaller equiaxed grains was obtained during hot extrusion.
- All the pilgering stages produce a ‘heterogeneous deformation structure’ increasing mechanical properties considerably and decreasing percentage elongation, hence necessitating intermediate annealing before next cold-working operation.
- In general, deformation (both hot extrusion, as well as pilgering) strengthened the material properties, while annealing enhanced grain coarsening by the way of recovery/recrystallization to optimize mechanical properties.

In the case of the tubular and sheet products, the microstructure is influenced by thermomechanical processing (TMP) steps used for the fabrication of Zirconium alloys components.

- In Zr-2 tubes, the microstructure is consists of the equiaxed grains, as it is in fully annealed condition.
- Zr-4 tubes microstructure shows elongated grains in working direction, as it is in stress relieved condition.
- The stress relieved condition in Zr-2.5%Nb alloy tube show α-Zr grains and fine β-Nb phase at α grain boundary.

  - The microstructure in Zr-1%Nb alloy tube consists of recrystallized grains.
  - SEM-EDS analisis for Zr-2 tubes show evenly distributed fine second phase particles, and indicate the presence of higher concentration of Fe, Cr and Ni compared to base material. In Zr-2 alloys, the partitioning of Fe between the two types of intermetallic phases leads to a more complex relationship between nominal composition and precipitate composition, giving a broad range of Fe/Cr ratio in $Zr(Cr,Fe)_2$, and Fe/Ni ratio in $Zr_2(Fe,Ni)$. Similarly for Zr-4 tubes show evenly distributed fine $Zr(Fe, Cr)_2$ precipitates and intermetallic particles within the grains with very high Fe/Cr ratios.

- EBSD maps show as-cast Zr-4 ingot has dendritic cast structure with small intermetallic second phase particles (Fe, Cr, Ni, Si, C) and along with SPPs at grain boundaries. Similarly, β quenched microstructure consists of Widmannstatten type α-plates. Microstructure of hot extruded billets and slabs indicates the presence of banded structure and dynamic recrystallisation. Cold worked pilgered structure is elongated in the direction of deformation; Cold work followed by annealing shows bright elongated structure along the working direction.
- TIG welded Zr-4 sample exhibited coarse acicular α structure in comparison to the fine acicular structure of EB welded sample. All welds exhibited a transformed grain structure/acicular α grains surrounded by prior β grain boundaries (Widmanstatten or basketweave structure).
- TIG welded Zr-4 exhibited a hardness value of 387VHN while the hardness of the base metal observed at 183VHN, and EB weld showed 197VHN. The increase in the hardness in the TIG weld region is due to increase in oxygen or nitrogen value.

5.1.2 Corrosion behavior of various Zirconium based alloys in boiling 11.5 M nitric acid

The major conclusions drawn from corrosion behavior of various Zirconium based alloys in boiling 11.5 M HNO_3 as per ASTM A262 Practice C for 240 h (5 periods of 48 h) and boiling 11.5 M HNO_3 in the Zirconium test loop facility for 1000 h are as follows:

- The corrosion rate obtained for as-cast ingots of unalloyed Zirconium, Zr-2, Zr-4 and Zr-1%Nb are 0.005, 0.005, 0.006 and 0.006 mpy respectively and corrosion rate of as-cast Zr-2.5%Nb ingot is 0.1 mpy.
- The corrosion rate obtained for tube Zr-2, Zr-4, Zr-2.5%Nb and Zr-1%Nb are 0.04, 0.02, 0.08 and 0.07 respectively and for autoclaved Zr-4 tube is 0.003 mpy.
- The corrosion rate of long-term corrosion loop test for as-cast ingots of unalloyed Zirconium, Zr-2, Zr-4 and Zr-1%Nb are 0.005, 0.006, 0.006 and 0.006 mpy respectively and for as-cast Zr-2.5%Nb ingot is 0.15 mpy.
- The corrosion rate of long-term corrosion loop test for tube made out Zr-2, Zr-4, Zr-2.5%Nb and Zr-1%Nb are 0.02, 0.02, 0.001 and 0.07 mpy respectively.
- Pilgered tube showed higher corrosion rate compared to as-cast ingot and autoclaved tube. It is caused by the elongated grain structure and evenly distributed fine $Zr(Fe,Cr)_2$ intermetallic particles within the grains and highly cold-worked surface area. Cast ingot have a large dendritic microstructure which results in moderate corrosion rate. However, due to the presence of thick black colored barrier oxide layer of ZrO_2, the autoclaved tubes exhibited negligible corrosion rate of 0.003 mpy in boiling nitric acid.
- The corrosion rate obtained for Zr-4 EB welded plate is zero mpy and TIG welded is 0.0005 mpy. EB weld exhibited superior corrosion resistance compared to TIG welded condition.
- The SEM surface morphology, after ASTM A262 practice C and long term loop test in boiling 11.5 M nitric acid for 1000 h, for unalloyed Zirconium, as-cast ingot Zr-2, as-cast

ingot & tube and Zr-4 as cast ingot, Zr-2.5%Nb as-cast ingot & tube and Zr-1%Nb as-cast ingot & tube shows smooth surface resulting in superior corrosion resistance of all the Zirconium alloys including Zr-4 TIG weld and Zr-4 EB weld samples.

- The LRS spectra of final pilgered and subsequently annealed Zr-4 tube and autoclaved Zr-4 samples, exposed to boiling liquid phase of for 1000 h, indicated a major peak around 175-180 cm^{-1} and minor peaks in the range 338-383 cm^{-1} correspond to monoclinic ZrO_2 phase. Similarly, the peak at 638-643 cm^{-1} and the minor peak at 272 cm^{-1} correspond to the tetragonal ZrO_2 phase. The peak at 479 cm^{-1} can be assigned to both monoclinic and tetragonal phase of ZrO_2. The shift in the peak positions also indicated the formation of monoclinic and tetragonal mixed phase of ZrO_2 in the passive films formed in the boiling liquid phase of nitric acid.
- The XPS analysis confirmed the passivity of Zr-4 in boiling 11.5 M nitric acid is due to the formation of thin ($\approx$ 3 nm) and a protective passive layer of ZrO_2.
- Insignificant corrosion rate was observed between different grades of Zirconium in boiling nitric acid. The effect of the metallurgical state after thermomechanical processing on the corrosion resistance of the Zirconium and its alloys indicated that the corrosion rate is unaffected by the metallurgical state. Since the corrosion of Zirconium is negligible, no maintenance and inspection are required for a radioactive environment, and extended plant component life can be realized.

5.2 Summary

This thesis emphasis the importance of several thermo-mechanical treatments required for processing the Zirconium alloys such as Zr-2, Zr-4, Zr-1%Nb and Zr-2.5%Nb. Characterization techniques like OM, SEM, SEM-EDS and XRD have been used in the present study to optimize the desired microstructure.

Microstructural evolution of the Zr-2 and Zr-4 samples follows the sequence:

As-cast ingot with dendritic structure → β-quenched Widmanstätten structure → hot extruded bimodal grain size → pilgered heterogeneous deformed structure → partially recrystallized structure (final annealed).

Similarly Zr-2.5% Nb and Zr-1% Nb for samples follow the sequence:

As-cast ingot with dendritic structure → β-quenched martensitic parallel plate morphology → hot extruded martensitic microstructure → pilgered heterogeneous deformed structure → α-Zr grains and fine β-Nb phase at α grain boundary (stress relieved).

Tensile testing and Vickers hardness measurements were used for the evaluation of mechanical properties like yield strength (YS), ultimate tensile strength (UTS) and micro-hardness at room temperature.

Three-electrode corrosion cell setup used to carry out the open circuit potential and the potentiodynamic polarization experiments to study the passivation behavior of Zirconium based alloys in 11.5 M nitric acid at room temperature has been described.

The optimized microstructure has been correlated with the obtained mechanical properties of the studied Zirconium alloys. Microstructural properties are depended strongly on the composition of the Zirconium alloy and thermo-mechanical processing conditions.

Corrosion behavior of Zirconium, Zr-2, Zr-4, Zr-1%Nb and Zr-2.5%Nb were evaluated in boiling 11.5 M nitric acid as per ASTM A262 practice-C (5 periods of 48 h) and in the Zirconium test loop facility for 1000h. SEM investigation of the samples surface subjected to practice C and Zirconium test loop facility has been studied.

Corrosion studies indicated that the corrosion rates for Zirconium based alloys as per ASTM A262 Practice C and in the boiling 11.5M HNO_3 in the Zirconium test loop facility are below 0.1 mpy. The corrosion rates for various as-cast and final product Zirconium alloys were negligible. The corrosion rates clearly indicated that these Zirconium alloys exhibited high corrosion resistance in boiling nitric acid medium. However, slightly higher corrosion rate was observed for Zr-2.5%Nb alloy samples because of two phase morphology of the alloy.

SEM investigations showed insignificant corrosion attack due to the formation of a smooth and compact passive film over the surface. LRS analysis confirmed that the high corrosion resistance behavior of these alloys are due to the formation of ZrO_2 passive film.

5.3 Scope for future work

1. In the present study, though, the corrosion rates were studied for 1000 h period. Corrosion loop test for tube made out various Zirconium based alloys showed very less corrosion rate. The performance of these alloys may be evaluated for 2000 h to study long term effect in boiling 11.5 M nitric acid on corrosion rate and morphology in the future work.
2. The results of the present study revealed that the corrosion rates for 1000 h corrosion loop test in boiling 11.5 M nitric acid is negligible. Similar studies may be carried out in vapour and condensate state to evaluate the corrosion rates.
3. Apart from the regular Zirconium based alloys like Zr-2, Zr-4, Zr-2.5%Nb and Zr-1%Nb tested during these studies, Effect of thermomechanical process on microstructural evolution, mechanical & corrosion properties may be carried out for newer alloys like Zirlo (Nb 1%, Sn 0.7-1%) and M5 (Nb 0.8-1.2 %) in the similar corrosive environment [30,91,92].

References

1. R. Krishnan, M. K. Asundi, "Zirconium alloys in nuclear technology", In: Proc. Ind. Acad. Sci.**4,** (1981), pp. 41-56.
2. D. G. Cacuci, "Handbook of Nuclear Engineering", Springer, (2010).
3. S. S. Bajaj and A. R. Gore, "The Indian PHWR", Nucl. Eng. Dec., 236, (2006), pp. 701-722**.**
4. S. Banerjee, J.K. Chakravarthy, J.S. Dubey, R.N. Singh, D. Srivastava, In, Proceedings of the Symposium Zirconium, ZIRC, (2002), p. 40.
5. A. B. Cheadle, C.E. Coleman, M. Ipohorski, in: Zirconium in the Nuclear Industry: Sixth International Symposium, ASTM STP 824, (1984), p. 210.
6. C.V. Sundaram, "Application related metallurgy of Zirconium, niobium and beryllium,"*Transactions. IIM*, (1986), pp. 12-27.
7. R. Adamson, P. I. Rudling, ZIRAT-14, Special topic report, Manufacturing Of Zirconium Alloys, *Advanced Nuclear Technology International*, (2004), pp. 2-4.
8. C. Coleman, M. Griffiths, V. Grigoriev, V. Kiseliov, B. Rodchenkov, and V. Markelov, "Mechanical Properties of Zr-2.5Nb Pressure Tubes Made from Electrolytic Powder," *J. of ASTM Int,* 4(10), 2007.
9. B. Cheadle, C. Coleman, and H. Licht, "CANDU-PHWR pressure tubes: their manufacture, inspection, and properties,"*Nucl. Technol,* (1982), pp. 413-425.
10. P. Mukherjee, P. M. G. Nambissan, P. Barat, P. Sen, S. K. Bandyopadhyay, J. K. Chakravartty, S. L. Wadekar, S. Banerjee, S. K. Chattopadhyay, S. K. Chatterjee, and M. K. Mitra, "The study of microstructural defects and mechanical properties in proton-irradiated Zr-1.0%Nb-1.0%Sn-0.1%Fe," *J. Nucl. Mater.*,297, no. 3, pp. 341-344, 2001.
11. G. K. Dey and S. Banerjee, "Decomposition of the β-Phase in Zr-20%Nb," *J. Nucl. Mater.,*125, (1984), pp. 219-227.
12. T.L. Yau, R. C. Sutherlin, "Corrosion of Zirconium and Zirconium Alloys," ASM Handbook, Volume 13B: Corrosion: Materials, (2005), pp. 300-324.
13. C. Lemaignan , Corrosion of Zirconium Alloy Components in Light Water Reactors , ASM Handbook, Volume 13C: Corrosion: Environments and Industries, (2005), pp. 415-420
14. Baldev Raj, U. Kamachi Mudali, Materials development and corrosion problems in nuclear fuel reprocessing plants, *Progress Nuclear Energy*, 48, (2006), pp. 283-313.

15. U. Kamachi Mudali, R.K. Dayal, J.B. Gnanamoorthy, Corrosion studies on materials of construction for spent nuclear fuel reprocessing plant equipment, *J.Nucl. Mater.,* 203, (1993), pp. 73-82.
16. S. Ningshen, U. Kamachi Mudali, G. Amarendra, Baldev Raj, Corrosion assessment of nitric acid grade austenitic stainless steels, *Corros. Sci.,* 51, (2009), pp. 322-329.
17. K. Kiuchi, H. Hayakawa, Y. Takagi, M. Kikuchi, Proc. of the Fourth International Conf. on Nuclear Fuel Reprocessing and Waste Management (RECOD-94), London, UK, vol. 3 (1994)
18. C. Bernard, J.P. Mouroux, J. Decours, R. Demay, J. Simonnet, Zirconium made equipment for the new La Hague reprocessing plants, in: Proceedings of the International Conference on Fuel Reprocessing and Waste Management, Sendai, Japan, RECOD 91, 2, 4-18 April, 1991, pp. 570–575.
19. P. Fauvet, F. Balbaud, R. Robin, Q.T. Tarans., A. Mugnier, D. Espinoux, Corrosion mechanisms of austenitic stainless steels in nitric media used in reprocessing plants, *J.Nucl.Mater.,* 375, (2008), pp. 52-64.
20. H. Chauve, J. Decours, R. Demay, M. Pelras, J. Simonnet, G. Turluer, Zirconium use for large process components, IAEA-TECDOC-421, (1987), pp. 165-192.
21. Rajamani Natarajan, Baldev Raj, Fast Reactor Fuel Reprocessing Technology in India, *J.Nucl. Sci. Tech*, 44, (2007), pp. 393-397.
22. U. Kamachi Mudali, A. Ravi Shankar, R. Natarajan, N. Saibaba, Baldev Raj, Application of Zirconium alloys for reprocessing plant components, *Nucl. Tech.*, 182, (2013), pp. 349-357.
23. A. Ravi Shankar, V.R. Raju, M. Narayana Rao, U. Kamachi Mudali, H.S. Khatak, Baldev Raj, Corrosion of Zr-4 and its welds in nitric acid medium, *Corros. Sci.*, 49, (2007), p. 3527.
24. Sunil Tonpe, N. Saibaba, R. N. Jayaraj, A. Ravi Shankar, U. Kamachi Mudali, Baldev Raj, Process development for fabrication of Zr-4 dissolver assembly for reprocessing of spent nuclear fuel, *Energy Procedia.*, 7, (2011), pp. 459-467.
25. K. Kapoor, Vivekanand Kain, T. Gopalkrishna, T. Sanyal, P.K. De, High corrosion resistant Ti-5%Ta-1.8%Nb alloy for fuel reprocessing application, *J.Nucl, Mater.,* 322, (2003), pp. 36-44.
26. C. Ganguly, Advances in Zirconium Technology for Nuclear Reactor Application, Proceeding of ZIRC 2003 Symposium, Mumbai, p.1

27. S. Banerjee, Role of basic research in the development of Zirconium Alloys for nuclear applications, Proceeding of ZIRC 2003 Symposium, Mumbai, p.40
28. K.V. Mani Krishna, S.K. Sahoo, I. Samajdar, S. Neogy, R. Tewari, D. Srivastava, G.K. Dey, Gaur Hari Das, N. Saibaba, S. Banarjee, Microstructural and textural developments during Zr-4 fuel tube fabrication, *J.Nucl.Mater.*, 383, (2008), pp. 78-85.
29. Bulletin of Alloy Phase Diagram, Vol. 4, No 2, (1983).
30. M. Sattari, R. A. Holt, and M. R. Daymond, "Phase transformation temperatures of Zr alloy Excel," *J. Nucl. Mater,* 435, (2013), pp. 241-249.
31. R. L. Tapping, "Materials performance in CANDU reactors: The first 30 years and the prognosis for life extension and new designs," *J. Nucl. Mater,* 383, (2008), pp. 1-8.
32. R. E. Smallman, "Modern Physical Metallurgy and Materials Engineering.", Sixth Edition, *Butterworth Heinemann,* 1999
33. G. W. Greenwood, "Modern physical metallurgy," *International Materials Reviews*, 30, (1985), pp. 302-302.
34. G. Y. Chin, "Competition Among Basal, Prism, and Pyramidal Slip Modes in HCP Metals", *Metall. Mater. Trans. B.*, 1, (1970), pp. 357-361.
35. E. Tenckhoff, "Deformation mechanisms, texture, and anisotropy in Zirconium and Zircaloy," in *ASTM STP 966* Philadelphia PA, p. 3, 1988.
36. J. Wang, I. J. J. Beyerlein, J. P. P. Hirth, and C. N. Tome, "Twinning dislocations on $\{10\bar{1}1\}$ and $\{10\bar{1}3\}$ planes in hexagonal close-packed crystals," *Acta Mater.*,59, (2011), pp. 3990-4001.
37. J. Christian and S. Mahajan, "Deformation twinning," *Prog. Mater. Sci.,* 39, (1995), pp.1-157.
38. D. G. Westlake, "Twinning in Zirconium, "*Acta Metall.*, 9, (1961), pp. 327-331.
39. H. Abdolvand, M. R. Daymond, and C. Mareau, "Incorporation of twinning into a crystal plasticity finite element model: Evolution of lattice strains and texture in Zr-2," *Int. J. Plast.,* 27, (2011), pp. 1721-1738.
40. S. K. Sahoo, V. D. Hiwarkar, I. Samajdar, and P. Pant, "Deformation twinning in Zr-2," *Mater. Sci.,* 702, (2010), pp. 838-841.
41. R. A. Holt, In-reactor deformation of cold-worked Zr-2.5%Nb pressure tubes, *J. Nucl. Mater,* 372, (2008), pp. 182-214.
42. S. Neogy, D. Srivastava, G. K. Dey, J. K. Chakravartty and S.Banerjee, Annealing studies on Zr-1Nb and Zr-1Nb-1Sn-0.1Fe alloys, *Trans. IIM.* 57, (2004), p. 509.

43. M.G. Fontana, Corrosion Engineering; third ed., Tata McGraw-Hill Education Private Limited, Delhi, India, 2005; 499.
44. A. Ravi Shankar, U. Kamachi Mudali, Electrochemical and surface studies on Zr-4 exposed to concentrated nitric acid, *Trans. IIM*, 62, (2009), pp.545-549.
45. A. Ravi Shankar, V.R. Raju, M. Narayana Rao, U. Kamachi Mudali, H.S. Khatak, Baldev Raj, Corrosion of Zr-4 and its welds in nitric acid medium, *Corros. Sci*., 49 (2007), pp.3527-3538.
46. IAEA-TECDOC-996, Waterside corrosion of Zirconium alloys in nuclear power plants.
47. C. Morant, J. M. Sanz, L. Galan, L. Soriano, F. Rueda, An XPS study of the interaction of oxygen with Zirconium, *Surface Science*, 218, (1989),pp. 331-345.
48. J. Jayaraj, A. Ravishankar, U. Kamachi Mudali, Electrochemical and passive characterization of a beta type $Ti_{45}Zr_{38}Al_{17}$ cast rod in nitric acid medium, *Electrochemical. Acta.*, 85, (2012),pp. 210-219.
49. Baldev Raj, H.S. Kamath, R. Natarajan, P.R. Vasudeva Rao, A perspective on fast reactor fuel cycle in India, *Prog. Nucl. Energy*, 47, (2005), pp. 369- 379.
50. U. Kamachi Mudali, A. Ravi Shankar, R. Natarajan, N. Saibaba, Baldev Raj, Application of Zirconium alloys for reprocessing plant components, *Nucl. Technol.* 182, (2013), p. 349
51. Mayasuki Takeunchi, Yuichi Suno , Yasuno Nakajima , Gunzo Uchiyama , Yauso Nojima and Sachio Fujine, Corrosion Behavior of Titanium Alloys in Hot Nitric Acid Condensate, *Journal of Energy and Power Engineering*, 7, (2013),pp.1090-1096.
52. Raphaël Robin, Fanny Balbaud, Pierre Fauvet, Nathalie Gruet, Benoit Gwinner, Corrosion Issues about the Materials of the French Fuel Reprocessing ,Proceedings of GLOBAL 2011,Makuhari, Japan, Dec. 11-16, 2011, Paper No. 360006.
53. ASTM E3-11 Standard for metallographic sample preparation.
54. ASTM 262A Practice “C” corrosion test
55. ASTM-E8/E8M-11 test procedure (Standard test method for tension testing of metallic materials)
56. B. Verlinden, J. Driver, I. Samajdar, and R. Doherty, "Thermo-mechanical processing of metallic materials". *Oxford: Elsevier,* pp.1-491, (2007).
57. F. J. Zanner and L. A. Bertram, "Vacuum arc remelting: An overview," in *NASA STI/Recon Technical Report*, 86, (1985), p. 16417.
58. R. L. Boxman, D. M. Sanders, and P. J. Martin, "Handbook of vacuum arc science and technology: fundamentals and applications", 1995.

59. F. Chinesta, E. Cueto, P. T. Moe, S. Storen, and H. Huetink, "Hot Metal Extrusion," *Adv. Mater. Forming,* (2007), pp. 207-223,
60. S.H. Hsiang and C.S. Liao, "Study on hot extrusion of tubes," *J. Mater. Processing Tech.,* 63. (1997), pp. 254-259.
61. P. V. Sivaprasad, S. Venugopal, C. H. J. Davies and Y. V. R. K. Prasad, "Identification of optimum process parameters for hot extrusion using finite element simulation and processing maps", Modell. Simu. Mater. Sci. Engg., 12, (2004), pp. 285-291.
62. H. Abe and M. Furugen, "Method of evaluating workability in cold pilgering," *J. Mater. Process. Technol.,* 212, (2012), pp. 1687-1693.
63. Ya. V. Frolov, Effect of Deformation Conditions on Mechanical Properties of Metal During Tube Cold Pilger Rolling, Pipe & Tube Production, UDC 621.774.36.
64. Hideaki Abe and Munekatsu Furugen, Method of Evaluating Workability in Cold Pilgering of Zirconium Alloy Tube, *Materials Transactions,* 51, (2010), pp. 1200 -1205.
65. J. Haq, A. Haq, and S. Banerjee, "Effect of cold working and annealing on the texture of Zr-2.5Nb pressure tubes," *Bull. Mater. Sci.,* 15, (1992), pp. 289-296.
66. R. G. Fleck, E. G. Price, and B. A. Cheadle, "Pressure Tube Development For Candu Reactors.," *Zirconium in the Nuclear Industry ASTMSTP 824,* (1984), pp. 88-105.
67. M. Ahmad, J. I. Akhter, M. A. Shaikh, M. Akhtar, M. Iqbal, M. A. Chaudhary, Hardness and microstructural studies of electron beam welded joints of Zr-4 and Stainless steel, *J.Nucl. Mater,* 301, (2002), pp. 118-121.
68. Bakish Robert Electron Beam Technology, John Wiley & Sons, Inc., New York, (1962).
69. C. Chi, C. Chao, “Characterization on electron beam welds and parameters forAZ31B-F extrusive plates,” *Journal of Material Processing Technology* 182, (2007), pp. 369-373.
70. V. Dey, D. K. Pratihar, G. L. Datta, M. N. Jha, T. K. Saha, A. V. Bapat, Optimization and prediction of weldment profile in bead-on-plate welding of Al-1100Plates using electron beam, International Journal of Advanced Manufacturing Technology, 48, (2010), pp. 513-528.
71. Paul E. Danielson, Metallographic Techniques for Zirconium and Zirconium Alloys, Teledyne Wah Chang Albany (TWCA) Publication.
72. Cottrell A H An introduction to metallurgy (London: Edward Arnold), 1967.
73. K. D. Vernon-Parry, "Scanning electron microscopy: An introduction," III-Vs Rev., 13, (2000), pp. 40-44.
74. J. Wilkinson and T. Ben Britton, "Strains, planes, and EBSD in materials science," *Materials Today,* 15.pp. 366-376, 2012.

75. F. J. Humphreys, "Characterisation of fine-scale microstructures by electron backscatter diffraction (EBSD)," *Scr. Mater.*, 51, pp. 771-776, 2004.
76. C. Hannon, "*Raman Spectroscopy*," in *Encyclopedia of Spectroscopy and Spectrometry,* 2010.
77. Sunil Tonpe, U. Kamachi Mudali, Effect of thermomechanical process on mechanical and corrosion properties of Zr-4 tubes of mock-up dissolver vessel, Journal Materials and Manufacturing Processes, 2015, (in Press), DOI:10.1080/10426914.2015.1090589
78. K. V.M. Krishna, S. K. Sahoo, I. Samajdar, S. Neogy, R. Tewari, D. Srivastava, G. K. K. Dey, G. H. Das, N. Saibaba and S. Banerjee, "Microstructural and textural developments during Zr-4 fuel tube fabrication," J. Nucl. Mater, 383(1-2), pp. 78-85, 2008.
79. H. Paul, M. Darrieula, N. Vanderesse , L. Litynska, M. Miszczyk, Microstructure of warm worked Zr -4, *Archives of metallurgy and materials*, 55, (2010), pp.1008-1019.
80. P. Zhao and R. A. Holt, "Microstructural Evolution and Micro-Texture in Zr-2.5Nb Tubes," *Mater. Sci. Forum,* 475-479, (2005), pp. 1421-1424.
81. E. Estela, P. A. Maria, E. Saggese, Welding Structures in Gas Tungsten Arc-Welded Zr-4, *Metallography,* 15, (1982), pp. 43-52.
82. D. Srivastava, G. K. Dey, and S. Banerjee, "Evolution of Microstructure during Fabrication of Zr-2.5 Wt pet Nb Alloy Pressure Tubes," *Metall. Trans. A,* 26, (1995), pp. 2707-2718.
83. Sunkulp Goel, R. Jayaganthan, I.V. Singh, D. Srivastava, G.K. Dey, N. Saibaba, Mechanical and microstructural characterizations of ultrafine grained Zr-2 produced by room temperature rolling, *Materials and Design,* 55, (2014), pp. 612-618.
84. A.R. Massih, T. Andersson, P. Witt, M. Dahlbäck, M. Limbäck, Effect of quenching rate on the β-to-α phase transformation structure in Zirconium alloy, *J.Nucl.Mater,* 322, (2003), pp. 138-151.
85. J P. Foster, J. Dougherty, M.G. Burke, J.F. Bates, S. Worcester, Influence of final recrystallization heat treatment on Zircaloy-4 strip corrosion, *J. Nucl. Mater,* 173**,** (1990), pp. 164-178.
86. A.R. Massih, M. Dahlbäck, M. Limbäck, T. Andersson, B. Lehtinen, Effect of beta-to-alpha phase transition rate on corrosion behavior of Zircaloy, *Corros. Sci.,* 48, (2006), pp. 1154-1181.
87. D. Srivastava, G. Dey, and S. Banerjee, "Evolution of microstructure during fabrication of Zr-2.5 Wt pet Nb alloy pressure tubes," *Metall. Mater. Trans.* A, 26, (1995), pp. 2707-

2718.

88. N. Saibaba, K. Vaibhaw, S. Neogy, K. V. Mani Krishna, S. K. Jha, C. Phani Babu and G. K. Dey, "Study of microstructure, texture and mechanical properties of Zr-2.5Nb alloy pressure tubes fabricated with different processing routes", *J. Nucl. Mater.*440, (2013). pp. 319-331.
89. C. Chauvy, P. Barberis, F. Montheillet, Microstructure transformation during warm working of β-treated lamellar Zr-4 within the upper α-range, *Materials Science and Engineering A*, 431, (2006), pp. 59-67.
90. V.D. Hiwarkar, S.K. Sahoo, I. Samajdar, A. Satpathy, K.V. Mani Krishna, G.K. Dey, D. Srivastav, R. Tewari, S. Banarjee, Defining recrystallization in pilgered Zr-4: From preferred nucleation to growth inhibition, *J.Nucl.Mater.*, 412, (2011), pp. 287-293.
91. R. Tewari, D. Srivastava, G. G. K. Dey, J. K. Chakravarty, and S. Banerjee, "Microstructural evolution in Zirconium based alloys," *J. Nucl. Mater*,383, (2008), pp. 153-171.
92. K.V. Mani Krishna, S.K. Sahoo, I. Samajdar, S. Neogy, R. Tewari, D. Srivastava, G.K. Dey, G. Hari Das, N. Saibaba, S. Banarjee, Microstructural and textural developments during Zr-4 fuel tube fabrication, *J.Nucl.Mater.*, 383, (2008), pp. 78-85.
93. G. Kumar, R. Singh, J. Singh, D. Srivastava, G.K. Dey, I. Samajdar, Defining the stages of annealing in a moderately deformed commercial Zirconium alloy, *J.Nucl.Mater.*, 466, (2015), pp. 243-252.
94. V. Deshmukh, Uppal Singha, Sunil Tonpe, N. Saibaba, Effect of process variables on texture and creep of preessurized heavy water reactor pressure tube, *Tran. IIM*, 63, (2010), pp. 397-402.
95. G. Choudhuri, S. Chakraborty, D. Srivastava, G.K. Dey, Phase field modelling of Widmanstatten plate formation in Zr-2.5Nb material, *Results in Physics*,3, (2013), pp. 7-13
96. Derek O. Northwood, John W. Robinson, ZhengJie, Microstructure and texture evolution during the annealing of cold-worked Zr-lwt%Nb , *Textures and Microstructures*, 13, (1991), pp. 133-154.
97. R.A. Holt, P. Zhao, “Micro-texture of extruded Zr-2.5Nb tubes, *”J.Nucl.Mater.*, 335, (2004), pp. 520-528

98. Y. Li, R. Rogge, R.A. Holt, “Development of local microstructure and crystallographic texture in extruded Zr-2.5Nb tubes,” *Materials Science and Engineering A*, 437, (2006), pp. 10-20.
99. Z. Jie, J. R. Robinson, D. O. Northwood, “A metallographic study of annealing of Zr-1 wt%Nb nuclear fuel sheathing, *Microstructural Science*, 17, (1989) ,pp.393-404.
100. Teodoro, J. E. Rosa, L. A. A. Terremoto, A. Teixeira, G. Lucki, and M. D. A. Damy, "Comparison Of The Mechanical Properties And Corrosion Resistance Of Zirlo And Other Zirconium Alloys," in *INAC* 2007, Santos, Brazil, pp. 1-6, (2007).
101. G. Sabol, "ZIRLO - An Alloy Development Success," *J. ASTM Int.*, 2, (2005), p. 12942.
102. S. Neogy, D. Srivastava, R. Tewari, R.N. Singh, G.K. Dey, S. Banerjee, Microstructural study of hydride formation in Zr-1Nb alloy, *J.Nucl.Mate.*, 322, (2003), pp. 195-203.
103. S. Neogy, D. Srivastava, J.K. Chakravarty, G.K. Dey, and S. Banerjee, Microstructural Evolution in Zr-1Nb and Zr-1Nb-1Sn-0.1Fe Alloys, *Metallurgical and Materials Transactions,* 38A, (2007), pp. 485-498.
104. S.K. Menon, S. Banerjee, and R. Krishnan: Metall. Trans. A, 1978, vol. 9A, pp. 1213-20.
105. C. Lemaignan, Zirconium Alloys: Properties and Characteristics, *Comprehensive Nuclear Materials,* 2, (2012), pp. 217-232.
106. R.V. Kulkarni, K.V. Mani Krishna, S. Neogy, D. Srivastava, E. Ramadasan, R.S. Shriwastaw, B.N. Rath, N. Saibaba, S.K. Jha, G.K. Dey, Mechanical properties of Zr–2.5%Nb pressure tube material subjected to heat treatments in $\alpha + \beta$ phase field, *J.Nucl. Mater,* 451, (2014), pp. 300-312.
107. N. Mozzani, Q. Auzoux, D. Le Boulch, E. Andrieu, C. Blanc, C.P. Scott, N. Barnel, Mechanical behavior of recrystallized Zr-4 under monotonic loading at room temperature: Tests and simplified anisotropic modeling, *J.Nucl.Mater.*, 447, (2014), pp. 94-106.
108. J. S. Leach and B. R. Pearson, The effect of foreign ions upon the electrical characteristics of anodic ZrO_2 films, *Electrochimica. Acta*, 29, (1984), pp.1271-1282.
109. H. Kajimura and H.Nagano, Passivity and its breakdown on Zirconium in high-temperature nitric acid, *Corros. Sci.*, 31, (1990), pp. 261-266.
110. B. Kim, C. Park, H. Kwon, “Effect of niobium on the electronic properties of passive films on Zirconium alloys,” J. *Electroanalytical. Chemistry.* 576, (2005), pp. 269-276.
111. B. Cox, Some thoughts on the mechanisms of in-reactor corrosion of Zirconium alloys. J.*Nucl. Mater.*,336,(2005), pp.331-368,

112. E. Hillner, D. G Franklin, J. D. Smee, *J. Nucl. Mater.* 278, (2000), p.334

113. A. Yilmazbayhan, E. Breval, A. T. Motta, R. J. Comstock, J. *Nucl. Mater*. 349, (2006), pp. 265-281.

114. Y. Jeong, H. Kim, T. Kim, Effect of β phase, precipitate and Nb-concentration in a matrix on corrosion and oxide characteristic of Zr-Nb alloys, J Nucl. Materials, 317, (2003), 1-12.

115. Sunil Tonpe, N. Saibaba, R.N. Jayaraj, A. Ravi Kumar, U. Kamachi Mudali, Baldev Raj, Process development for fabrication of Zr-4 dissolver assembly for reprocessing of spent nuclear fuel, *Energy. Procedia,* 7, (2011), pp. 459-467.

116. Te-Lin Yau, Zirconium for nitric acid solutions, Fourth ASTM symposium on Titanium and Zirconium in Industrial applications, Philadelphia, PA, 10–11 October, (1984), pp. 57-68.

117. H. Nagano, H. Kajimura, K. Yamanaka, Corrosion resistance of Zirconium and Zirconium-titanium alloy in hot nitric acid, *Mat Sci.Eng A.*,198, (1995), pp. 127-134.

118. C. Kato, T. Motooka, and M. Yamamoto, Global 2007, Advanced Nuclear Fuel Cycles and Systems, Boise, Idaho, USA, Sept. 2007, pp.245-250.

119. U. Kamachi Mudali, A. Ravishankar, S. Ningshen, Girija Suresh, Ravikumar Sole, K. Thyagarajan, Materials Development and Corrosion Issues in the Back End of Fuel Cycle, *Energy Procedia*, 7, (2011), pp. 468-473.

120. J. Jayaraj, K. Thyagarajan, C. Mallika and U. Kamachi Mudali, Corrosion behaviour of Zirconium, Titanium, and their alloys in simulated dissolver solution of fast breeder reactor spent nuclear fuel using Zr-4 mock up dissolver vessel, *Nuclear Technology*, 191 (2015) http://dx.doi.org/10.13182/NT14-90.